

Techniques in Kalman Filtering for Autonomous Vehicle Navigation

Philip Andrew Jones

**Thesis submitted to the faculty of Virginia Polytechnic Institute and State University in
partial fulfillment of the requirements for the degree of**

**Master of Science
in
Mechanical Engineering**

Committee Members

**Dr. Alfred Wicks
Dr. John Bird
Dr. Kathleen Meehan**

May 5, 2015

Blacksburg Virginia

Keywords:

Kalman Filter, Extended Kalman Filter, Navigation, IMU, GPS

Techniques in Kalman Filtering for Autonomous Vehicle Navigation

Philip Jones

ABSTRACT

This thesis examines the design and implementation of the navigation solution for an autonomous ground vehicle suited with global position system (GPS) receivers, an inertial measurement unit (IMU), and wheel speed sensors (WSS) using the framework of Kalman filtering (KF). To demonstrate the flexibility of the KF several methods are explored and implemented such as constraints, multi-rate data, and cascading filters to augment the measurement matrix of a main filter. GPS and IMU navigation are discussed, along with common errors and disadvantages of each type of navigation system. It is shown that the coupling of sensors, constraints, and self-alignment techniques provide an accurate solution to the navigation problem for an autonomous vehicle. Filter divergence is discussed during times when the states are unobservable. Post processed data is analyzed to demonstrate performance under several test cases, such as GPS outage, and the effect that the initial calibration and alignment has on the accuracy of the solution.

Acknowledgments

I would like to thank all of those who made it possible for me to complete this important step in my academic career. Firstly, my parents, who have always been there and supported my decisions to help me become the person I am today. To my patient fiancé Rachel, whose words of encouragement always kept me motivated. To my peers, colleagues, and friends who have made this adventure educational and enjoyable.

Also, a special thanks to my committee members is due. To Dr. Al Wicks for his ability to keep the big picture in focus, Dr. John Bird for never hesitating to give useful and sincere advice, and Dr. Kathleen Meehan, for her helpful feedback and guidance on writing this thesis.

Nomenclature

A	Dynamic plant model
{B}	Body frame
β	Pitch
C	Measurement matrix
{ECEF}	Earth centered earth fixed frame
ϵ	Innovation Error
F_k	Linearized State Dynamics Matrix
f_b	Body accelerations
g_iⁿ	Plumb bob acceleration
γ	Heading
h	Altitude
{I}	Inertial frame
K_k	Kalman Gain
λ	Longitude angle
M_k	A priori estimation covariance matrix
{N}	Navigation frame
v	Measurement Noise
ω_x ω_y ω_z	Body angular rates
Ω_e	Earth rotation rate amplitude (rad/s)
ω_b	Body Angular Rates
ω_{en}^n	Transport Rate
ω_{ie}^e	Earth rate in navigation frame
ω_{imu}	IMU noise
ω_{nb}^b	Body angular rates
P_k	Estimation Error Covariance
ϕ	Latitude angle

Φ	State Transition Matrix
Q_k	Process Noise Covariance Matrix
\mathbf{r}	Position vector from inertial frame
$\dot{\mathbf{R}}^*$	Angular rates in nav. frame (compact)
${}^N_B\mathbf{R}$	Rotation matrix from Body to Navigation
${}^N_E\mathbf{R}$	Rotation matrix from Earth to Navigation
\mathbf{R}_k	Measurement Noise Covariance Matrix
$\boldsymbol{\theta}$	Body attitude vector
θ	Roll
$\dot{\mathbf{v}}_e^n$	Ground acceleration of vehicle
$\hat{\mathbf{x}}_k$	State estimate
$\tilde{\mathbf{x}}_k$	Estimation error
$\hat{\mathbf{x}}_k^-$	A priori state estimate
$\hat{\mathbf{x}}_k^+$	Posteriori state estimate
\mathbf{x}	State vector
\mathbf{y}	Measurement Vector
$\hat{\mathbf{y}}_k$	Estimated measurement vector
\mathbf{y}_{GPS}	GPS measurement vector
\mathbf{y}_{WSS}	WSS measurement vector

Table of Contents

Chapter 1: Introduction	1
1.1 Autonomous Ground Vehicles	2
1.2 State Estimation.....	5
1.3 Fusing Navigation Sensors.....	5
1.4 Thesis Overview.....	7
Chapter 2: Navigation Background and Theory.....	9
2.1 Navigation Background.....	9
2.2 Inertial Navigation Systems	18
2.3 GPS Navigation.....	29
2.4 Conclusion.....	34
Chapter 3: The Kalman Filter.....	35
3.1 Introduction	35
3.2 Noise and Disturbances	37
3.3 General Kalman Filter Model	41
3.4 Extended Kalman Filter	45
3.5 Constrained Kalman Filter Methods	47
3.6 Other Notable Kalman Filter Methods.....	49
Chapter 4: Kalman Filter Application	52
4.1 Process Model and State Vector Realization	52
4.2 Measurements.....	54
Chapter 5: System Interface	61
5.1 Hardware Used.....	61
5.2 A Look at Alternative Models Using Different Sensor Suites.....	64

Chapter 6: Results	72
6.1 Attitude Estimation	72
6.2 Test Case One – Full EKF Model	79
Chapter 7: Conclusions and Future Work	86
7.1 Filter Model Construction	86
7.2 Standalone Sensor Platforms.....	87
7.3 Process and Measurement Noise.....	88
7.4 Benefits of Adaptation	88
7.5 Future Work	89
Bibliography	90

List of Acronyms

- AKF (Adaptive Kalman Filter)
- DBW (Drive by Wire)
- DR (Dead Reckoning)
- ECEF (Earth Centered Earth Fixed)
- EKF (Extended Kalman Filter)
- GDOP (Geometric Dilution of Precision)
- GLONASS (Global Navigation Satellite System)
- GPS (Global Positioning System)
- IAE (Innovation Based Adaptive Estimation)
- IMU (Inertial Measurement Unit)
- INS (Inertial Navigation System)
- KF (Kalman Filter)
- LIDAR (Light detection and ranging)
- MMAE (Multiple Model Adaptive Estimation)
- SLAM (Simultaneous Localization and Mapping)
- UKF (Unscented Kalman Filter)
- VDOP (Vertical Dilution of Precision)
- WSS (Wheel Speed Sensor)

List of Figures

Figure 1-1 Autonomous Vehicle Subsystem Design Framework.....	3
Figure 2-1: Roll, Pitch, and Yaw Rates $\omega_x, \omega_y, \omega_z$	12
Figure 2-2: ECEF, N, G, I, B Coordinates	14
Figure 2-3: Geodetic Coordinates Planar Figure	15
Figure 2-4: GPS Functional Diagram	31
Figure 2-5: GDOP.....	34
Figure 3-1: Basic Kalman Filter	36
Figure 3-2: General Dynamic System.....	38
Figure 3-3: Gaussian Random Variable.....	39
Figure 3-4: Block Diagram of Kalman Filter	41
Figure 4-1: GPS Latitude and GPS Accuracy for a non-moving Vehicle	58
Figure 5-1: Vehicle Structure.....	61
Figure 5-2: GPS and WSS Dead-Reckoned Position and Error	66
Figure 5-3: IMU Velocity and Uncertainty	67
Figure 5-4: Kalman filter with Cascaded Attitude Estimate.....	71
Figure 6-1: Differenced Acceleration Measurements and Navigation Frame Alignment Angles	73
Figure 6-2: Norm of the Covariance of Zeroth Order Navigation Alignment.....	74
Figure 6-3: Filtered Attitude Estimate During Same Run	75
Figure 6-4: IMU Integrated from Acceleration with no Roll or Pitch Measurements.....	76
Figure 6-5: Navigation Frame Angular Drift.....	77
Figure 6-6: Reduction of Integration Drift with Bias Corrections.....	78
Figure 6-7: IMU Dead Reckoned Trajectory with Bias Corrected Gyros and Roll and Pitch Calculation	78
Figure 6-8: Northing Velocity Comparison.....	79
Figure 6-9: Northing Position and Estimated Variance for Straight Line	80
Figure 6-10: GPS Pop for Northing Trajectory and Kalman Estimate Rejection.....	81
Figure 6-11: Northing Velocity - GPS vs. Kalman Estimation	81
Figure 6-12: GPS Pop for Easting Trajectory and Kalman Estimate Rejection	82
Figure 6-13: GPS Outage for Straight Line Trajectory	83

Figure 6-14: GPS Outage During Two Intervals and Estimated Performance 84
Figure 6-15: Northing Velocity and Estimate Variance 84

List of Tables

Table 2-1 Coriolis and Centripetal Acceleration at Different Vehicle Speeds at 21 degrees Latitude	21
Table 2-2 Vehicle Speed and Magnitude of the Transport Rate.....	23
Table 2-3 Comparison of Different IMUs	28
Table 2-4 Error Sources and Relative Contributions [5]	33
Table 3-1 Linear Kalman Filter Algorithm.....	44
Table 3-2 Extended Kalman Filter Algorithm	46
Table 5-1 IMU Performance Characteristics	63

Chapter 1: Introduction

The combination of mechanical systems coupled with electronics and software defines a type of technology that is now convention. Automobiles are a perfect example of fusion of sleek, functional, and ergonomic mechanical design, with the capability to preemptively brake, correct for lane departure, and parallel-park with modern technology. The cost of sensing and combining sensor data through microcontrollers has dramatically decreased, catalyzing the growth of technology to reach an age where cars drive themselves and humanoid robots can balance on their own. A common thread between automobiles, autonomous cars, and robots is the need to interpret the data received from the sensors installed on each platform. The art of state estimation specifically addresses the interpretation of sensor data to define the dynamic state of a system, e.g. the velocity, position, or orientation of a robot. This information can provide the necessary feedback to tell the controller what to do next, e.g. to start braking if an object is too close.

The Kalman filter is one such method of state estimation, which has been applied and adapted for the last 60 years in applications ranging from space missions to robotics. It is one of the most used tools in state estimation and control due to its robust nature and applicability to many mechatronics systems including robotics, aircraft, automation, and much more. The Kalman filter is implemented via a computer program and has the framework to easily combine data from multiple sensors, and utilize the physical and mathematical description of the system so that the best estimate of the dynamic state may be achieved. In the context of autonomous vehicles, which by nature utilizes many sensors to define the state of the system, they are a perfect platform to exercise Kalman filtering because every task depends on some interpretation of sensor data. More specifically, for an autonomous vehicle to drive from one place to another, navigation may be performed with the available sensors on board.

Navigation in and of itself is a well-studied topic [1], [2], [3], and has developed a sophisticated infrastructure which allows one to know their position to within several meters anywhere on the planet. Satellite radio navigation such as Global Positioning System (GPS), Galileo, and Global Navigation Satellite System (GLONASS) is commonly installed standard on cell phones and

vehicles. Many modern systems such as autonomous vehicles or missiles require precise kinematic awareness above and beyond the jogger tracking distance traveled for calories burned. In fact, satellite navigation is only one method of navigation used; other hardware and techniques such as, inertial navigation systems, and odometers, celestial navigation, and landmark association are commonly utilized to supplement the GPS navigation solution and generate a better knowledge of one's position. Fusion of the data coming in from many such sources is a delicate process but may provide a more accurate solution to navigation be facilitated by the application of Kalman filters.

This thesis focuses on sensor fusion in the context of autonomous ground vehicle navigation using Kalman filtering (KF) methods to achieve the fusion of the global positioning system (GPS), inertial navigation, and other auxiliary forms of sensing. The framework of the KF allows for fundamental navigation equations to be incorporated into a structure that can handle many sources of sensed data, and provide a minimum variance estimate of the perceived world. The theory behind navigation is discussed, as well as an introduction to the theory and practical uses of the KF. The work in this thesis is largely instructive and of a reviewing nature, but applied and demonstrated using autonomous vehicle data. The implementation uses a multi-rate, self-aligning and tuning cascaded extended KF which is robust to GPS faults and outages and returns an estimate of position, velocity, and body attitude (state variables) of the host vehicle.

1.1 Autonomous Ground Vehicles

An autonomous vehicle is usually described as one that has the ability to sense the surrounding world, make decisions based on the sensed information, and apply controls and actuate itself to get from one place to another. Typically, this requires several subsystems that can be integrated together, Figure 1-1 shows a generalized example of a hypothetical framework of subsystems for an autonomous ground vehicle. In this example, there are four main subsystems which are all connected via system interface. Drive-by-wire (DBW) is a subsystem which physically controls the vehicle through actuation, such as steering, throttle, and brake actuators. Perception observes the environment for obstacles or hazards, localization determines the position and orientation of

the vehicle, and the autonomy subsystem handles the logistics given information provided by the other subsystems, such as an obstacle avoidance trajectory.

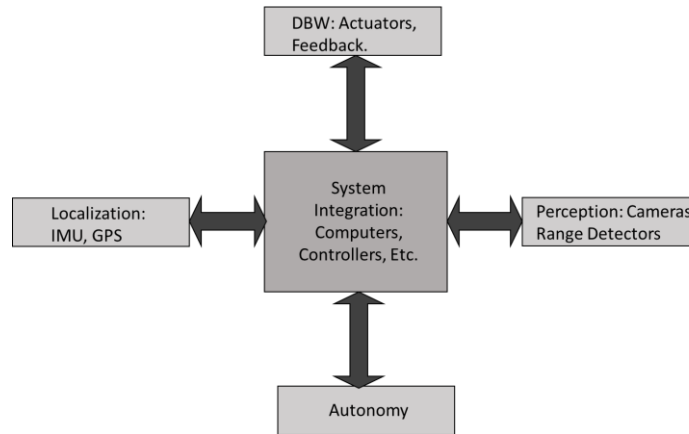


Figure 1-1 Autonomous Vehicle Subsystem Design Framework

The inspiration for this work comes from the growth in development of autonomous vehicles, and their need for a precise, and smooth, navigation solution which includes the position, velocity and orientation, or attitude [4]. The navigation solution/estimate is used as the closed loop control feedback for an autonomous vehicle, so the accuracy of the estimate limits the performance of the controller. Accordingly, precise state estimates will mean the control decisions are operating with high fidelity. Conversely, a noisy, biased, scaled or other erred state estimate will cause the controller to have unpredictable and likely undesirable behaviors.

In terms of autonomous vehicles operating with GPS, IMU, and WSS, it is inevitable that the sensors will be subject to error to each of these systems. For instance, GPS is known to have geometric (GDOP), multipath, delays caused by the atmosphere, and clock offsets [2], [5]. Similarly, the IMU provides accelerations and angular rotation rates which must be integrated, a common problem is that this leads to drift due to noise and other error in the sensors [6], [7]. Finally, WSSs are susceptible to wheel slip, causing an inaccurate representation of how far the vehicle has traveled when dead reckoning [8].

1.1.1 Drive by Wire and Localization

There are many subsystems which must be implemented and connected in order to control the vehicle. The main axes which must be controlled, such as steering, throttle, and brake is often called the drive-by-wire (DBW) system [9]. This is the control required to physically move the vehicle from one position to another. The vehicle will also be equipped with a number of sensors in several forms, such as wheel speed sensors, steering angle potentiometers, throttle positioning sensors, GPS and IMUs to measure the state of the vehicle.

1.1.2 Perception and Mapping

There are many other factors which must be considered when implementing an autonomous vehicle, as one of the biggest concerns is safety. While sensor such as GPS, speedometers, IMUs etc. provide information about the vehicle dynamic and kinematic state, there is still much to know about the outside environment. Perception is paramount, as it will find obstacles relative to itself and its path, and pass the information to a computer to ensure the obstacle is avoided. Perception is the monitoring of the surroundings through a range of sensors such as light detection and ranging (LIDAR), ultrasonic sensors, and visible and infrared cameras [10]. Perception can also aid in the navigation solution and simultaneous localization and mapping (SLAM) which develops a map at the same time navigation occurs [11]. For this reason, autonomous vehicles are typically equipped with perception hardware which is designed to monitor the outside environment. In addition to research on perception hardware, other areas of significant research in perception for lane and pedestrian detection over the last decade are machine learning and the detection and classification of objects. References [12], [13], and [14] are but a few examples of research studies in these areas.

The subsequent chapters will discuss the design process of the localization system, with regards to an adequately instrumented, non-holonomic ground vehicle as the platform. While this is a largely studied topic, both in terms of cost, speed, and performance optimization [15] [16] [17] [2], the purpose of the work here is to demonstrate flexibility and utility of the Kalman filter with empirical results.

1.2 State Estimation

State estimation is the determination of the dynamic state of a system, such as position, velocity, and attitude, and is vital in the successful control of any dynamical system. For example, the control of an autonomous vehicle requires that its position and velocity be known so that it may drive from one point to another. Other applications such as autonomous farming [18], robotic vision [19], and industrial robotics [20] are all examples of relatively new technologies which have stemmed from the fundamental science of sensing and control.

Autonomous vehicles are an interesting platform to study in terms of state estimation because of the variety of sources of information from sensors which may be applicable, such as GPS and inertial measurement unit (IMU) data. GPS and IMUs are different sensors by nature, GPS receives radio signals from an antenna and IMUs measure the movement of a tiny mass on a spring. However, GPS offers absolute readings of global position and velocity at low sampling rates (1-50 Hz) [21] whereas IMUs provide higher frequency acceleration and rotation data (~100 Hz) where the rigid body modes of a ground vehicle are in the 1-4 Hz range [22]. In a significant, and exploitable way, the differences in these sensors complement each other and can work in harmony to generate an accurate and precise state estimate resistant to the flaws of either one individually [23].

The motivation for this work is to develop design criteria for navigation in the context of an autonomous vehicle through the examination of state estimation of position and location. The principal focus is on fusing GPS, IMU and WSS readings for autonomous ground vehicle application and to discuss different methods of handling faults such as GPS outage or wheel slip. This type of fusion problem for navigations is typical in applications for navigation for ground, aerial, and even missiles [15] [16] [23] [24] [25] [26] [27] [28] [29].

1.3 Fusing Navigation Sensors

This thesis discusses the techniques of data fusion from many sensors that measure different parameters associated with navigation and to gain insight into the limitations of the sensors and numerical algorithms as applied to autonomous ground vehicles. The works of Cooper [30],

Sukkarieh [31], and Wendel [16] delve in to certain aspects of the navigation solution, regarding different filtering algorithms such as information filtering versus extended Kalman filtering, linearization, numerical integration and coordinate transformations, calibration and alignment, and the method of coupling the GPS and inertial measurement unit. This thesis will also evaluate Kalman filtering methods, sensor failures, and the construction of the filter model to quantify how well the navigation solution can be achieved under different scenarios, e.g. GPS, WSS, IMU failure.

One of the underlying problems when attempting to obtain an accurate navigation solution for computer navigation is the fusion of several types of data that are captured at different rates. The Kalman filter is a widely accepted method used to handle this problem. This thesis will look at the use of extended and linear Kalman filters for propagating state estimates forward despite the availability of measurements from the existing sensors.

Another challenge in the navigation problem is that in order to combine GPS and inertial measurements, this data must be transformed into the same coordinate system. Discussed in detail in Chapter 2, the basic premise is to transform them both to a locally level coordinate system which has an origin based on the start of a trajectory and has orthogonal components, for example pointing north, east, and down. In order to do this transformation, the vehicles body attitude must be determined as the inertial navigation system remains fixed to the vehicles orientation in a configuration known as a strapdown configuration [32].

Finally, because the nature of a ground vehicle incorporates nonholonomic constraints, methods of constrained Kalman filtering will be presented as a way of improved the accuracy of the filter as discussed in [33] and [34] (and many more) which have aiding the inertial navigation solution and prevent the drifting effect of integrating inertial measurements and wheel velocity measurements.

1.4 Thesis Overview

This thesis will discuss the theory, formulation, and application of Kalman filtering techniques in dealing with the fusion of GPS, IMUs, and auxiliary sensors for a precise and smooth navigation solution. The data presented in this work is post processed, however, the implementation is developed in such a way that online processing is feasible in regards to algorithm speed and data processing. Special attention is considered for GPS outage and dead reckoning performance is evaluated during such an event. The baseline assumptions associated with Kalman filtering are examined and evaluated for the use of the sensor platform used in the filter. A review of other approaches is also presented.

The Kalman filter, or equivalently the optimal linear quadratic estimator, will be presented with a discussion on assumptions, simplifications, and modifications which make practical implementation possible. There are examples provided in the appendix to show concept and design, but the main focus of application is GPS and WSS aided IMU navigation. The performance will be evaluated to determine which sensors and combinations thereof provide the most useful information regarding the navigation solution.

Chapter 2 provides background information to the navigation problem and associated sensor fusion methods from other authors. The error introduced into doing such as a transformation and its effect on integrated acceleration and angular rates is also discussed. Satellite navigation, error, corrections, and effect on the navigation solution is also presented.

Coordinate systems and transformations are discussed to setup the construction of the Kalman filter in chapter 3. Thus, Chapter 3 will focus on the nomenclature and underlying theory required to implement the Kalman filter and its extensions. Process noise and measurement noise are discussed as well as a brief introduction to different types of random variables. Since there have been many adaptations to the Kalman filter, several of them are presented in a general sense with citations and sources for the interested reader.

Chapter 4 looks at the development of the extended Kalman filter given the navigation equations presented in chapter two. The full, non-linear system of equations is used in this implementation. Switching mode measurement vectors are presented in the event that the observability of the system model changes during implementation, such as GPS outage. Selection of process and measurement noise is also examined.

Chapter 5 will detail the hardware specifications for these experiments and discuss estimated statistical properties and how they are implemented into the model. An evaluation of stand-alone sensor platforms is simulation, such as WSS dead reckoning using heading angle and IMU integration for position. The dynamic states will be defined and a corresponding state space model will be derived. Next, the IMU framework, i.e. three axis accelerometer, and three axis gyroscope will be described with a similar discussion on error, bias, and assumptions.

Chapter 6 is the results section which shows how the Kalman filter performs under different hypothetical scenarios, such as rapid IMU alignment when GPS heading information is unavailable, instantaneous spikes in GPS positional changes also known as GPS pop, and GPS outage.

Chapter 7 presents concluding remarks regarding the different performance evaluations of the different filter modes.

Chapter 2: Navigation Background and Theory

This chapter is designed to give the reader background information on past and current navigation techniques and their implementations. The Kalman filter and its relevance and utility as a navigation framework is discussed along with other authors' implementations.

Coordinate transformations are presented as each sensor, i.e. IMU, GPS, and WSS must be related to a unified coordinate system.

Strapdown inertial navigation theory is described and presented as well as error characteristics, such as noise, bias, scale factor, coning and sculling, and their relative impact on the sensor outputs. An investigation at the relative influence of Coriolis and centripetal acceleration under different driving conditions is presented as well.

Satellite navigation and the infrastructure are discussed along with ephemerides, error sources, corrections, and differential GPS. Discussion on the minimum number of satellites required for receiver clock compensation and the difference between tightly and loosely coupled INS/GPS navigation is described.

2.1 Navigation Background

Navigation is the process or activity of accurately ascertaining one's position and planning and following a route. Technology has advanced and navigation can now be done with computers and the aid of sensors, such as IMUs and GPS.

2.1.1 Types of Navigation Systems

Today, navigators rely on GPS, which is a class of satellite, radio navigation. GPS has become very accurate with an available 20 Hz update rate and down to sub-meter level accuracy through the use of OmniSTAR differential GPS [35]. However, there are some downsides to satellite navigation in that there are ionospheric delays, geometric dilution of precision, noise, and multipath errors [2] which degrade the accuracy of the position measurement. Occasionally, the

errors may cause abrupt pops, where the position may jump from one location to another. At times, this effect can cause jumps which exceed several meters. In the case of autonomous ground vehicle control, such a drastic jump in position may cause abrupt control inputs to correct the discrepancy in anticipated versus measured trajectory. GPS is also a line-of-sight sensor, meaning the GPS satellites must be visible to the receiver's antennas. In heavy forestry or urban environments, satellite visibility may be severely diminished and the dependence on GPS alone will degrade the integrity and robust nature of the state estimate. For this reason, it is valuable to supplement the navigation solution with other sensory information that may be used in the navigation computation.

For example, common navigation systems include INS, which consist of accelerometers which measure body accelerations, and gyroscopes that measure angular rate. Inertial navigation can be found in the guidance systems of aircraft, missiles, maritime equipment, ground vehicles, and robots [36], [37], [38]. Typically an INS will have error compensation built directly in it and gravity vector estimation, whereas an inertial measurement unit (IMU) has no such error compensation [37]. The INS is hailed due to its high sampling rates and passive nature [3]; not needing external equipment such as GPS satellites or using laser scanners which emit distinct spectrum to the environment. INS have been used in the aerospace industry and widely accepted as a successful navigation system since the 1930s [37]. However, INS are corrupted by error, such as bias, g sensitive drift, misalignment, and noise which in turn affects the inertial navigation solution [39]. Ultimately, the desired output of an inertial measurement unit will be position, velocity, and attitude (or orientation) which will require an integration of the measured accelerations and angular rate outputs [32].

The IMU, unless equipped with an absolute attitude sensor such as a magnetometer or tilt sensor, has no knowledge of orientation in relation to the other coordinate frames and must rely on a set of initial conditions and integrations to maintain the body attitude knowledge needed to transform measurements into the other coordinate systems. Since there is no absolute information on the orientation, velocity or position, integration of angular rates will lead to a drifting orientation, and twice integrating accelerations with both bias and random error will cause a drift in position and velocity.

Furthermore, the orientation is used in the calculation of position via coordinate transformations, such that any error in the orientation will also propagate through to the velocity and position components in the new coordinate frame.

Although satellite navigation and the IMU are the two main sensor suites that comprise the navigation system in this work, it is not uncommon to use auxiliary sensors to supplement the navigation solution. Sensors such as magnetometers, or tilt sensors [31], [27] provide an absolute body orientation and heading which reduce or eliminate the drift caused by integrating gyroscope data for body attitude. For example, the use of the steering angle for an Ackerman steered vehicle coupled with forward vehicle speed and a kinematic relationship can describe angular rotation rates which can be coupled with the other sensor information [11]. Wheel speed sensors (WSS), or odometers, are used in dead reckoning (DR), which is the process of integrating velocity or acceleration to obtain position. These sensors have the drawback of being sensitive to wheel slip and only provide information for a single degree of freedom in the body coordinate system.

This study will use a dual antenna GPS with differential GPS availability, tactical grade IMU, and WSS to analyze the effectiveness in obtaining a navigation solution under different sensor outages or availability. Accordingly, without an absolute heading reference system (AHRS), an evaluation of the IMU as a heading reference will be performed in the event of loss of GPS signal and thus the vehicle is required to depend on internal sensing. The method of synchronizing these sensors to a unified coordinate system is presented below.

2.1.2 Coordinate Systems

To begin the discussion of navigation, it is important to understand the different coordinate systems which orient each navigation system, i.e. Earth frame, inertial frame, geodetic, and navigation, et cetera. Specifically, there are five coordinate systems that will be used in this paper and these are the body frame {B}, earth centered earth fixed frame {ECEF}, inertial frame {I}, and the geodetic frame {G} also referred to as world geodetic system (WGS-84).

The body frame {B} is assumed to be fixed to the vehicle, it rotates and traverses with the vehicle [36]. The IMU located onboard the host vehicle is typically considered to be aligned with the body frame {B} and is used to denote the directions of the accelerations and axes of rotational motion of the body. Figure 2-1 shows typical orientation of the body frame which is also aligned with the sensing axes of the IMU. For strapdown navigation systems, the body frame is used as a reference to transform the linear accelerations and rotational velocities into {N} or {ECEF}.

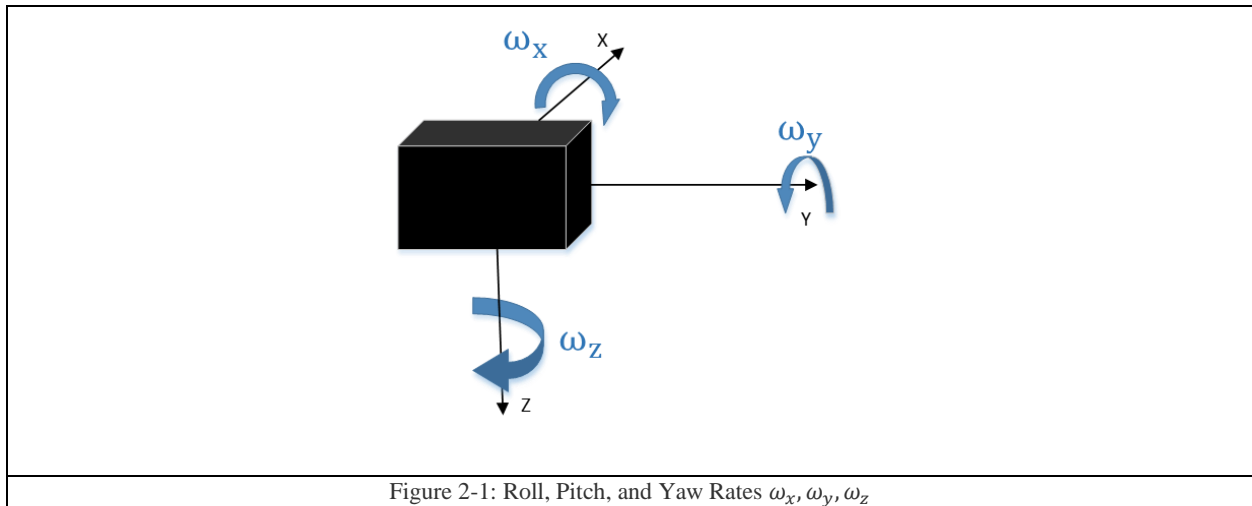


Figure 2-1: Roll, Pitch, and Yaw Rates $\omega_x, \omega_y, \omega_z$

Figure 2-1 shows the direction of sensing axes for a typical body frame, which is also aligned with the inertial measurement unit.

The inertial frame {I} is fixed in space and aligned with the center of the earth such that once every ~24 hours the earth frame {ECEF} is aligned with it. The navigation solution may be resolved in this frame, but the ground speed of the vehicle must be transformed into {I}.

Another frame of reference is the earth centered earth fixed {ECEF} frame, which is fixed with the rotating earth, and provides a Cartesian representation of the position of the vehicle with respect to the center of the earth. Due to the rotation of the earth, this causes a Coriolis acceleration which can be compensated for in the navigation equation but tends to have a relatively small impact over short periods of time. A common implementation of the {ECEF} representation is to use the earth frame reference without compensating for Coriolis effect and subsequently transform the earth frame to have an orthogonal component normal to the earth's surface and the corresponding plane to be tangent to the earth's surface [32].

A similar, but more comprehensive version of the transformed {ECEF} representations is the navigation {N} frame, which moves with the vehicle and is locally level on the earth's surface with an orthogonal axis pointing down towards the center of the earth. This coordinate system accounts for the both the Coriolis effect from the earth rotating, the vehicle travelling on the earth's surface causing a Coriolis term, and centripetal acceleration caused by a moving vehicle on the earth's surface [32]. In this context, the navigation frame will share a moving common origin with the body frame. A benefit of this frame is that the gravitational vector can be used for a coarse alignment technique in order to align and solve for components of the body frame attitude with respect to the navigation frame while the vehicle is stationary, thus providing initial conditions before integration of the IMU data.

Geodetic {G} is an earth-fixed model but is in polar coordinates and accounts for the eccentricity of the earth (latitude (ϕ), longitude(λ), and elevation (h)) [5]. Typically, this is given to users wanting to know their absolute position on the earth, and is not used in any computation in this work.

All of the coordinate frames are derived out of what's known as the inertial frame, which is fixed relative to the earth's rotation. This becomes especially important when discussing the strapdown inertial navigation equations as they are written in the inertial frame initially, and transformed into the navigation equation through the Coriolis theorem which is described later.

As one can see in Figure 2-2, the ECEF coordinates place an origin at the earth's center, O, and the location of a vehicle can be described relative to the center of the earth through standard Cartesian coordinates. Geodetic latitude and longitude were formulated to give the user their location relative to the equator and prime meridian in polar coordinates. This method is typically used to give a user location information but is still not necessarily the frame of choice for computation for navigation. GPS will typically give location in terms of latitude, longitude, and height above the ellipsoid (HAE) which assumes an ellipsoidal Earth model opposed to a spherical model. Figure 2-2 represents a *geocentric* earth, but the navigation equations are modified to account for the ellipsoidal earth.

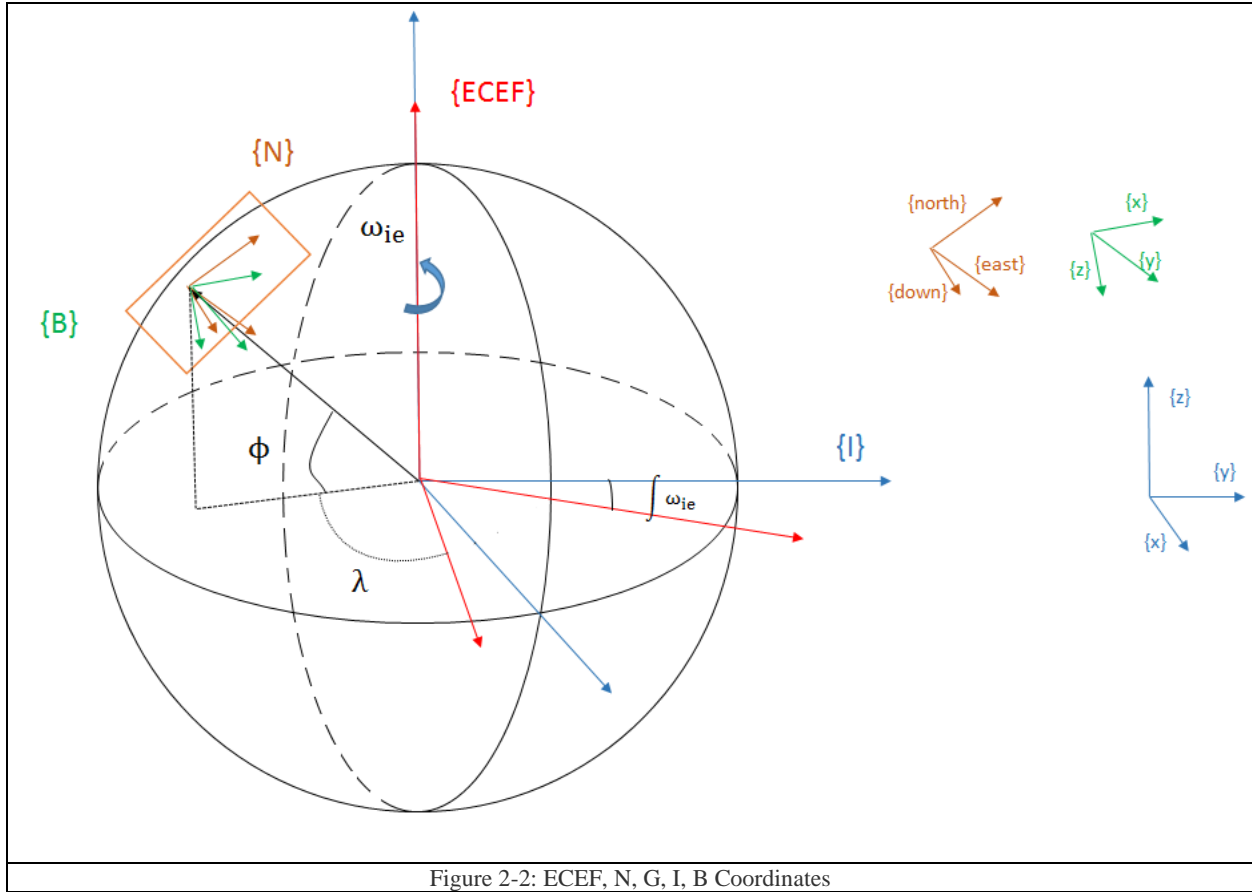


Figure 2-2: ECEF, N, G, I, B Coordinates

Figure 2-2 shows all of the coordinate systems used in this thesis. The inertial frame is fixed in space, while the ECEF frame shares a common vertical axis but rotates about it. Since the navigation frame is locally flat, the plane is drawn on the surface for reference. The body frame and navigation frame in this work share a common origin, but are not necessarily aligned in attitude.

For the navigation in this work, the typical coordinate frame to apply the fusion of all of the sensor data is the locally level frame $\{N\}$, which accounts for Coriolis and centripetal effects of the rotating earth and rotating coordinate system of the moving vehicle. However, a simplification due to the relative effects of the Coriolis terms will be examined later, which makes it similar to a transformed earth frame mechanization as presented in [32].

2.1.3 Geodetic Coordinates to Navigation Frame

Firstly, given geodetic coordinates and assuming the earth is an ellipsoid, as in Figure 2-3, the expressions for finding ECEF coordinates are functions of the eccentricity, N , and the geodetic longitude λ , latitude ϕ , and height h . These Cartesian coordinates are given by the following expressions [5],

	$x_{ECEF} = (N + h) \cdot \cos(\phi) \cdot \cos(\lambda),$	2-1
--	--	-----

	$y_{ECEF} = (N + h) \cdot \cos(\phi) \cdot \sin(\lambda),$	2-2
--	--	-----

	$z_{ECEF} = \left(\frac{b^2}{a^2} \cdot N + h\right) \cdot \sin(\phi),$	2-3
--	---	-----

where $a = 6378.137 \text{ km}$ is the semi-major axis, $b = 6356.75231425 \text{ km}$ is the semi-minor axis, and N is the radius of curvature of the ellipsoid illustrated in Figure 2-3 and is defined as the perpendicular line from the altitude of the ECEF coordinate that continues until crossing the z axis and can be given by the following:

	$N = \frac{a^2}{\sqrt{a^2 \cdot \cos^2(\phi) + b^2 \cdot \sin^2(\phi)}}$	2-4
--	--	-----

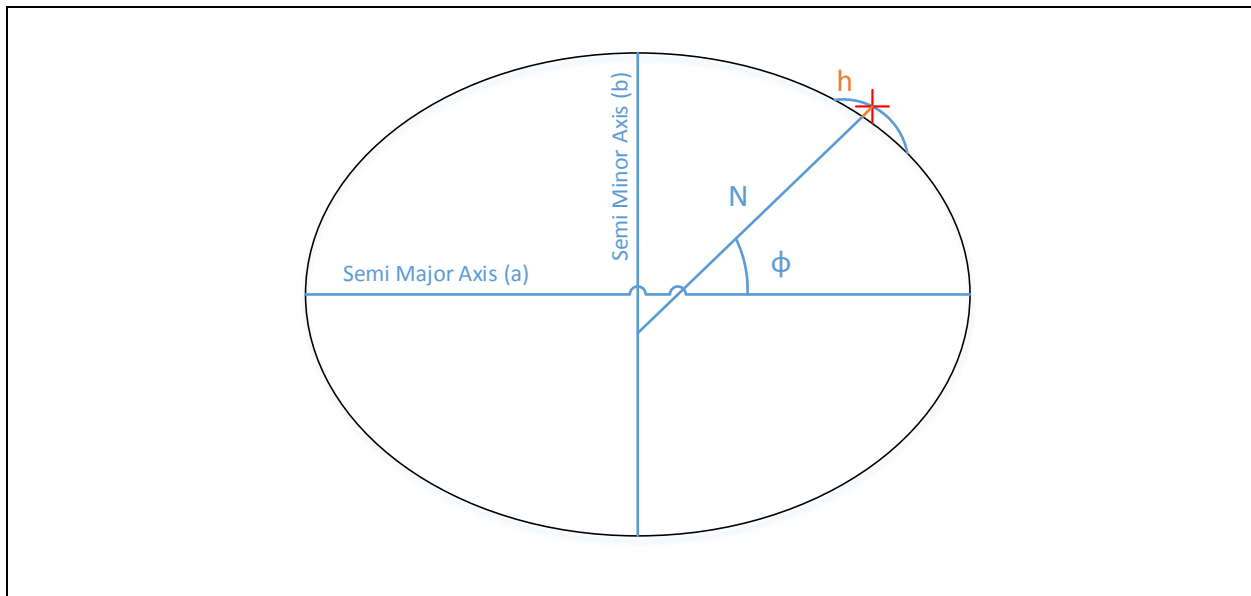


Figure 2-3: Geodetic Coordinates Planar Figure

Figure 2-3 shows that in order to account for an ellipsoidal earth, a perpendicular line with the surface is drawn until it intersects the semi minor axis of the Earth.

In order to transform ECEF coordinates into {N}, it can be shown that a series of two rotations must be completed to transform them and in this work, the Euler angle rotation method is used. For example, if a coordinate frame is rotated about x, and then y using the Euler method, the first rotation occurs about the x axis of the original frame and the second rotation occurs about the y axis is the now rotated frame. This is opposed the fixed angle notation, which requires all rotations to be about the fixed, non-moving reference frame [40].

By observation of Figure 2-2, it can be shown that, in order to transform the {ECEF} coordinates into the {N} frame, a rotation about the z_{ECEF} axis by λ , followed by a rotation about the new axis noted as y'_{ECEF} by ϕ . This transformation will point the previous x_{ECEF} in the local north direction, y_{ECEF} will point towards the east, and the z_{ECEF} will point down towards the center of the Earth. The series of rotations is shown to be,

	${}^N_E \mathbf{R} = \begin{bmatrix} \cos(\lambda) & -\sin(\lambda) & 0 \\ \sin(\lambda) & \cos(\lambda) & 0 \\ 0 & 0 & 1 \end{bmatrix} \cdot \begin{bmatrix} \cos(\phi) & 0 & -\sin(\phi) \\ 0 & 1 & 0 \\ \sin(\phi) & 0 & \cos(\phi) \end{bmatrix}$ $= \begin{bmatrix} -\cos(\lambda) \cdot \sin(\phi) & -\sin(\lambda) \cdot \sin(\phi) & \cos(\phi) \\ -\sin(\lambda) & \cos(\lambda) & 0 \\ -\cos(\lambda) \cdot \cos(\phi) & -\sin(\lambda) \cdot \cos(\phi) & -\sin(\phi) \end{bmatrix}$	2-5
--	---	-----

It is also noted that the notation used in this work is drawn from [40] where the subscript and superscript relationship on the rotation matrix means frame {E} relative to {N}. A convenient property of rotation matrices is that they belong to a special orthogonal group $SO(3)$ which is an orthonormal set which has the following properties [40],

	$\mathbf{R}^{-1} = \mathbf{R}^T = \mathbf{R},$	2-6
--	--	-----

where \mathbf{R} is a generic rotation matrix from one coordinate system to another. This means that one must simply take the transpose of that rotation matrix in order to transform from one coordinate system to another or vice versa.

Since the desired coordinates are relative to a given origin, the $\{N\}$ coordinates can be given by Equation 2-7 using the rotational transformation matrix given in equation 2-5.

	$\{N\} = {}^N_E \mathbf{R} \cdot [\mathbf{X}_k - \mathbf{X}_0]$	2-7
--	---	-----

where \mathbf{X}_k is the Cartesian vector $[x_{ECEF} \ y_{ECEF} \ z_{ECEF}]^T$ in $\{E\}$ at time k and \mathbf{X}_0 is the origin of choice in $\{E\}$. N is the Cartesian vector representing the position of the host in $\{N\}$.

2.1.4 Body Frame to Navigation Frame

The body frame also requires a transformation into the $\{N\}$ frame so that accelerations and angular rates may be compatible with the GPS measurements. Again, the vehicle is assumed to have 6 degrees of freedom (DOF): 3 orthogonal linear components in $\{B\}$, $[x_B \ y_B \ z_B]^T$ and three orthogonal rotational components, or attitude, $[\theta \ \beta \ \gamma]^T$ which are roll, pitch, and yaw, respectively.

It is assumed that the host vehicle undergoes these three rotations relative to the navigation frame $\{N\}$ and it is through these rotations that the linear components of acceleration, velocity, and position from the IMU may be updated in the navigation frame. Specifically, the body is assumed to undergo the rotations in order of roll θ , pitch β , and yaw γ since, matrix multiplication is non-commutative. The rotation matrix is given by the following which can be found in a number of works on the topic [31],

	${}^N_B \mathbf{R} = \begin{bmatrix} \cos(\gamma) & \sin(-\gamma) & 0 \\ \sin(\gamma) & \cos(\gamma) & 0 \\ 0 & 0 & 1 \end{bmatrix} \cdot \begin{bmatrix} \cos(\beta) & 0 & \sin(\beta) \\ 0 & 1 & 0 \\ \sin(\beta) & 0 & \cos(\beta) \end{bmatrix} \cdot \begin{bmatrix} 1 & 0 & 0 \\ 0 & \cos(\theta) & \sin(-\theta) \\ 0 & \sin(\theta) & \cos(\theta) \end{bmatrix}$ $= \begin{bmatrix} \cos(\beta) \cdot \cos(\gamma) & -\cos(\theta) \cdot \sin(\gamma) + \sin(\theta) \cdot \sin(\beta) \cdot \cos(\gamma) & \sin(\theta) \cdot \sin(\gamma) + \cos(\theta) \cdot \sin(\beta) \cdot \cos(\gamma) \\ \cos(\beta) \cdot \sin(\gamma) & \cos(\theta) \cdot \cos(\gamma) + \sin(\theta) \cdot \sin(\beta) \cdot \sin(\gamma) & \sin(-\theta) \cdot \cos(\gamma) + \cos(\theta) \cdot \sin(\beta) \cdot \sin(\gamma) \\ \sin(-\beta) & \sin(\theta) \cdot \cos(\beta) & \cos(\theta) \cdot \cos(\beta) \end{bmatrix}$	2-8
--	--	-----

which maps the body frame into the navigation frame. To find these angles in the preceding equation, Section 2.2.3 will present the vector rate equations to obtain these.

2.2 Inertial Navigation Systems

In order to navigate with an inertial based measurement system, one is required to integrate the output of the IMU, given a set of initial conditions of position, velocity and attitude. Inertial navigation has the advantage that it has a high sampling rate and can passively measure the dynamics, i.e. without external aids such as location beacons or satellites, of the vehicle and provide an estimate of position, velocity, and attitude of the host vehicle. Inertial navigation is typically broken down into two configurations: gimbaleed and strapdown inertial navigation systems (SINS) [37]. While SINS is used throughout this work, the operation of both are described below.

2.2.1 Gimbaled Inertial Navigation

In a gimbaleed configuration, the orientation of the inertial navigation system is compensated such that it has a constant orientation nominally pointed north, east, and down for each of the orthogonal components. Conversely, a strapdown configuration is such that the IMU is rigidly fixed to the body, or vehicle, and is thus changing orientation with respect to the navigation frame in time. Due to the expensive nature of gimbaleed systems, which require multi-axis actuation to maintain its orientation, gimbaleed systems are less commonly used for common applications [37]. Strapdown systems are less expensive, but have the disadvantage that in order to obtain attitude information, they must be numerically transformed into the proper coordinate system.

2.2.2 Strapdown Inertial Navigation

The strapdown inertial navigation equations used in this work are derived in Ref. [32], which work off of the principal that a triad of accelerometers measures the specific force (force normalized by mass) of a given point in a fixed, non-moving inertial frame of reference. An expression to map the body frame accelerations into the navigation frame and compensate for Coriolis, centripetal, and gravitational effects is presented in this sections will then be used in subsequent sections regarding the Kalman filter implementation.

For precise, long-term navigation, it is common to compensate for both Coriolis, centripetal, and gravitational acceleration, caused by the rotation of the Earth and the local gravity field, as integration errors will grow significantly over long periods of time. For this reason, the Earth's rotation rate, which is the cause of Coriolis acceleration, is compensated in the navigation equations. For short-term navigation it is common to just compensate for gravity and not necessarily for Earth's rotation and, thus, Coriolis force.

The following strapdown navigation equations are fully derived in Titterton [32], which details how to transition from a fixed inertial frame, to a fixed earth frame, and finally, into the navigation frame. Using body frame accelerations and rotation rates as sensed by the IMU, the coordinate frames are aligned and can be used as an expression of motion as a differential equation.

The navigation equation as written in the navigation frame {N} is given by [32]:

	$\dot{\mathbf{v}}_e^n = {}^n\mathbf{R}_b \cdot \mathbf{f}_b - (2\boldsymbol{\omega}_{ie}^e + \boldsymbol{\omega}_{en}^n) \times \mathbf{v}_e^n + \mathbf{g}_I^n,$	2-9
--	---	-----

where $\dot{\mathbf{v}}_e^n = [\ddot{N} \quad \ddot{E} \quad \ddot{D}]^T = \left[\frac{d^2N}{dt^2} \quad \frac{d^2E}{dt^2} \quad \frac{d^2D}{dt^2} \right]^T$ is the acceleration in the navigation frame with each component being one of northing position (N), easting position (E), and height in the positive down frame (D) as shown in Figure 2-2. ${}^n\mathbf{R}_b \cdot \mathbf{f}_b$ are the body accelerations transformed into the navigation frame.

$(2\boldsymbol{\omega}_{ie}^e + \boldsymbol{\omega}_{en}^n) \times \mathbf{v}_e^n$ is the Coriolis acceleration as experienced by the vehicle moving on the surface of the earth and is comprised of the earth's rate of rotation in the navigation frame as a function of latitude ϕ shown below [32].

	$\boldsymbol{\omega}_{ie}^n = [\Omega_e \cos(\phi) \quad 0 \quad \Omega_e \sin(\phi)]^T$	2-10
--	--	------

crossed with the ground speed of the vehicle \mathbf{v}_e^n . The rotation of the earth is given by $\Omega_e = 7.292115 \times 10^{-5} \frac{rad}{s}$. Recall that ${}^n\mathbf{R}_b$ is the rotation matrix that is used to transform the body frame accelerations into the navigation frame.

The term [32],

	$\boldsymbol{\omega}_{en}^n = \begin{bmatrix} \dot{E} & \dot{N} & \dot{E} \cdot \tan(\phi) \end{bmatrix}^T \begin{bmatrix} R_E + h \\ R_N + h \\ R_N + h \end{bmatrix}^{-1},$	2-11
--	---	------

is called the transport rate and is caused by the motion of the navigation frame with respect to the fixed earth frame. R_E is the transverse radius [32],

$$R_E = \frac{a(1-e^2)}{(1-e^2 \sin^2 \phi)^{3/2}},$$

and R_N is the meridian radius [32],

$$R_N = \frac{a}{(1 - e^2 \sin^2 \phi)^{1/2}},$$

where a is the semi-major axis of the earth given by $a = 6378.137$ km, and $e = \sqrt{1 - \frac{b^2}{a^2}}$ is the eccentricity of the ellipsoidal earth.

Finally [32],

	$\mathbf{g}_l^n = \mathbf{g} - \boldsymbol{\omega}_{ie}^n \times [\boldsymbol{\omega}_{ie}^n \times \mathbf{r}] = \mathbf{g} - \frac{\Omega_e^2 (R+h)}{2} [\sin(2\phi) \quad 0 \quad 1 + \cos(2\phi)]^T,$	2-12
--	---	------

is referred to as the plumb-bob acceleration as it is the experienced force caused by a gravity field along with the centripetal acceleration due to the rotation of the earth. By design of the navigation frame, $\mathbf{g} = [0 \quad 0 \quad -9.789 \frac{m}{s^2}]$ is the acceleration as caused by the local gravitational field as defined in Hawaii according to Ref. [41].

The geodetic coordinates may also be written as a function of the northing, easting and downing velocity as [32],

	$\dot{\phi} = \frac{\dot{N}}{R_N + h}$ $\dot{\lambda} = \frac{\dot{E} \cdot \sec(\phi)}{R_E + h}$ $\dot{h} = -\dot{D}$	2-13
--	--	------

Table 2-1 shows the specific force experienced by the accelerometer for different vehicle speeds. Note that the plumb bob acceleration is constant at a given latitude regardless of the vehicle speed.

Vehicle Speed (N, E, D) $\left(\frac{m}{s}\right)$	Total Coriolis Acceleration $\left(\frac{m}{s^2}\right)$	Total Plumb Bob Acceleration $\left(\frac{m}{s^2}\right)$
[0, 0, 0]	0	$g_{nom} - 3.121 \times 10^{-5}$
[1, 2, 0]	0.000292	~
[2, 2, 0]	0.000482	~
[4, 4, 0]	0.000965	~

Table 2-1 Coriolis and Centripetal Acceleration at Different Vehicle Speeds at 21 degrees Latitude

It is also noted that a singularity will exist in the navigation equations due to the fact that the transport rate and latitude and longitude are dependent on $\frac{1}{\cos(\phi)}$, which is singular for $\phi = \frac{\pi}{2}$. This is overcome with what is known as α – *wander* methods, which rotate the navigation frame such that the northing direction is pointed away from the poles of the earth [37]. This is noted, but not used in this work because all of the measurements were taken at lower latitudes ~21° which is far enough away from the poles to be a nonissue.

From the previous equations, namely Equation 2-9, defines the differential equation which governs the model for the Kalman filter used in the overall fusion of data. However, it is still required that the rotation matrix ${}^N\mathbf{R}_B$ be calculated in real time to transform the body acceleration rates into the navigation frame. The next section is dedicated to the rate vector equations.

2.2.3 Rate Vector Equations

In general, the strapdown inertial problem of resolving attitude from the gyroscope is dealt with in a number of ways to try to reduce the error and to perform more quickly and efficiently. The problem is typically presented as a non-linear differential equation which is solved through numerical methods such as an Euler or Runge Kutta Methods [42], [43], [44].

Again from Ref. [32], the rate equations for roll, pitch and gamma in the navigation frame are defined as shown in 2-14.

	$\dot{\theta} = \omega_x + (\omega_y \cdot \sin(\theta) + \omega_z \cdot \cos(\theta)) \cdot \tan(\beta)$ $\dot{\beta} = \omega_y \cdot \cos(\theta) - \omega_z \cdot \sin(\theta)$ $\dot{\gamma} = \frac{(\omega_y \cdot \sin(\theta) + \omega_z \cdot \cos(\theta))}{\cos(\beta)}$	2-14
--	--	------

Collectively, these three angular rate and corresponding angles will be given as $\dot{\Theta} = [\dot{\theta}, \dot{\beta}, \dot{\gamma}]^T$ which are the roll, pitch, and heading rates in the navigation frame.

For convenience, equation 2-14 can be written as:

	$\dot{\mathbf{R}}^* = \begin{bmatrix} 1 & \sin(\theta) \tan(\beta) & \cos(\theta) \tan(\beta) \\ 0 & \cos(\theta) & -\sin(\theta) \\ 0 & \frac{\sin(\theta)}{\cos(\beta)} & \frac{\cos(\theta)}{\cos(\beta)} \end{bmatrix} \begin{bmatrix} \omega_x \\ \omega_y \\ \omega_z \end{bmatrix}.$	2-15
--	---	------

The sensors used to measure body frame angular rates $\omega_b = [\omega_x \ \omega_y \ \omega_z]^T$ also measure the rotational rate of the earth along with the navigation frame rate with respect to the Earth.

Accordingly, from Ref. [32],

	$\omega_{nb}^b = \omega_{ib}^b - {}^b_n\mathbf{R}[\omega_{ie}^n + \omega_{en}^n],$	2-16
--	--	------

where again, $\omega_{ie}^n = 7.2921 \times 10^{-5} \frac{rad}{s}$, which is the rotation rate of the earth. Equation 2-16 states that the body rate with respect to the navigation frame is equal to the total angular velocity as measured by the gyroscopes referenced from a fixed inertial frame minus the earth's rotation in the navigation frame plus the navigation frame rotation rate with respect to earth all transformed into the body frame. A list of transport rate angular velocities is given in Table 2-2.

Vehicle Speed $\left(\frac{m}{s}\right)$	Magnitude of the Transport Rate Induced Angular Velocities $\left(\frac{rad}{s}\right)$
[0, 0, 0]	0
[1, 2, 0]	3.5571×10^{-7}
[2, 2, 0]	4.5950×10^{-7}
[4, 4, 0]	9.1901×10^{-7}

Table 2-2 Vehicle Speed and Magnitude of the Transport Rate

There are different methods of handling the integration of the rotation rate vector, including the direction cosines and quaternions. This work simply uses the Euler expressions as mentioned above with integration of the rate equations taking place in the framework of the Kalman filter directly as shown in chapter 3. Mathematically, these methods will produce the same result [26] but have different computational load.

Methods for IMU integration to resolve accelerations into positions and velocities, and angular rates into attitude is done thoroughly in [43], [45] which is a two volume series on the subject. References [43] and [45] suggests a two-part approach to integration which utilizes a low order (fast) integration method at high frequencies and a higher order method at a lower frequency. The purpose for this is to maintain high resolution at lower computational cost. The advantage of higher order integration is that for a first order Euler method, the local truncation error is on the order of δt^2 whereas for higher order integration methods, such as a Runge Kutta method, the local truncation error is of the order δt^4 [46].

2.2.4 INS Calibration and Alignment of the Host Vehicle

One of the first challenges for inertial navigation is that of initial alignment and calibration, which without the presence of an AHRS, the IMU must align itself based on prepackaged alignment procedures. Initial alignment and calibration is used to find the initial conditions of the attitude before attempting to navigate or integrate the inertial measurements. This is substantial due to the fact that the compensation of gravity in the inertial navigation equations, and the subtraction of such a large acceleration will cause a significant amount of drift during integration if the angles are not correct. The vehicle or IMU will start from an initial pose, whether on an incline or otherwise skewed from a locally flat plane. While the vehicle is stationary is an ideal time to compute the roll or pitch angle before the vehicle begins its trajectory. If the initial conditions are off by even a small amount, beginning a series of integrations under these conditions will inevitably compromise the solution for a reasonable position estimate given the IMU.

There are many works and analysis done on the initial alignment of the host vehicle for inertial navigation systems. In [34] and [47], external tilt sensors is used to estimate the bias terms on the accelerometer when using the gravity vector to estimate roll and pitch angles. Rapid alignment techniques for heading are also studied, e.g. [48] who also shows that Euler angle based integration is slower than the rotation vector counterpart. It is also often desired to estimate sensor biases during alignment as the vehicle is stationary, references [49], [50], [51] are a few examples which exercise different methods of doing this.

The approach used in this study is of aligning the body frame to the navigation frame is using the gravity vector, which by design aligns with the vertical unit vector in $\{N\}$, and using accelerometer outputs to estimate which direction the z axis on the accelerometer is pointing. This projection will lead to the ability to find the roll and pitch angles derived from equation 2-8. For examples on different methods of achieving initial alignment and calibration, see [7], [49], [52], [50].

With higher grade inertial gyroscopes, it is possible to extend this capability to estimate the heading angle through sensing Earth's rotation and again assuming a stationary vehicle, [2], [37].

Both techniques for the alignment of roll and pitch require a stationary vehicle to ensure that the measurements are only measuring the motion of Earth and gravity. High speed algorithms are often desired such that the vehicle is not required to be stationary for long periods of time for recalibration [24], [48].

The solution to the initial alignment of an IMU used in this work is to resolve the initial conditions of attitude given a stationary host vehicle using the accelerometers output which is done in many works including references [47], [31]. The accelerations acting on the stationary vehicle are that of gravity and a Coriolis force caused by the rotation of the earth as seen from equation 2-9. During coarse alignment, the effects of the earth's rotation rate are ignored and it is assumed that only gravity is acting on the accelerometers. Recall that the navigation plane assumes a flat Earth in the vicinity of the positional excursion. Accordingly, this means that gravity will point along just one of the orthogonal directions in {N} along the vertical component. When the vehicle is not moving, one of the only accelerations experienced by the IMU will be that of gravity, $\mathbf{a}_N = [0 \ 0 \ g_{nom}]$, where g_{nom} is the nominal gravitational constant and this term varies about the earth.

By taking the transpose of ${}^N_B\mathbf{R}^T = {}^B_N\mathbf{R}$, and using $\mathbf{a}_B = {}^B_N\mathbf{R} \cdot \mathbf{a}_N$ one can then write the following,

	$\begin{bmatrix} a_B^x \\ a_B^y \\ a_B^z \end{bmatrix} = \begin{bmatrix} \cos(\beta) \cdot \cos(\gamma) & \cos(\beta) \cdot \sin(\gamma) & \sin(-\beta) \\ -\cos(\theta) \cdot \sin(\gamma) + \sin(\theta) \cdot \sin(\beta) \cdot \cos(\gamma) & \cos(\theta) \cdot \cos(\gamma) + \sin(\theta) \cdot \sin(\beta) \cdot \sin(\gamma_s) & \sin(\theta) \cdot \cos(\beta) \\ \sin(\theta) \cdot \sin(\gamma) + \cos(\theta) \cdot \sin(\beta) \cdot \cos(\gamma) & \sin(-\theta) \cdot \cos(\gamma) + \cos(\theta) \cdot \sin(\beta) \cdot \sin(\gamma_s) & \cos(\theta) \cdot \cos(\beta) \end{bmatrix} \begin{bmatrix} 0 \\ 0 \\ g \end{bmatrix}$	2-17
--	--	------

Multiplying through, we can see that for a stationary vehicle with misalignment angles that,

	$\mathbf{a}_b = \begin{bmatrix} \sin(-\beta) \\ \cos(\beta) \cdot \sin(\theta) \\ \cos(\beta) \cdot \cos(\theta) \end{bmatrix} \cdot g$	2-18
--	---	------

Which is an analytical solution for finding the initial angles θ and β based on measured acceleration data. However, \mathbf{a}_b is a measurement vector which contains noise and disturbances from external sources, such as wind or engine vibrations. This work will use an external filter to

estimate the roll and pitch, and augment the measurement matrix with the outputs of that filter. A similar method was proposed in [51], which uses an extended Kalman filter using a gyrocompassing technique to estimate azimuth angle.

Another issue is that γ , or the heading angle, is unobservable and may not be calculated from this expression. However, if the rotation of the earth is measured by a high precision gyroscope, the heading may also be initially aligned in a process called gyrocompassing with gyroscope errors and resolution to be several orders of magnitude smaller than the rotation rate of the earth [37].

It is shown in Ref. [36] that the rotational velocity in the navigation frame due to a non-moving vehicle can be given by equation 2-19.

	$\boldsymbol{\omega}_n = [\Omega_e \cos(\phi) \quad 0 \quad \Omega_e \sin(\phi)]^T$	2-19
--	---	------

$$\begin{bmatrix} \omega_x \\ \omega_y \\ \omega_z \end{bmatrix} = \mathbf{R}_{N}^B \begin{bmatrix} \Omega_e \cos(\phi) \\ 0 \\ \Omega_e \sin(\phi) \end{bmatrix}$$

where Ω_e is the earth rotation rate nominally about the earth's z axis. Jiang [53] provides an error analysis regarding scale factors and biases and how they influence the coarse alignment. Jiang shows methods of calculating drift error, skew misalignment angles, and scale factor by means of comparing the IMU output to the expected output given the earth rates.

This work will use coarse alignment techniques to estimate initial attitude, not including heading from gyrocompassing, and will use a cascaded filter with an augmented measurement vector. In this framework, gyroscope bias is estimated and compensated for on the output of the gyroscopes and is developed in Chapter 4.

2.2.5 IMU Measurement Error Sources

The preceding navigation equations hold true if there is no error in the measurement. In reality this is not true, so it is worthwhile to look at error commonly found in IMU measurements. Before a complete discussion on IMU error sources can be given, it is important to understand some of the parameters which pose limitations to the measurements. These parameters are

range, scale factor, sample rate, bias, bias drift, and bias instability which, in general apply to both accelerometers and gyroscopes.

Range quantifies the limits of which the sensor can measure, and for gyroscopes is usually given in deg/s or rad/s. Resolution of the measurement will be dependent on the range and data type of the measurement, for example a 1000 deg/sec gyroscopic operating range with 32 bit resolution will have $\frac{1000}{2^{32}} = 2.33 \times 10^{-7}$ deg/sec resolution.

Scale factor is the aspect which translates the output voltage signal to the actual value for angular velocity along its respective axes. In many cases there is a slight non-linear relationship which may be represented as an error based on the full scale range vs. a linear regression fit.

Sample rate determines how quickly the acquisition system will be able to update its measurement. A lower sample rate will result in a lower quality signal. Higher grade inertial sensors will have upwards of 1000 Hz sampling rate.

Bias is the amount of DC offset present in the measurement. Essentially this is phantom acceleration or angular rate as reported by the IMU.

For gyroscopes, it is common to list the bias instability which is how the gyroscope bias changes over time. The Allan variance technique was developed to determine this value. The Allan variance calculation is done by averaging data in equal sized bins of a given sample set, finding the variance of those averages, and then increasing the size of the bins and repeating the variance calculation. An optimal bin size is then found and the data is averaged to have the minimum variance in bias. The variance of the bias measurements of this minimum point is called the Allan variance [54]. Analyzing the slope of this curve gives the angular random walk as well, which is induced by noise in the sensor.

Typical error characteristics for several types of inertial measurement units are given in Table 2-3 [55],

Parameter	Rate Grade	Tactical Grade	Inertial Grade
-----------	------------	----------------	----------------

Angle Random Walk $^{\circ}/\sqrt{hr}$	>0.5	0.5-0.05	<0.001
Bias Drift, $^{\circ}/hr$	10-1000	.1-10	<.01
Range ($^{\circ}/sec$)	50-1000	>500	>400

Table 2-3 Comparison of Different IMUs

2.2.6 Error Propagation

A simplified examination of how the error propagates through the navigation equations, similar to Sukkarieh's [31] perturbation model, we can observe how the integration error term propagates to the overall navigation solution. This type of integration and transformation error tends to accumulate quickly because integration of both accelerations and angular rates are coupled as shown below.

To find the error in the overall solution, and to quantify how sensitive the solution is to these errors, the error associated with the accelerometers and gyroscopes is given by the following simplified angular rate equations and navigation frame accelerations from 2-15 and 2-9, respectively.

	$\dot{\Theta} = \mathbf{R}^*(\Theta) \cdot (\omega_B + \epsilon_{\omega}),$	2-20
--	---	------

where ϵ_{ω} is a generic error term associated with each gyroscope sensing direction.

Similarly, the acceleration measurements can be given by Equation 2-21,

	$\mathbf{a}_B^* = \mathbf{a}_B + \epsilon.$	2-21
--	---	------

Here, \mathbf{a}_B^* is the measured body acceleration vector for the x, y and z directions, \mathbf{a}_B is the actual acceleration as experienced by the host vehicle and ϵ is a generic error vector associated with any given measurement and includes terms such as bias, scale factor, misalignment et cetera or noise.

To find the change in attitude over a given time interval, integrating 2-20 shows,

	$\boldsymbol{\Theta} = \mathbf{R}^*(\boldsymbol{\Theta}) \cdot \boldsymbol{\omega}_B \cdot \delta t + \mathbf{R}^*(\boldsymbol{\Theta}) \cdot \boldsymbol{\epsilon}_\omega \cdot \delta t.$	2-22
--	---	------

And integrating 2-21 yields,

	$\mathbf{v}_B = \mathbf{a}_B \cdot t + \boldsymbol{\epsilon} \cdot t,$ $\mathbf{p}_B = \frac{1}{2} \cdot \mathbf{a}_B \cdot t^2 + \mathbf{v}_B \cdot t + \boldsymbol{\epsilon} \cdot t^2,$	2-23
--	--	------

Where \mathbf{v}_B , \mathbf{p}_B are the position and velocity in the {B} frame.

However, recall that the velocity and position in {N} are functions of not only the acceleration but of the body attitude as well, i.e.

	$\mathbf{V}_N = {}^N\mathbf{R}(\boldsymbol{\Theta}) \cdot \mathbf{v}_B,$ $\mathbf{P}_N = {}^N\mathbf{R}(\boldsymbol{\Theta}) \cdot \mathbf{p}_B,$	2-24
--	---	------

From Equation 2-26 it can be seen that the error in position grows with the square of time.

Combining equations 2-24 and 2-23 and shows that error growth is related to the integration of the accelerations and those from the transformations into the navigation frame.

2.3 GPS Navigation

This section outlines some of the concepts of GPS navigation, including basic principles, error sources, corrections, and modern methods of implementation into a sensor fusion protocol.

As of now there are 31 GPS satellites in orbit, with at least 24 active at all times to ensure a minimum of 6 satellites be visible, or line of sight, at all times [56]. Along with the United States GPS constellations system, there are other similar constellations as developed by Russia, Europe and China. Global Navigation Satellite System (GLONASS) is a Russian version of GPS, Galileo is the European version. Some GPS receivers are capable of tracking satellites from multiple constellations to improve the position estimate.

GPS operates on radio navigation to broadcast information that allows a receiver to parse and use that information to calculate the receiver's position. The data sent from the satellite is known as the ephemerides, and consist of the space vehicle number, time, orbital position, and correction terms for estimated errors due to, e.g. the procession of the earth [5]. The carrier frequencies are separated as $L1 = 1.575$ GHz, and $L2 = 1.2276$ GHz, for civilian and military access, respectively.

Before the year 2000, only a single band was available for civilian access and this was also corrupted by noise, known as selective availability, to limit the accuracy of GPS to a 100m radius. However, because this error was artificially manufactured, the error was the same for all near-by receivers which could then be determined and corrected for, which was one of the driving factors in the development of differential GPS.

Accordingly, differential GPS is the ability to use a well-known position of a stationary receiver, and broadcast the measured error term associated with each satellite. A GPS receiver that has a subscription to differential GPS may experience accuracies down to sub-meter, even centimeter range [35]. The subscription includes access to differential GPS stations, which have very precise information regarding its position and can estimate the pseudorange errors to each satellite. This deterministic error is then broadcast and local receivers in the area are thought to contain the same error. Although the restricted access was lifted in 2000, differential is still used to compensate for other naturally occurring errors in the GPS signals, such as delays caused by the ionosphere.

2.3.1 GPS Principles

GPS works on radio communications, high precision timing, and decades of improvements to existing technologies. The first basic principle is radio navigation, which uses triangulation and the time of flight of the radio signal to determine the range of the receiver to each satellite. The user's position may be found through knowledge of the positions of each satellite and the users distance to each satellite. In theory, a minimum of 3 satellites is required for 3 dimensional positioning using the intersection of three spheres.

However, GPS receiver clocks do not have the precision needed to be synchronized with the satellite clocks, so a fourth satellite (all equipped with highly accurate, corrected, atomic clocks) is used to estimate the receiver clock error. This is done as part of the solution in solving for the position [2].

In order for GPS to operate, three primary segments are required: a control station, the space segment, and the receiver or end user as shown in Figure 2-4 [5]. The control segment is concerned with tracking all of the satellites and generating what is known as the almanac. The almanac contains all ephemerides information on all of the GPS satellites. The space segment is a satellite constellation which broadcasts the almanac data as well as their own position or ephemeris information. The receiver segment is the end user, which will use the satellite information to ascertain its own position.

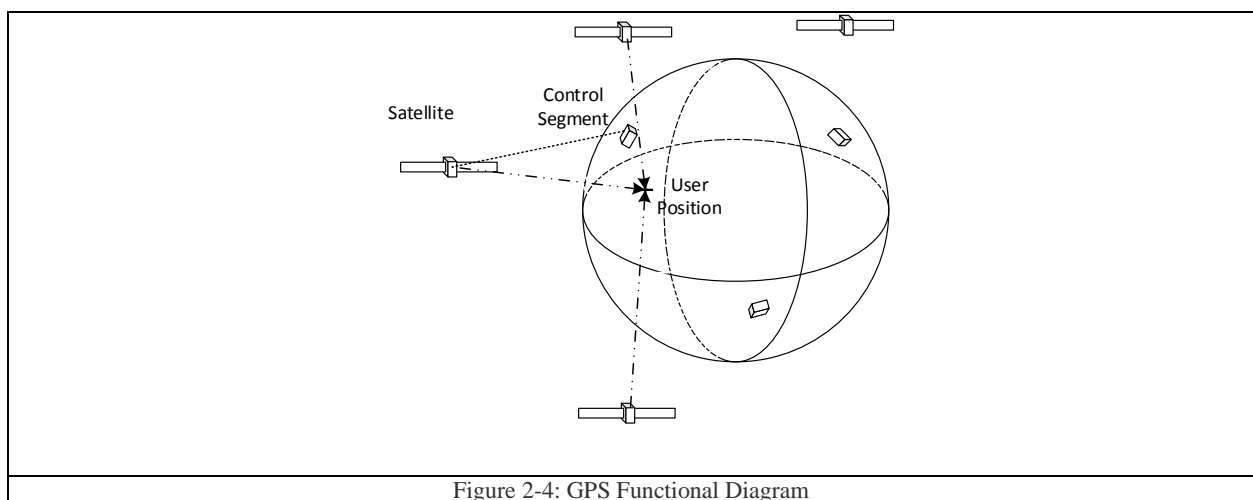


Figure 2-4: GPS Functional Diagram

Figure 2-4: GPS Functional Diagram shows the different segment associated with GPS operation, the control stations which track each satellite and send the satellite its estimated position, the space segment (satellites), and finally the end user [5].

2.3.2 GPS Corrections and Implementation

Time is one of the most critical aspects of accurate GPS positioning; therefore, each satellite must have very accurate timing capabilities. Even though GPS satellites have high precision atomic clocks, satellite timing errors could still affect accuracy of tens of meters if not compensated for by the control segment. In fact, this is part of a satellite ephemerides message, which is modeled as a second order time dependent polynomial [5]. Just as a satellite can have an

error in its clock source, it is much more prominent in inexpensive GPS receivers which usually operate on quartz crystal oscillators that do not have the type of precision for accurate modeling.

Since the error in the receiver clock is the same compared to all of the satellite clock signals, one can see that this unknown receiver bias can be calculated based on a fourth satellite's information in addition to the three required for the position based on the three-dimensional calculation. Most receivers will do this automatically, without the need for the user to do this computation.

However, depending on the level of hardware being used, one may get very low level and include clock offsets and error into the total navigation model, which includes the IMU navigation, in a tightly coupled navigation configuration [2], [25], [57].

There are two general methods of GPS/IMU integration, tightly coupled and loosely coupled integration, which deals with the way the filter is structured. Generally speaking, a loosely coupled model will have a position and velocity estimate from the GPS receiver and uses this as the vehicle states to model the error dynamics. Tightly coupled systems will augment parameters of the GPS, such as ephemerides, error sources, and integer ambiguities directly into the Kalman filter as vehicle states but increases the order of the system significantly [2] [58] [59]. There are many things to think about when implementing GPS and IMU sensors, such as dimensions, necessity, and simplifications which depends on the required accuracy of the application.

2.3.3 GPS Error Sources

There are also other sources of error which include incorrect ephemeris data, multipath and measurement noise on the receiver. One method of eliminating some of these errors is through the use of differential GPS. Often times, the assumed position of the satellite may not be accurate, and each satellite is required to estimate its own position in between updates from the control segment. This leads to a biased estimate if the satellite is estimating an incorrect position. Sending the wrong pseudorange information will then affect the knowledge of the receiver. Other error includes multipath, which involves receiving reflections of the original satellite signal off of buildings or trees. The ionosphere delays the signal based on the total electron content, which varies throughout the day when the sun is emitting solar radiation, for example.

Clock error is demonstrated in Figure 2-5, as that effects the pseudorange accuracy directly. A tabulated list of error values and characteristics found in Ref. [42] are shown in Table 2-4.

Error	Typical Error Value (1σ m)	Type
Receiver Clock	1.5	Random
Ephemerides	4	Bias
Ionosphere + Troposphere	2-30+2	Bias
Multipath	2-5+	Multipath
Noise	.5	Random
Resolution	1.5	Random

Table 2-4 Error Sources and Relative Contributions [5]

Another source of error is caused by dilution of precision, which is caused by error in the pseudorange error from each satellite. Figure 2-5 illustrates the bounds of positional error for each satellite with the shaded region as the potential position of the receiver. The optimal configuration for 2D navigation is to maximize the area between all satellites and receivers, and for 3D it is a maximized volume. Geometric dilution of precision and estimated positional error as calculated by the receivers is used in the construction of the Kalman filter model.

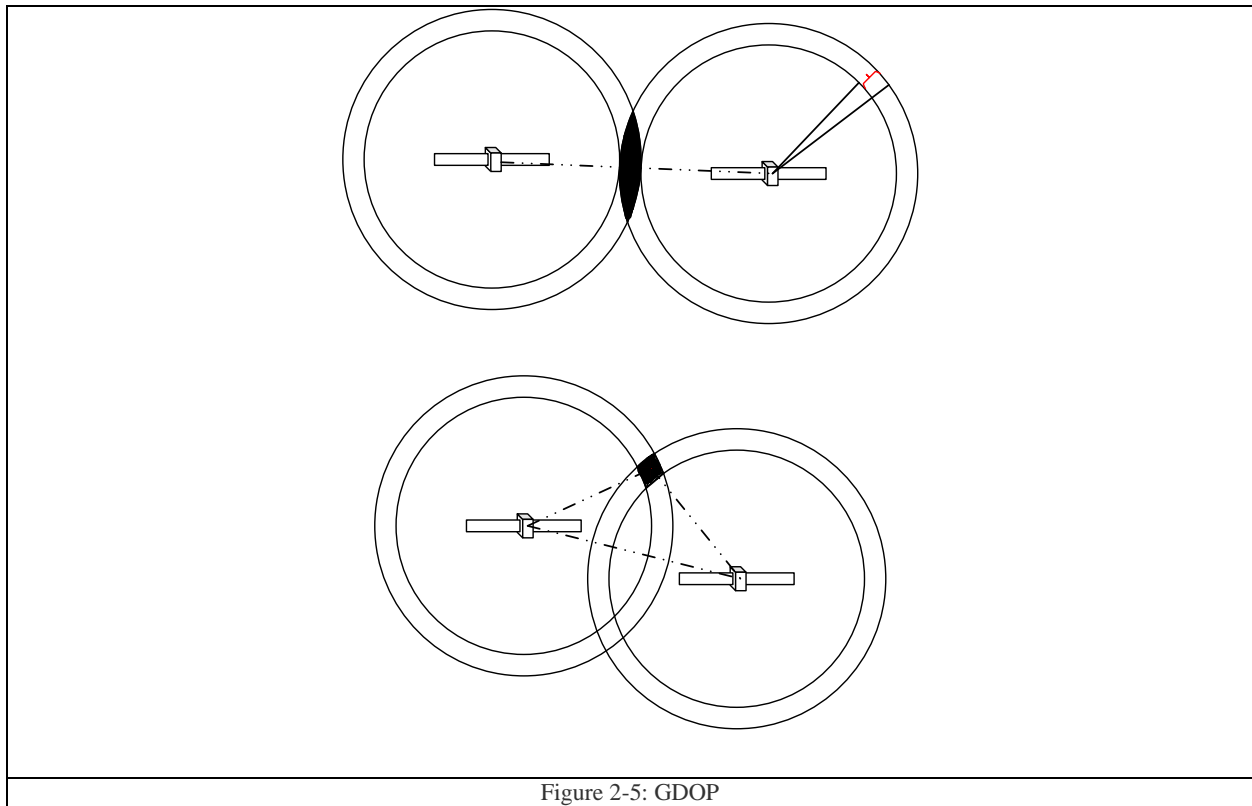


Figure 2-5: GDOP

Figure 1-1 Shows dilution of precision based on two satellites performing triangulation in a place. Each ring circling the satellite corresponds to the amount of random error for each pseudorange. The end effect is dependent on the position of the user, and how minimal the area of the shaded region is. It turns out that in order to minimize the GDOP error, one should maximize the area between satellites and the receiver as shown above. In three dimensions, this corresponds to maximizing the volume to minimize the error.

2.4 Conclusion

Inertial and GPS navigation are very large topics which contain a lot of literature which exceeds the scope of this work. This work will focus on the application of said technologies in a loosely coupled configuration based on the equations presented. The reader is referred to [2] and [5] for a thorough discussion on some of the topics briefly mentioned in this text. Coordinate systems and transformations were discussed such that fusion of data from different coordinate systems may be fused in the subsequent chapters.

Chapter 3: The Kalman Filter

3.1 Introduction

This chapter presents Kalman filtering and the application to navigation. A brief discussion on random variables is given to provide context of the assumption of which the Kalman filter was originally developed. The linear Kalman filter (KF) derivation is shown, and from there, the equations for the extended Kalman filter (EKF) are also developed. Modifications such as the unscented KF (UKF), adaptive KF (AKF), the information filter, and the constrained KF are all discussed, as they have become valuable additions to the original filter framework.

A Kalman filter is a linear quadratic state estimator given a dynamic state space model, a group of measurements, and knowledge of statistics surrounding the model and its measurements [60]. The Kalman filter was originally designed to estimate the state of a system with stochastic inputs and noisy measurements [61] in the early 1960s which stemmed from the work of Norbert Wiener [62] but was tailored to the state space framework used in many controls applications [63]. The formulation considers the second order statistics of both the process and measurement noise of which probability distribution is known [61]. An optimal, closed form solution for the estimation error and minimum covariance was developed using the knowledge of the probability distributions, which was implementable in the state space framework used for control.

Figure 3-1 shows the basic relationship between a dynamic system, e.g. a vehicle, with measured outputs and known inputs. The output of the Kalman filter is an estimated state, which minimizes the estimation error covariance.

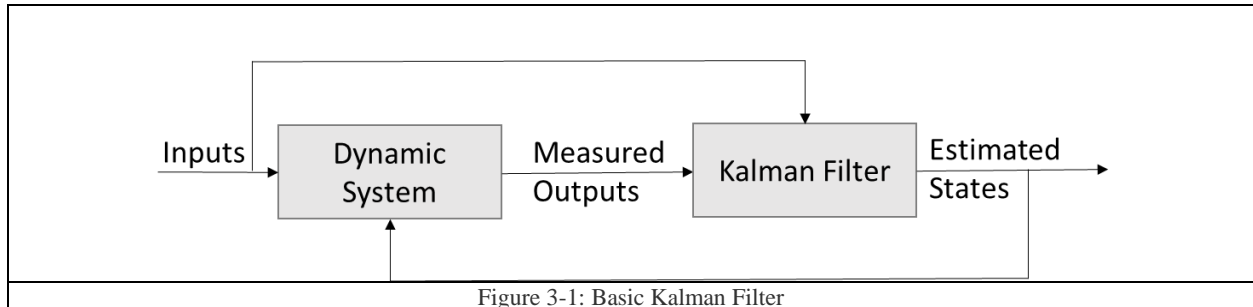


Figure 3-1 illustrates that there is a truth model which has inputs and outputs that are fed into the Kalman filter to output the estimated states.

One of the limiting assumptions in the derivation of the original KF was that of linearity, so the extended Kalman filter was developed to deal with nonlinear systems through a first order approximation of the governing nonlinear functions [60]. Since nonlinear systems are typical in a controls environment, such as polar to Cartesian transformations, it is necessary to extend the framework of the linear KF to nonlinear systems. This is one of the more common uses of filter used today, and it was used almost immediately after it was developed in high risk applications such as the 1969 Apollo 11 mission [37].

However, the EKF is also limited in that the first order linearization compromises the optimality of the error covariance and thus the accuracy of the state estimate [60]. Higher order extended Kalman filters can reduce the truncation error and propagate higher order statistics by means of using more terms in the Taylor series expansion; however, it is at the cost of increased computational complexity. More recently, nonlinear Kalman filtering has found new form, i.e. Unscented Kalman filtering (UKF), which relies on an unscented transformation of the statistics to propagate them to what would be an equivalent third order Taylor series approximation in the EKF chassis [64], without the need for linearization or function approximations.

Adaptive Kalman filtering (AKF) methods have been proposed to take some of the guesswork out of modeling the stochastic variables in the Kalman filter, and in a real-time manner estimate the statistical characteristics of the measured signals and update the governing equations accordingly. The distinguishing bodies of AKF are those that estimate measurement noise variance, and those that estimate process noise variance, and thus adapting to time-varying statistics, or non-stationary data. Hide et. al [16] evaluated adaptive techniques, namely the multiple model adaptive estimator (MMAE) for low cost GPS/INS integration and showed that adaptive filters outperformed . Much of the theory of the adaptive methods can be found in [65], [29], but a couple general methods are discussed later in the chapter.

The purpose of the Kalman filter is to estimate the state of a dynamic system and is often referred to as an observer model or state estimator. It requires a model of the dynamic system of interest, however, this model is usually only an estimated model of the real world dynamics. The general assumption in a Kalman filter is that there is some dynamic system which is measured by sensors, and a known control input is applied to the dynamic system. With the inputs, outputs, and an estimate of the system dynamics model, one can generate an estimate of the state variables and thus provide estimated full state feedback for the controller. For this research, the desired estimate is that of position, velocity, and body attitude so that the computer may apply the appropriate controls to go from one place to another.

3.2 Noise and Disturbances

As mentioned previously, Kalman filters are linear quadratic estimators under the assumption of Gaussian white process and measurement noise, and yields the optimal estimation error covariance based on this criteria. However, rarely is it seen that noise is plainly white. Further yet, the covariance can be proven to be the optimal solution given uncorrelated random data in time and amongst measurement axis.

The discussion on the formulation begins with an overview of the stochastic terms which appear in the derivation of the Kalman filter.

3.2.1 Process Noise vs. Measurement Noise

To answer the question on what process and measurement noise are, the dynamic system block from Figure 3-1 is expanded in Figure 3-2 showing where the process and measurement noise are injected precisely.

The general model considered is one that takes on the following form in continuous time.

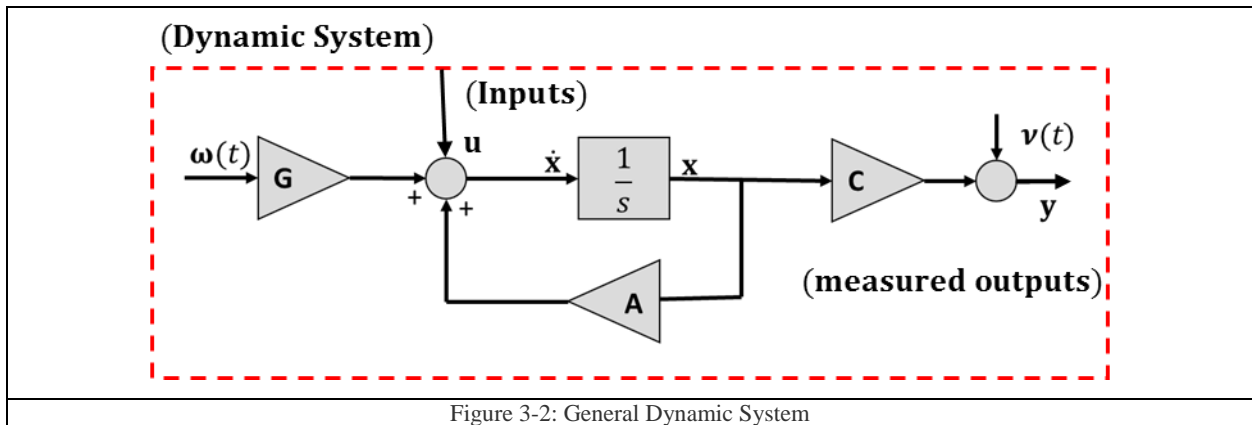


Figure 3-2: General Dynamic System

Figure 3-2 shows the general flow of a dynamical system under the presence of process noise and measurement noise.

Figure 3-2 can be written mathematically as,

	$\dot{\mathbf{x}}(t) = \mathbf{A} \cdot \mathbf{x}(t) + \mathbf{G} \cdot \boldsymbol{\omega}(t)$	3-1
--	--	-----

where \mathbf{x} is a $n \times 1$ dynamic state vector, \mathbf{A} is the $n \times n$ dynamic coefficient matrix, \mathbf{G} is the process noise distribution matrix, and $\boldsymbol{\omega}(t) = \mathcal{N}(0, \boldsymbol{\sigma}_{\omega}^2)$ is process noise. Process noise is in general, caused by disturbances through the environment and is *assumed* to have a Gaussian distribution. An environmental example could be that of a plane flying through gusts of wind, the wind applies a force but is perhaps not measurable. The implementation of the Kalman filter requires a baseline assumption of what the distribution of the wind is, and not necessarily the input itself.

The right hand side of Figure 3-2 above yields the measured *output* of the system in Equation 3-2,

	$\mathbf{y}(t) = \mathbf{C} \cdot \mathbf{x}(t) + \mathbf{v}(t),$	3-2
--	---	-----

where $\mathbf{y}(t)$ is the $p \times 1$ measurement vector, \mathbf{C} is the $p \times n$ measurement matrix and $\mathbf{v} = \mathcal{N}(0, \sigma_v^2)$ is the $p \times 1$ measurement noise vector. Measurement noise is brought into the observation model through sensor dynamics and error. Again, one of the major assumptions is that both the process noise $\omega(t)$ and the measurement noise $\mathbf{v}(t)$ are Gaussian random variables (RV).

3.2.2 Gaussian White Noise

White noise is characterized by an infinite power spectral density, meaning equal power over all frequencies, that follows a normal Gaussian distribution with zero mean and is independent of all other samples in the time series.

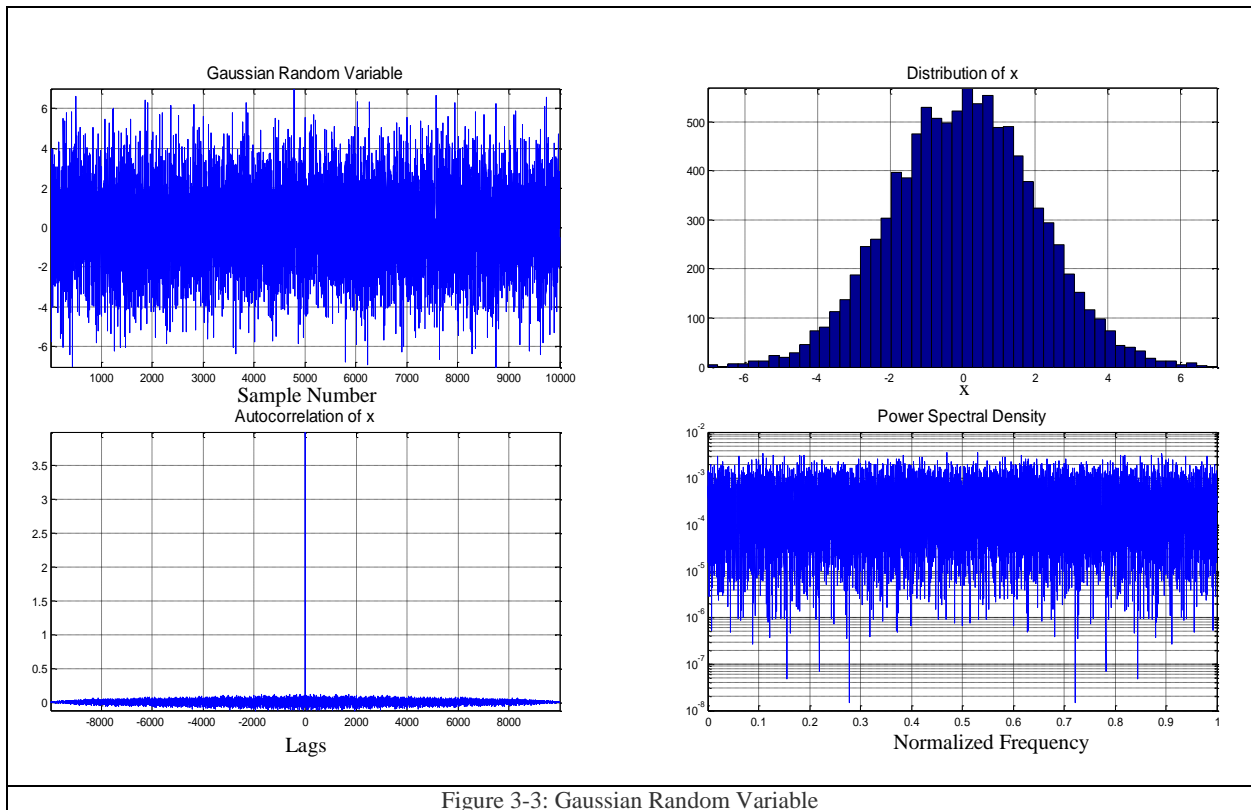


Figure 3-3: Gaussian Random Variable

Figure 3-3 shows an example of a Gaussian random variable. The top left figure is the signal itself, $x = \mathcal{N}(0, \sigma^2)$ which defines x as a random variable with zero mean and σ^2 variance. As one can see, the variable is only perfectly correlated at zero lag from the autocovariance plot, and has an infinite power spectral density.

This type of RV yields the following properties of two separate random variables x and y shown in the equations from 3-3.

	$E\{x \cdot y\} = E\{x\} \cdot E\{y\}$ $p(x, y) = p(x) \cdot p(y)$ $E\{x \cdot y\} = 0$	3-3
--	---	-----

Where x, y are two random variables, $E\{x \cdot y\} = \int_{-\infty}^{\infty} \int_{-\infty}^{\infty} x \cdot y \cdot p(x)p(y) dx dy$ is the expected value, and $p(x)$ is the probability density function. The equations in 3-3 states that the expected value, of two random variables are uncorrelated, independent, and orthogonal. These properties are used in Section 3.3 when developing the Kalman filter.

Contrasting Gaussian white noise, there are other noise sources which may not necessarily have the same ideal properties as above. Among these other types of noise are exponentially correlated noise, harmonically coupled noise, random walks, random constant (bias), band limited noise, and many more. In real world situations, it is likely to encounter non-white noise which will also degrade the optimality of the Kalman filter solution.

Shaping filters (SF) are one method of handling non-white noise, which can be augmented into the Kalman filter itself [37]. SF are used when a non-white noise distribution is known, and assume a white noise input to the SF with a colored noise output which is then augmented to the rest of the system. Applying this technique allows the baseline stochastic input to be white, with the output of the SF, i.e. colored noise, acting as the input to the remaining filter.

3.3 General Kalman Filter Model

A derivation for the linear, discrete time homogenous system will be presented that follows the derivation from Zarchan [66]. The equations of the Kalman filter start with the following discrete time version of the dynamic system of equations given in 3-1 and 3-2 which can be mathematically derived from Figure 3-4 [37].

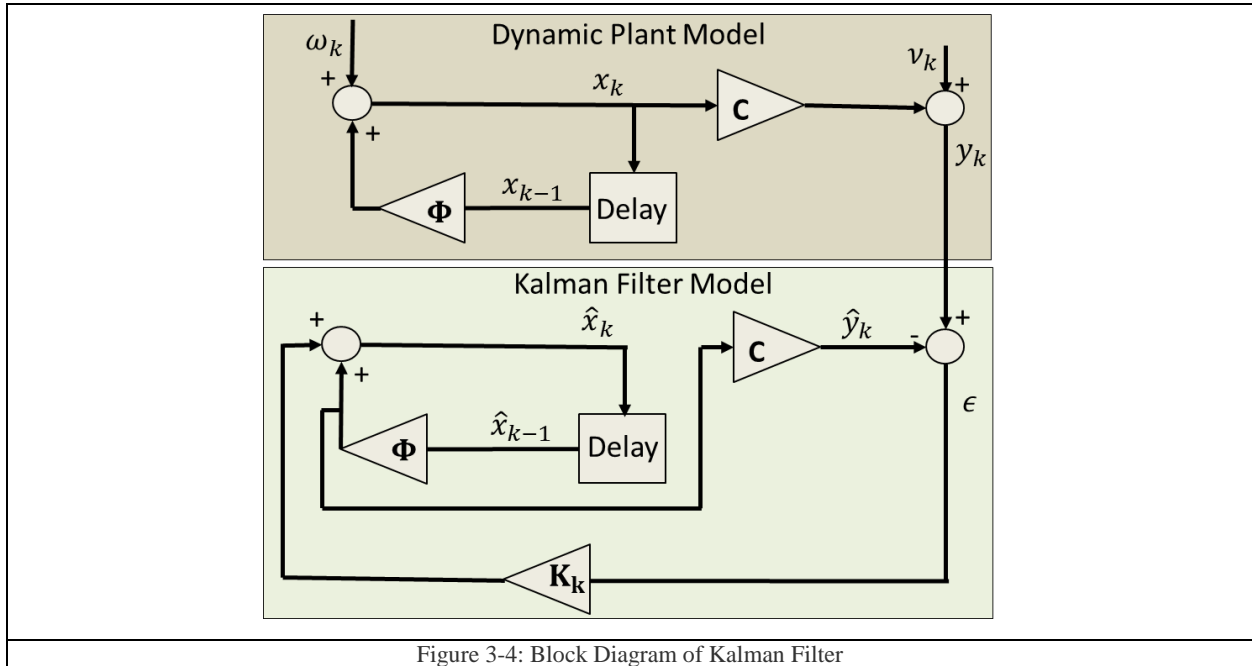


Figure 3-4: Block Diagram of Kalman Filter

Figure 3-4 shows a linear, homogenous discrete time Kalman filter model and truth model which are used in the following derivation. This is the same as an expanded version of Figure 3-1 except with no inputs, no state feedback, and is in discrete time.

The discrete time equations regarding the linear, homogenous KF as shown above are the state vector,

	$\mathbf{x}_k = \Phi \cdot \mathbf{x}_{k-1} + \omega_k,$	3-4
--	--	-----

and the output,

	$\mathbf{y}_k = \mathbf{C} \cdot \mathbf{x}_k + \mathbf{v}_k,$	3-5
--	--	-----

where $\mathbf{x}_k \in \mathbf{R}^n$ is the true state vector of the dynamic plant at time k, $\Phi = e^{At}$ is the $n \times n$ state transition matrix, ω_k is a discrete random process termed process noise, \mathbf{v}_k is measurement noise, and $\mathbf{y}_k \in \mathbf{R}^p$ is the measured output. The estimated state and output is given as the estimated state vector,

	$\hat{\mathbf{x}}_k = \Phi \hat{\mathbf{x}}_{k-1} + \mathbf{K}\epsilon,$	3-6
--	--	-----

the estimated output,

	$\hat{\mathbf{y}}_k = \mathbf{C}\Phi \hat{\mathbf{x}}_{k-1},$	3-7
--	---	-----

Where $\hat{\mathbf{x}}_k$ is the $n \times 1$ estimated state vector at time k, $\mathbf{K} \in \mathbf{R}^{n \times p}$ is the error gain, or Kalman gain, $\hat{\mathbf{y}}_k$ is the estimated output at time k, and ϵ is called the output error term which is defined in Equation 3-8 as,

	$\epsilon = \mathbf{y}_k - \hat{\mathbf{y}}_k.$	3-8
--	---	-----

The estimation error at time k is defined as,

	$\tilde{\mathbf{x}}_k = \mathbf{x}_k - \hat{\mathbf{x}}_k,$	3-9
--	---	-----

Substituting Equations 3-4 and 3-6 into Equation 3-9 gives,

	$\tilde{\mathbf{x}}_k = \Phi \mathbf{x}_{k-1} + \omega_k - (\Phi \hat{\mathbf{x}}_{k-1} + \mathbf{K}\epsilon),$	3-10
--	---	------

where $\tilde{\mathbf{x}}_k$ is the estimation error at time k. We can then substitute $\hat{\mathbf{y}}_k$ from Equation 3-6 and \mathbf{y}_k from 3-5 in ϵ to obtain the expression in Equation 3-11 for the estimation error.

	$\tilde{\mathbf{x}}_k = (\mathbf{I} - \mathbf{K}\mathbf{C})\Phi \tilde{\mathbf{x}}_{k-1} + (\mathbf{I} - \mathbf{K}\mathbf{C})\omega_k - \mathbf{K}\mathbf{v}_k$	3-11
--	--	------

By definition, the estimation variance is defined as,

	$\mathbf{P}_k = E(\tilde{\mathbf{x}}_k \tilde{\mathbf{x}}_k^T).$	3-12
--	--	------

Using the following identities based on the assumption of Gaussian noise and uncorrelated measurement and process noise,

	$E(\mathbf{v}_k \mathbf{v}_k^T) = \mathbf{R}_k$ $E(\boldsymbol{\omega}_k \boldsymbol{\omega}_k^T) = \mathbf{Q}_k$ $E(\boldsymbol{\omega}_k \mathbf{v}_k^T) = E(\tilde{\mathbf{x}}_k \mathbf{v}_k^T) = E(\tilde{\mathbf{x}}_k \boldsymbol{\omega}_k^T) = 0.$	3-13
--	---	------

The second equation of 3-13 is representative of the discrete time process noise matrix, which has a continuous time analog \mathbf{Q} . In typical applications, process noise is considered a continuous time random variable and must be discretized. Equation 3-14 is an expression to find the discrete time process noise matrix [66],

	$\mathbf{Q}_k = \int_0^{\delta t} \boldsymbol{\Phi}(\tau) \mathbf{Q} \boldsymbol{\Phi}^T(\tau) d\tau,$	3-14
--	--	------

where δt is the sampling time.

After squaring equation 3-11, taking the expectation and substituting equation 3-13 into the term for \mathbf{P}_k , the covariance of the estimation error will be,

	$\mathbf{P}_k = (\mathbf{I} - \mathbf{K}\mathbf{C})\mathbf{M}_k(\mathbf{I} - \mathbf{K}\mathbf{C})^T + \mathbf{K}\mathbf{R}_k\mathbf{K}^T,$	3-15
--	---	------

where $\mathbf{M}_k = \boldsymbol{\Phi}\mathbf{P}_{k-1}\boldsymbol{\Phi}^T + \mathbf{Q}_k$ is often termed the priori covariance. The next step is to find \mathbf{K} which is found through solving,

	$\frac{\partial [tr(\mathbf{P}_k)]}{\partial \mathbf{K}} = \mathbf{0},$	3-16
--	---	------

for \mathbf{K} , where $tr(\mathbf{P}_k)$ is the trace of \mathbf{P}_k .

Solving Equation 3-15 yields,

	$\mathbf{K} = \mathbf{M}_k \mathbf{C} (\mathbf{C} \mathbf{M}_k \mathbf{C}^T + \mathbf{R}_k)^{-1},$	3-17
--	--	------

and finally the updated covariance is found using the new gain from Equation 3-17,

	$\mathbf{P}_k = (\mathbf{I} - \mathbf{K} \mathbf{C}) \mathbf{M}_k.$	3-18
--	---	------

The algorithm to use a linear, homogenous Kalman filter is given in Table 3-1, in order to start estimation, initial conditions of the state estimate and the assumed distribution must be provided, hence $\hat{\mathbf{x}}(0) = \hat{\mathbf{x}}_0, \mathbf{P}(0) = \mathbf{P}_0$.

$\hat{\mathbf{x}}(0) = \hat{\mathbf{x}}_0, \mathbf{P}(0) = \mathbf{P}_0$	Initialize state estimate and covariance
$\hat{\mathbf{x}}_k^- = \Phi \hat{\mathbf{x}}_{k-1}^+$	Predict the next state estimate (A priori Estimate)
$\mathbf{M}_k = \Phi \mathbf{P}_{k-1} \Phi^T + \mathbf{Q}_{k-1}$	Predict the covariance
$\mathbf{K}_k = \mathbf{M}_k \mathbf{C} (\mathbf{C} \mathbf{M}_k \mathbf{C}^T + \mathbf{R}_k)^{-1}$	Solve for the 'Kalman Gain'
$\mathbf{P}_k = (\mathbf{I} - \mathbf{K}_k \mathbf{C}) \mathbf{M}_k$	Update the covariance based on Kalman gain
$\hat{\mathbf{x}}_k^+ = \hat{\mathbf{x}}_k^- + \mathbf{K}_k (\mathbf{y}_k - \mathbf{C} \hat{\mathbf{x}}_k^-)$	Find the new state estimate given measurement \mathbf{y}_k (Posteriori Estimate)

Table 3-1 Linear Kalman Filter Algorithm

A term that will be used later is called the innovation error, it is the actual measurement minus the predicted measurement which is also given in Equation 3-8,

	$\mathbf{e}_k = \mathbf{y}_k - \mathbf{C} \Phi \hat{\mathbf{x}}_{k-1}.$	3-19
--	---	------

A metric of filter performance can be found using what's known as the innovation covariance which is defined as [67],

	$\mathbf{R}_e = \mathbf{C} \mathbf{M}_k \mathbf{C}^T + \mathbf{R}_k,$	3-20
--	---	------

and comparing it to the actual innovation error covariance which can be found using windowed autocorrelations. How close these two values are represents how well the assumed statistical properties are to the actual ones which can be found while the filter is running [67]. This property is exploited for adaptive estimators, namely the innovation adaptive estimator which is discussed in further detail in section 3.6.3

The extended Kalman filter as presented in [66] is shown in the following section.

3.4 Extended Kalman Filter

One of the limitations to the Kalman filter is that the system model is assumed to be linear, so the extended Kalman filter was developed to handle the case of nonlinear dynamics. In spirit, the EKF uses a first order linearization of the nonlinear system to propagate the statistics forward, whereas the dynamic equations of motion may be integrated. However, this truncates the estimate of the covariance and optimal gain to first order accuracy. The contrast from the linear Kalman filter is shown below.

Starting with a homogenous nonlinear system with stochastic inputs,

	$\dot{\mathbf{x}} = f(\mathbf{x}, \boldsymbol{\omega}),$ $\mathbf{y}_k = c(\mathbf{x}_k, \mathbf{v}_k),$	3-21
--	--	------

and defining the state estimate as the same known function,

	$\hat{\mathbf{x}}_k = f(\hat{\mathbf{x}}_{k-1}^+),$ $\mathbf{y}_k = c(\hat{\mathbf{x}}_k^-),$	3-22
--	---	------

Where the definitions remain the same from the previous section, except now f and c are nonlinear functions dependent on the state of the system.

Equations 3-23 and 3-24 show the first order linearized dynamic system of equations (Jacobians) as,

	$\mathbf{F}_k \approx \left. \frac{\partial f(\mathbf{x})}{\partial \mathbf{x}} \right _{\mathbf{x}=\hat{\mathbf{x}}_k^-}$	3-23
--	--	------

and,

	$\mathbf{C}_k \approx \left. \frac{\partial c(\mathbf{x})}{\partial \mathbf{x}} \right _{\mathbf{x}=\hat{\mathbf{x}}_k^-}$	3-24
--	--	------

This first order approximation can be extended to higher order algorithms, such as second or third order approximations. However, the evaluation of the Hessian is required to do so. Assuming a first order approximation for the Taylor series expansion of 3-23 and 3-24, results in

	$\Phi_k = e^{\mathbf{F}_k \delta t} \approx \mathbf{I} + \mathbf{F}_k \delta t$	3-25
--	---	------

The algorithm for the EKF is provided in Table 3-2.

$\hat{\mathbf{x}}(0) = \hat{\mathbf{x}}_0, \mathbf{P}(0) = \mathbf{P}_0$	Initialize state estimate and covariance
$\hat{\mathbf{x}}_k = f(\hat{\mathbf{x}}_{k-1}^+)$	Predict the next state estimate
$\hat{\mathbf{x}}_k^- = \hat{\mathbf{x}}_{k-1}^+ + \hat{\mathbf{x}}_k \delta t$	Numerically Integrate
$\mathbf{F}_k = \left. \frac{\partial f(\mathbf{x})}{\partial \mathbf{x}} \right _{\mathbf{x}=\hat{\mathbf{x}}_k^-}$ $\mathbf{C}_k = \left. \frac{\partial c(\mathbf{x})}{\partial \mathbf{x}} \right _{\mathbf{x}=\hat{\mathbf{x}}_k^-}$	Find the first order approximations linearizing about the priori state estimate
$\mathbf{M}_k = \Phi_k \mathbf{P}_{k-1} \Phi_k^T + \mathbf{Q}_{k-1}$	Predict the covariance
$\mathbf{K}_k = \mathbf{M}_k \mathbf{C}_k (\mathbf{C}_k \mathbf{M}_k \mathbf{C}_k^T + \mathbf{R}_k)^{-1}$	Solve for the ‘Kalman gain’
$\mathbf{P}_k = (\mathbf{I} - \mathbf{K}_k \mathbf{C}_k) \mathbf{M}_k$	Update the covariance based on Kalman gain
$\mathbf{x}_k^+ = \hat{\mathbf{x}}_k^- + \mathbf{K}_k (\mathbf{y}_k - c(\hat{\mathbf{x}}_k^-))$	Find the new state estimate given measurement \mathbf{y}_k

Table 3-2 Extended Kalman Filter Algorithm

The notation here stems from a hybrid continuous-discrete time model, where the a priori estimate is based on evaluating a continuous function at the estimate found at the previous time step and then numerically integrating for a discrete time state estimate. This algorithm here represents an implementable algorithm for discrete time computation.

3.5 Constrained Kalman Filter Methods

State constraints are another useful tool when implementing a Kalman filter if knowledge of physical or mathematical limitations exist. The methods for the constrained linear and nonlinear Kalman filter are described in [68], such as model reduction, perfect measurements, estimate projection, probability density function truncation, gain projection, and soft constraints. The benefit in a constrained Kalman filter is that if one has prior knowledge of the bounds of the state, then a constraint may be applied to keep the estimate within those bounds. Stochastic constraints may also be used when the precise constraint is unknown or there is limited knowledge of the constraint equations, allowing slack in the constraint and thus creating a soft constraint architecture. Constrained Kalman filters have applications in spacecraft attitude estimation, vision aided inertial navigation, target tracking, robotics, and GPS/INS navigation [68], [69], [70].

For linear systems, state equality and inequality constraints will take the following form [68],

	$\mathbf{D}\mathbf{x} = \mathbf{d},$ $\mathbf{D}\mathbf{x} \leq \mathbf{d}.$	3-26
--	--	------

Where \mathbf{D} is a $l \times n$ matrix consisting of l linear constraint equations and \mathbf{d} is the constraint boundary.

For the platform used in this work in regards to ground vehicle navigation, it is particularly useful to use the rigid, non-holonomic constraints of the ground vehicle, which assume the vehicle cannot move from side to side nor jump up off of the ground. However, for a vehicle on soft terrain such as dirt, or a vehicle that may climb hills, a rigid constraint that may be violated

due to side slip or hill climbing. This can be handled by a stochastic constraint which models the constraints as perfect measurements with added measurement noise [33], [34].

In this work, utilization of the perfect measurement method as in [31] will aid in the navigation solution by observing the nonholonomic limitations of the vehicle.

The methods outlined in the survey [33] are the perfect measurement method, which augment the measurement matrix and assume zero measurement noise as shown in Equation 3-27,

	$\begin{bmatrix} \mathbf{y} \\ \mathbf{d} \end{bmatrix} = \begin{bmatrix} \mathbf{C} \\ \mathbf{D} \end{bmatrix} \mathbf{x} + \begin{bmatrix} \mathbf{v} \\ \mathbf{0} \end{bmatrix}.$	3-27
--	--	------

In this method, the constraint equation appears as an augmented term in the measurement matrix.

If the constraint is rigid, then the noise term is deemed zero, which yields the perfect measurement constraint. If, however, there is potential for violation of this constraint, one can assign an amount of uncertainty to this term and assign a measurement noise term to the measurement covariance matrix [26], [31]. Contrasting a rigid equality constraint in the architecture of the perfect measurement method, a soft constraint is implemented by considering a RV as part of the constraint relationship given in Equation 3-28.

	$\mathbf{D}\mathbf{x} = \mathbf{d} + \mathbf{v}_d,$	3-28
--	---	------

where \mathbf{v}_d is a random process which is typically assumed to be Gaussian noise. This fits into the framework of Equation 3-27,

	$\begin{bmatrix} \mathbf{y} \\ \mathbf{d} \end{bmatrix} = \begin{bmatrix} \mathbf{C} \\ \mathbf{D} \end{bmatrix} \mathbf{x} + \begin{bmatrix} \mathbf{v} \\ \mathbf{v}_d \end{bmatrix}.$	3-29
--	--	------

This method is commonly used in work regarding autonomous ground vehicles as it is a convenient way to apply non-holonomic constraints by restricting the motion of the vehicle from moving along the body y axis and z axis. This is also convenient because the soft constraint of having a stochastic term allows for a certain amount of slip in the vehicle motion [34]. The

notion of this is that the vehicle slips within certain bounds, and can be modeled to account for more or less slip according to the driving conditions.

3.6 Other Notable Kalman Filter Methods

3.6.1 Unscented Kalman Filter

Similar to the EKF the Unscented Kalman Filter (UKF) was developed to address the truncation errors as caused by the first order linearization of nonlinear systems through what is known as the unscented transform (UT). The premise is that it is easier to estimate the probability distribution function of a nonlinear function than to estimate the function itself [71]. The UKF can accurately estimate the distribution of the estimate up to second order accuracy. As shown in equations 3-23 and 3-24, the first order approximation in the EKF limits the accuracy for functions whose higher order terms affect the solution to the state estimate.

The context of which the Unscented Kalman Filter is presented in under the assumption that the states undergo a nonlinear transformation from polar to Cartesian coordinates. Due to the nonlinear transformation of which the navigation problem would be an ideal candidate to use the UKF [27], [72].

3.6.2 The Information Filter

The information space is another adaptation to the Kalman filter which uses information space as opposed to the covariance space. The essence of information space is to quantify the information available by using the inverse of the covariance matrix as a means of propagating statistics forward. This essentially means inverting the estimate covariance and transforming the state estimate accordingly, which implies that as covariance gets smaller, the amount of information becomes large. For example, if the variance of a signal estimate is small, then the inverse would be large – meaning ‘a large amount of information.’ This means that a state estimate can start off with zero information, or infinitely large variance [37]. This has been used in several works by Dissayeka in his work with IMU/GPS for ground vehicles such that this method of handling data from multiple sensors reduces the effect of cross correlation between the sensors [34] superior to the EKF or KF.

3.6.3 Adaptive Kalman Filter

One of the main drawbacks of Kalman Filtering is the assumption that the process noise and measurement noise terms are considered constant, and the baseline assumption of the covariance terms may not be true. Adaptive Kalman filtering (AKF) uses algorithms to find the true theoretical covariance terms based on the innovation error and sensor data available in real-time [65]. Multiple Model Adaptive Estimation (MMAE) and Innovation-Based Adaptive Estimation (IAE) have been used in Kalman filtering for GPS/INS navigation [16], [29] to adapt to time changing statistics and to find the true covariance terms of the system. The techniques for these adaptive schemes are shown in Mohammed [29], where the MMAE algorithm is based on several Kalman filter models, each with different covariance matrices, run in parallel. MMAE then converges to the optimal value. Conversely, IAE uses the innovation sequence from equation 3-9 and looks at the autocorrelation function of a windowed set of data. This problem then becomes a tuning problem to find the appropriate window size for the application, and the results may vary significantly based on the window size.

3.6.4 Multi-Rate Data and Cascaded Models

One of the benefits of using a Kalman filter is the fact that data may come into the system at different rates, and depending on what data is available a simple change in observation matrix is done to complete the innovation sequence. For this work, models are switched between different availability of data, i.e. GPS + WSS +IMU data vs. IMU data only, and have the flexibility to change over every time step.

A cascaded model can be implemented such that certain parameters such as sensor error or calibration parameters may be estimated [73], [74]. Essentially, a cascaded Kalman filter may be used to estimate certain state variables in a decentralized framework that can then be fed into the measurement vector in the main Kalman filter estimating the desired state variables.

For this work, a cascaded type approach is used for initial alignment of the host vehicle model, whereas roll and pitch are estimated in a separate, linear Kalman filter is then used as an

augmented measurement to the main filter similar to the work of [51]. This will be discussed in more detail in chapter 5.

This chapter discussed the KF and algorithms needs to construct the Kalman filter and extended Kalman filter as used in chapter four. Other methods and of filtering, and extensions of filtering were discussed, although not implemented in this work.

Chapter 4: Kalman Filter Application

This chapter presents the construction of the Kalman filter using the navigation equations presented in chapter 2 and the measurement models associated with the different sensor configurations, such as GPS outage or a stationary vehicle model. Accordingly, the process and measurement noise covariance matrix design is discussed and designed for each sensor platform.

4.1 Process Model and State Vector Realization

The Kalman filter model developed in this work and used in experiments is based on the navigation frame model as presented by the strapdown equations from Section 2.2.2 and the rate vector equations from Section 2.2.3 . The state vector is given by Equation 4-1,

	$\mathbf{x} = [N \ E \ D \ \dot{N} \ \dot{E} \ \dot{D} \ \theta \ \beta \ \gamma],$	4-1
--	---	-----

Which is the northing, easting and downing position and velocity as well as the body attitude, roll, pitch, and heading angle in the navigation frame. These states are further be categorized into 3D position, velocity, and attitude as,

	$\mathbf{P} = [N \ E \ D]^T,$	4-2
--	-------------------------------	-----

and

	$\mathbf{V} = [\dot{N} \ \dot{E} \ \dot{D}]^T,$	4-3
--	---	-----

and

	$\boldsymbol{\theta} = [\theta \ \beta \ \gamma]^T,$	4-4
--	--	-----

respectively.

The system dynamics model will be designed to have IMU measurements embedded in the framework, constructed in a way such that they appear in the equations as follows,

	$\mathbf{f}_b = [f_x \quad f_y \quad f_z]^T,$	4-5
--	---	-----

and

	$\boldsymbol{\omega}_b = [\omega_x \quad \omega_y \quad \omega_z]^T,$	4-6
--	---	-----

where \mathbf{f}_i is the body frame accelerations and ω_i is the body frame rotation rates for $i = x, y, z$.

The continuous, nonlinear, dynamic system of equations are augmented from equations 2-9 and 2-14,

	$\dot{\mathbf{x}} = f(t, \mathbf{x}) = \begin{bmatrix} \dot{\mathbf{P}} \\ \dot{\mathbf{V}} \\ \dot{\boldsymbol{\Theta}} \end{bmatrix} = \begin{bmatrix} \mathbf{V} \\ {}^N\mathbf{R}(\boldsymbol{\Theta}) \cdot \mathbf{f}_b - (2\boldsymbol{\omega}_{ie}) \times \mathbf{V} + \mathbf{g} \\ \mathbf{R}^*(\boldsymbol{\Theta}) \cdot \boldsymbol{\omega}_b \end{bmatrix} + \boldsymbol{\omega}$	4-7
--	--	-----

Recall $(2\boldsymbol{\omega}_{ie}) \times \mathbf{V}$ is the Coriolis force experienced caused by the rotation of the earth and rotation of the vehicle at speed \mathbf{V} and $\boldsymbol{\omega}$ is some process noise assumed to be present.

The implementable, discrete time equations to find the a priori state estimate, the above function is evaluated and the previous state estimate with accelerations and angular rates from the IMU,

	$\hat{\mathbf{x}}_k^- = f(\hat{\mathbf{x}}_{k-1}^+) = \begin{bmatrix} \hat{\mathbf{V}}_{k-1} \\ {}^N\mathbf{R}(\hat{\boldsymbol{\Theta}}_{k-1}) \cdot \mathbf{f}_{b,k} - (2\boldsymbol{\omega}_{ie}) \times \hat{\mathbf{V}}_{k-1}^+ + \mathbf{g} \\ \mathbf{R}^*(\hat{\boldsymbol{\Theta}}_{k-1}) \cdot \boldsymbol{\omega}_{b,k} \end{bmatrix},$	4-8
--	--	-----

and

	$\hat{\mathbf{x}}_k^- = \hat{\mathbf{x}}_{k-1}^+ + \dot{\hat{\mathbf{x}}}_k^- \times \delta t$	4-9
--	--	-----

Which is the a priori state estimate based on the integration of the accelerometers and gyroscopes.

In order to propagate the statistics as well and solve for the Kalman gains, the state transition matrix is found through finding the Jacobian of f ,

	$\mathbf{F} = \left. \frac{\partial f}{\partial \mathbf{x}} \right _{\hat{\mathbf{x}}_k^-} .$	4-10
--	---	------

In the event that there were no other measurements other than the IMU, it is possible to integrate 4-8 to obtain position, velocity and attitude. This is how inertial navigation could be done if GPS or WSS data became unavailable. It is noted, however, that without velocity or position measurements the solution drifts as a random walk due to the integration of the noisy signal, or worse the integration of bias and other error sources will lead to a much worse drift. This is demonstrated in chapter 6.

4.2 Measurements

Following the development of the process model is the development of the measurement model, which combines the sensor information from both the wheel speed sensors and GPS. The GPS provides position, velocity, and heading when utilizing dual antennas or the vehicle is in motion. The GPS measurement vector is given by the following,

	$\mathbf{y}_{\text{GPS}} = \begin{bmatrix} \mathbf{P} \\ \mathbf{V} \\ \theta \\ \gamma \end{bmatrix} + \mathbf{v}_{\text{GPS}} .$	4-11
--	--	------

Accordingly, the estimated GPS measurements are,

	$\hat{\mathbf{y}}_{\text{GPS}} = \begin{bmatrix} \hat{\mathbf{P}}_k^- \\ \hat{\mathbf{V}}_k^- \\ \hat{\theta}_k^- \\ \hat{\gamma}_k^- \end{bmatrix}$	4-12
--	--	------

Similarly, the WSS data may also be transformed into the state space by,

	$\mathbf{y}_{wss} = \begin{bmatrix} v_{wss} \\ 0 \\ 0 \end{bmatrix} + \mathbf{v}_k$	4-13
--	---	------

which provides an estimated measurement of,

	$\hat{\mathbf{y}}_{wss} = {}^b_n\mathbf{R}(\boldsymbol{\theta}) \cdot \hat{\mathbf{v}}_k^-$	4-14
--	---	------

The following scenarios describing measurement vectors correspond to sensor availability. For example, the measurement vector will change dimension and structure if GPS signal is lost or if a single antenna is unavailable.

The nature of the Kalman filter in this context allows the computer to switch from one measurement model to another for every time step which has different data available.

4.2.1 Full Measurement Vector

In the case that GPS and WSS data are available, the predicted measurement vector will take the following form.

	$\hat{\mathbf{y}}_k = c(\hat{\mathbf{x}}_k^-) = \begin{bmatrix} \hat{x}_{1,k}^- \\ \hat{x}_{2,k}^- \\ \hat{x}_{3,k}^- \\ \hat{x}_{4,k}^- \\ \hat{x}_{5,k}^- \\ \hat{x}_{6,k}^- \\ {}^b_n\mathbf{R}(\hat{x}_{7,8,9,k}^-) \times [\hat{x}_{4,k}^- \quad \hat{x}_{5,k}^- \quad \hat{x}_{6,k}^-]^T \\ \hat{x}_{8,k}^- \\ \hat{x}_{9,k}^- \end{bmatrix}$	4-15
--	---	------

Where $x_{i,k}^-$ is the a priori state variable for $i = 1,2, \dots, 9$ at time k .

Where GPS provides measurements of the northing, easting, and downing position and velocity, dual GPS provides heading γ and roll angle θ . The redundant measurement terms for

${}^b_n\mathbf{R}(\hat{\mathbf{x}}_{7,8,9,k}^-) \times [\hat{\mathbf{x}}_{4,k}^- \quad \hat{\mathbf{x}}_{5,k}^- \quad \hat{\mathbf{x}}_{6,k}^-]^T = \dot{N}, \dot{E}, \dot{D}$ come from the wheel speed sensor signal transformed into the navigation equation.

4.2.2 GPS Outage Vector

In the event of GPS outage, information is lost regarding position and attitude. For this reason, the filter switches to a mode which relies solely on the integration of IMU data and the absolute velocity measurement as provided by the wheel speed sensor.

	$\hat{\mathbf{y}}_k = c(\hat{\mathbf{x}}_k^-) = {}^b_n\mathbf{R}(\hat{\mathbf{x}}_{7,8,9,k}^-) \times [\hat{\mathbf{x}}_{4,k}^- \quad \hat{\mathbf{x}}_{5,k}^- \quad \hat{\mathbf{x}}_{6,k}^-]^T$	4-16
--	---	------

Where the previous expression is generated from 4-14.

In this situation, six out of the nine state variables are not measured, and accordingly not observable. For this reason, during times of GPS outage, the Kalman filter moves to rely heavily on the integration of equation 4-8. Due to the fact that integrating random signals leads to a random walk and time varying variance, one would suspect that the estimation uncertainty would also increase during this time. A section in the results is dedicated to the performance of the Kalman filter and its ability to track its own performance.

Finally, the alignment stage of the vehicle allows the IMU measurement to estimate the roll and pitch of the vehicle. For this implementation, the estimated roll and pitch angles are also used in the measurement vector when the vehicle is stationary, and the measurement matrix is updated accordingly.

4.2.3 Process and Measurement Noise

The selection of the process and measurement noise terms largely drives the performance characteristics of the estimate, and can often be used to tune the filter until the performance is deemed acceptable. Loosely, the measurement and process noise terms are analogous to the

amount of trust there is- in either the process model or in the measurements. Specifically, if the process noise terms are weighted significantly lower than the measurements, then the a priori estimate will have more weight in the final estimate at time k .

Measurement noise can be found empirically based on sensor performance through the collection of data while no inputs are present. Process noise is typically considered a continuous random variable caused and determined by the physical processes or environment of the dynamic system [75], but this is dependent on having a knowledge beforehand what those inputs may be. In many cases this is not necessarily the case, and process noise must be estimated based on best judgment. Furthermore, for the implementation of the Kalman filter presented in Chapter 3, discrete time process noise is required. For this work the process model presented is a function of IMU outputs, thus any noise associated with those outputs will also contribute to the external disturbance noise.

Measurement noise can be found empirically through processing of data on the sensors. For this work, the GPS receiver computes the estimated *accuracy* of the filter, which is a function of DOP, delays, receiver clock bias, orbital errors, or multipath and shown in Table 2-4.

GPS accuracy is usually given as a confidence level, that it is within $\langle xx \rangle$ meters $\langle yy \rangle\%$ of the time [56], which doesn't necessarily mean that the GPS measurements are centered about the true position. However, the measurements obtained may not necessarily be centered about the true position, the spread may be about some other biased point. Take for example, an set of GPS data taken while the vehicle is stationary and corresponding accuracy values as calculated by the receiver in Figure 4-1.

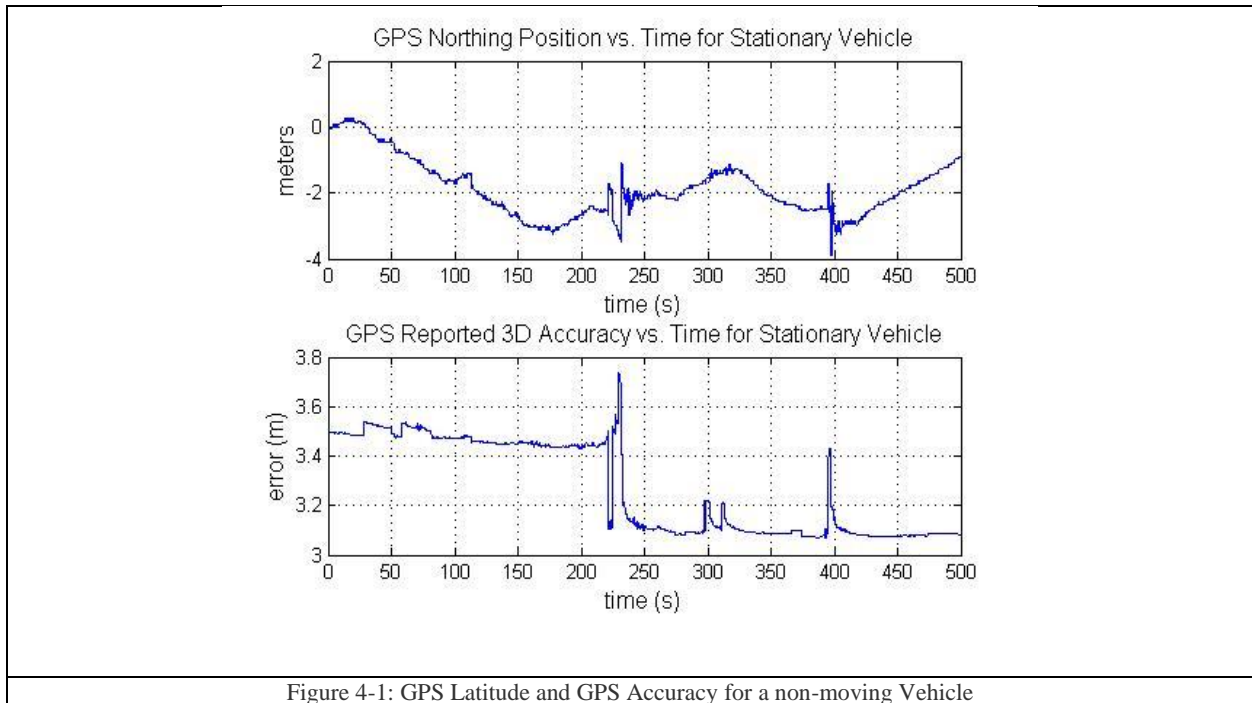


Figure 4-1: GPS Latitude and GPS Accuracy for a non-moving Vehicle

Figure 4-1 shows the position in time for a vehicle that is not moving and the corresponding receiver accuracy. Although the vehicle is not moving, the solution tends to move, at times nearly 4 meters from the initial position.

While the assumption of Gaussian noise is violated, the measurement noise term is still obtained in real time as the GPS accuracy reading as suggested by [26]. The accuracy provided by the receiver is still representative of the where the measurement is in relation to the actual position. Similarly, GPS velocity accuracy is also used in the measurement covariance matrix.

The WSS component of the measurement noise matrix is given by the variance of the WSS. However, WSS are known to have nearly zero variance, but this is not to say that the measurement is perfect. The wheel encoders on the vehicle are subject to wheel slip, which gives an inaccurate measurement in the velocity of the body frame. Furthermore, if one were to put the near zero variance for the measurement, the filter would only trust the WSS, treating it as a perfect measurement. For this work, the manufacturer suggested noise value of 0.1m/s was used.

Accordingly, since the WSS is in the body frame and must be transformed into the navigation frame, the covariance matrix will also need to be transformed into the navigation frame using equation 4-17,

	$\mathbf{R}_{wss} = \begin{bmatrix} \sigma_{wss}^2 & 0 & 0 \\ 0 & \sigma_{slip}^2 & 0 \\ 0 & 0 & \sigma_{vert}^2 \end{bmatrix},$	4-17
--	--	------

where σ_{slip}^2 and σ_{vert}^2 are the design parameters for side slip and vertical travel respectively.

From a strictly application standpoint, process noise is also a way to bound the uncertainty of the model and characterizes how much ‘trust’ the engineer has in the mathematical model. For example, in [37], it is suggested that process noise be determined by examining the limits in performance of the vehicle, i.e. mean squared velocity or acceleration, and use this as the covariance matrix.

For this work, the process noise covariance matrix was determined from the outputs of the IMU, $f_x, f_y, f_z, \omega_x, \omega_y, \omega_z$, while the vehicle was at rest. Considering only the first term of equation 4-7, it can be written as the following,

	${}^N\mathbf{R}(\boldsymbol{\Theta}) \cdot (\mathbf{f}_b + \boldsymbol{\omega}_{imu}) = {}^N\mathbf{R}(\boldsymbol{\Theta}) \cdot \mathbf{f}_b + {}^N\mathbf{R}(\boldsymbol{\Theta}) \cdot \boldsymbol{\omega}_{imu},$	4-18
--	--	------

Where $\boldsymbol{\omega}_{imu}$ is a vector containing the noise terms on each axis. By observation, a conservative of the maximum value for the variance at any given time, due to the fact that the rotation matrix is orthonormal, would simply be $\Sigma_i \omega_{imu}$, or the sum of all three random variables. It follows also that the variance of the sum of three random variables’ variance is the sum of each of those three random variables, and thus

	$\sigma_N^2 = \sigma_E^2 = \sigma_D^2 = \sigma_{f_x}^2 + \sigma_{f_y}^2 + \sigma_{f_z}^2.$	4-19
--	--	------

Similarly, the process variance for the angular rate equations can also be derived from the IMU gyroscope output through a similar analysis as,

	$\sigma_{\theta}^2 = \sigma_{\omega_x}^2 + \sigma_{\omega_y}^2 + \sigma_{\omega_z}^2$ $\sigma_{\beta}^2 = \sigma_{\gamma}^2 = \sigma_{\omega_y}^2 + \sigma_{\omega_z}^2.$	4-20
--	---	------

The overall process noise matrix becomes,

	$\mathbf{Q} = \text{diag}([0 \quad 0 \quad 0 \quad \sigma_N^2 \quad \sigma_E^2 \quad \sigma_D^2 \quad \sigma_{\theta}^2 \quad \sigma_{\beta}^2 \quad \sigma_{\gamma}^2])$	4-21
--	---	------

And recall from equation 3-14 that $\mathbf{Q}_k = \int_0^{\delta t} \boldsymbol{\phi}(\tau) \mathbf{Q} \boldsymbol{\phi}^T(\tau) d\tau$ in discrete time.

The Kalman filter model presented in this section is based on a full extended Kalman filter with switching observability modes, from full observable with GPS and WSS measurements, to dependency of the integration of IMU outputs only. The process model noise terms are dependent on the noise associated with the IMU output, and the measurement noise is terms are related to GPS provided accuracy, and manufacturer suggested uncertainty for the WSS. The next section outlines the hardware configuration and an examination of individual sensor platforms used in this thesis and their viability as standalone navigation platforms.

Chapter 5: System Interface

This chapter will discuss the system interface of the platform used, specifications of each sensor, relative locations, and electrical interface. Also presented are several test cases of stand-alone inertial navigation, WSS dead reckoning with GPS provided heading (to evaluate the effect of slip), and a stationary vehicle calibration method to estimate the roll and pitch angles of the IMU.

5.1 Hardware Used

The vehicle sensor suite consists of a 6 axis, navigation grade IMU, dual antenna GPS, two large pass band wheel encoders, which are all synchronized in time by a navigation computer using pulse per second (PPS) signal from the GPS receiver clock. The sensor configuration is illustrated in Figure 5-1 with a top down view and the z axis pointing into the page.

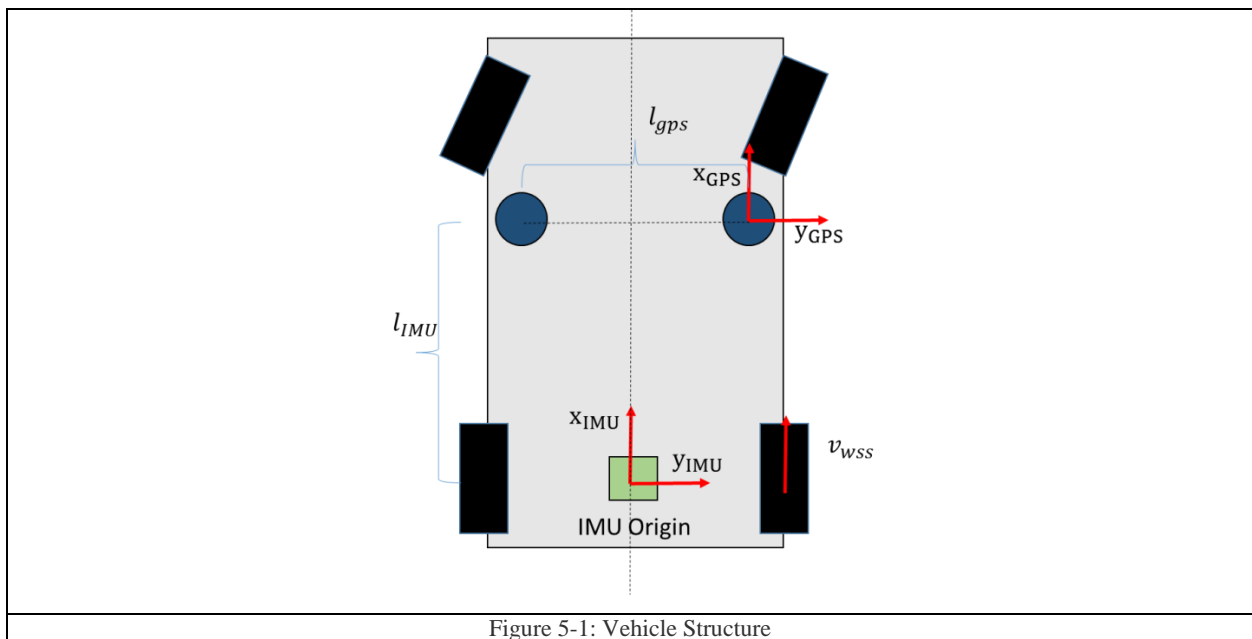


Figure 5-1: Vehicle Structure

Figure 5-1 shows the relative locations of each of the sensors mounted on the vehicle and the directions of the sensing axes.

Because the GPS, IMU, and wheel speed sensors all have different origins, the moment arms can be accounted for through transformation matrices much like the rotation matrices presented in chapter two.

A simplistic method of aligning the origins of the axes is by simply adding the vector in the navigation frame. This is done by finding the difference between the two origins in the navigation frame and transforming it into the body frame.

	$P_{align} = {}^N_B R \begin{bmatrix} l_{imu} \\ l_{GPS} \\ z \\ -h \end{bmatrix}$	5-1
--	--	-----

Where l_{imu} is the distance from the IMU origin to the intersection of the y axis on the GPS origin, l_{GPS} is the distance from each antenna which has a center along the vehicles center, and h is the height from the z axis to the GPS. In order to align the IMU and the GPS, the origin is selected to be the IMU center. Accordingly, each measurement calculated by the GPS in the {N} frame will then have P_{align} subtracted from it.

	$\begin{bmatrix} N \\ E \\ D \end{bmatrix}_{GPS \text{ Aligned}} = \begin{bmatrix} N \\ E \\ D \end{bmatrix}_{GPS} - P_{align}$	5-2
--	---	-----

5.1.1 Electrical Interface

The communications protocol used for this system consisted of a UDP protocol over Gigabit Ethernet which could be configured to deliver messages from GPS, IMU, and the wheel speed sensors. Each update occurred as the measurements were decimated and synchronized using the GPS PPS signal. The IMU was sampled at 100Hz, the WSS was sampled at 50Hz, and the GPS signals were sampled at 20Hz.

5.1.2 IMU

The IMU used for these experiments consists of a navigation grade vibrating beam accelerometer and MEMS gyroscope and with a 1000 Hz update rate but is decimated by the navigation computer to 100 Hz while applying a coning and sculling algorithm to minimize the effects of engine vibration. The IMU performance characteristics are summarized in Table 5-1.

Synchronized (GPS) Sample Rate (Hz)	100
Gyroscope Range (deg/sec)	1000
Accelerometer Range	30g
Angular Random Walk $\frac{deg}{\sqrt{hr}}$.06
Bias Stability (deg/hr)	1.0

Table 5-1 IMU Performance Characteristics

However, it should the values provided above only show the accuracy under laboratory conditions. In real-case applications, body vibrations from the engine, bumpy roads, and inaccurate initial conditions on the body attitude will degrade the accuracy of the IMU outputs.

5.1.3 GPS

The GPS system used in this research has a dual antenna configuration oriented such that heading and roll angle are observed from GPS readings. The antennas are capable of measuring GPS in the L1 and L2 bands, Omnistar differential GPS subscription, and GLONASS L2 frequency. The horizontal positional accuracy can achieve up to 1.5 meter accuracy to 10 cm level accuracy depending on the availability of Omnistar and dilution of precision. The GPS receiver also calculates automatically the estimated accuracy of 3D position and velocity, in meters and m/s according to the fix type and GDOP.

When both antennas have signals a suitable number of satellites to obtain a positional awareness, the navigation computer also calculates heading and roll angle, and their corresponding estimated accuracies. If only one GPS antenna is available, heading may be calculated using one GPS antenna if the vehicle is moving.

5.1.4 Auxiliary Sensors

The wheel speed sensors for these experiments are series quadrature speed and direction sensors which provide two signals 90° phase shifted from each other. The resolution for this sensor can range from 1Hz to 15 kHz and is robust to air gap uncertainty to provide accurate signals. The

tone ring is designed to fit inside the wheel rim for each rear wheel and has 19 teeth per revolution. Calibration was performed by calculating the rollout of the wheel and correlating that to the speed of the pulses. Wheel speed will vary according to the tire diameter which changes under different tire pressure and ground surface hardness.

Steering angle sensors were not employed during these tests; however, with their use it would have been possible to add additional constraints to the vehicle model and measure the centripetal acceleration. However, in the strapdown navigation configuration, it is adequate to use just the inertial measurement unit and GPS receivers.

5.2 A Look at Alternative Models Using Different Sensor Suites

Before discussing the data fusion methods, it is worthwhile to look at some of the raw sensor data and the characteristics that can be extracted under different scenarios. A performance evaluation of each sensor platform, i.e. IMU, WSS, and GPS as standalone sensors is performed. Specifically, a linear Kalman filter is presented which references a trajectory given by the GPS data and estimates the navigation solution with WSS data to see how well a linear Kalman filter works without the presence of GPS or IMU aiding.

5.2.1 Linear Kalman Filter Implementation Using WSS and Heading Information

The wheel speed sensors offer a method of dead reckoning which fortunately has very little noise associated with the measurements and little error. However, they only measure the true speed of the vehicle under the ideal circumstances that the wheels are not slipping. The wheel speed sensors also have the effect that they may only measure in the body coordinate frame $\{B\}$ along the vehicles x axis. For this reason, heading angle, as computed using GPS measurements must be used to complete this implementation of the dead reckoning solution. The most basic method of navigation would consist of using heading angle and body velocity for a two dimensional navigation approach.

To perform this navigation solution, a linear Kalman filter is proposed based on the following simplified state vector,

	$\mathbf{x} = [N, E, \dot{N}, \dot{E}, \gamma]$.	5-3
--	---	-----

For this version of the Kalman filter, only the heading angle is considered for the attitude and not the roll or pitch angles.

For the state dynamics matrix, first order models will be considered for the NED directions, and zeroth order models for the attitude. The reason for this is because velocity is a measured state both by the GPS and through a transformation into the {N} frame by the wheel speed sensor. Accordingly, for the attitude representation, it was shown that a zeroth order model in estimating this signal sufficed for the purpose of attitude estimation.

To build the model for this, a set of augmented first and zeroth order systems was constructed.

	$\mathbf{A} = \begin{bmatrix} 0 & 0 & 1 & 0 & 0 \\ 0 & 0 & 0 & 1 & 0 \\ 0 & 0 & -\frac{1}{\tau_N} & 0 & 0 \\ 0 & 0 & 0 & -\frac{1}{\tau_E} & 0 \\ 0 & 0 & 0 & 0 & 0 \end{bmatrix},$	5-4
--	---	-----

Where τ_x is a northing and easting time constant which places a pole in the left half plane.

Typical values for ground vehicles are 13-16 seconds [37]. Finding the state transition matrix $e^{\mathbf{A}\delta t}$ yields,

	$\Phi_k = \begin{bmatrix} 1 & 0 & \delta t & 0 & 0 \\ 0 & 1 & 0 & \delta t & 0 \\ 0 & 0 & e^{-\frac{\delta t}{\tau_N}} & 0 & 0 \\ 0 & 0 & 0 & e^{-\frac{\delta t}{\tau_E}} & 0 \\ 0 & 0 & 0 & 0 & 1 \end{bmatrix}.$	5-5
--	---	-----

Similarly, since we are assuming zero input, the output measurement equation will take the following form

	$\mathbf{y} = \begin{bmatrix} \sin(\gamma) \cdot v_{WSS} \\ \cos(\gamma) \cdot v_{WSS} \\ \gamma \end{bmatrix} + \begin{bmatrix} {}^n\mathbf{R}_b \cdot \mathbf{v}_{WSS} \\ v_{h_{GPS}} \end{bmatrix} = \begin{bmatrix} \dot{N} \\ \dot{E} \\ \gamma \end{bmatrix}$	5-6
--	---	-----

Figure 5-2 shows the use of the heading data and body velocity to characterize the performance of the WSS in the event of driving in a straight line. The WSS data was integrated and compared to the absolute position given by the GPS.

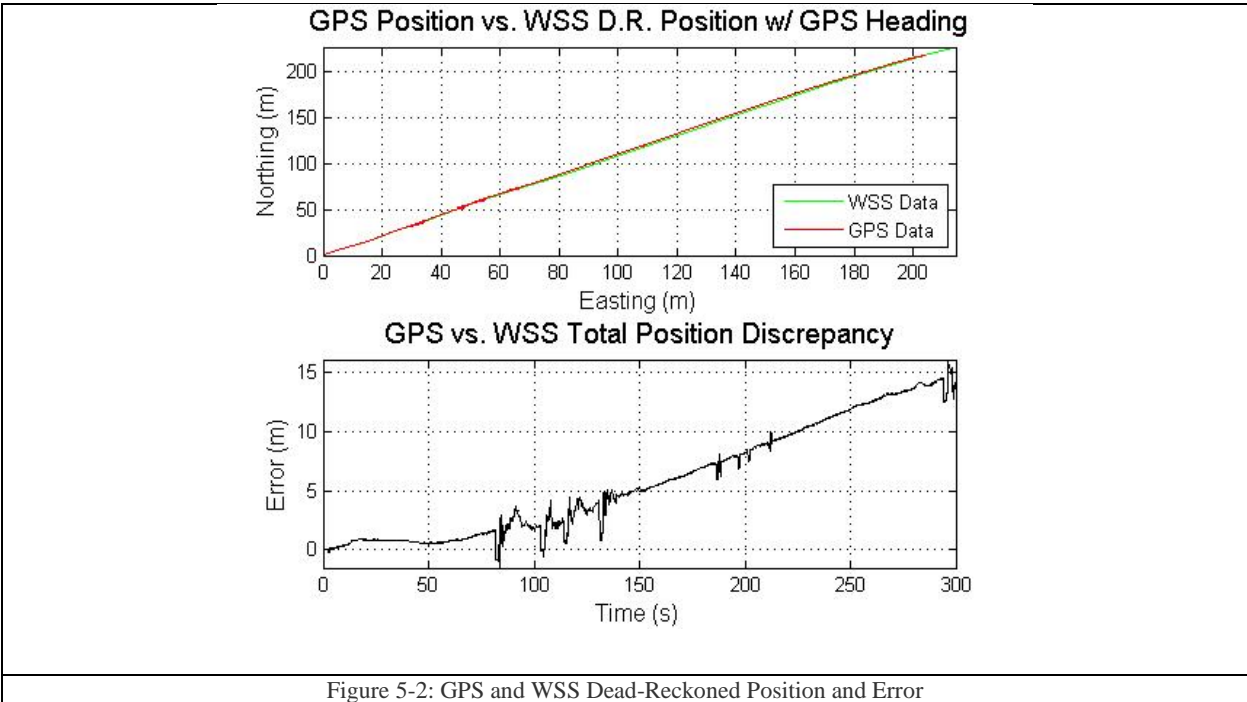


Figure 5-2: GPS and WSS Dead-Reckoned Position and Error

Figure 5-2 Show GPS position, a dead reckoned WSS solution using a first order KF and the error between the GPS solution and the WSS solution. In the subplot above, the WSS shows that it extends past the GPS calculated position. The error reaches about 15 meters, but it is clear that GPS pop is occurring.

From the figure above, it is clear that the WSS integration causes a significant amount of drift in the WSS dead reckoned solution. Over 280 meters, the positional discrepancy from the dead reckoned solution was around 15 meters.

5.2.2 Standalone IMU Navigation Solution

In order to use the IMU navigation solution, it is necessary to integrate both the rate vector equation for attitude in the navigation frame and also the accelerations into velocity and position. If we consider just a standalone IMU with no external outputs, i.e. , i.e. $c(\mathbf{x}) = \emptyset$, neither position, velocity nor attitude is observable; it is solely integrated rate data from the IMU which is subject to drift.

An artifact of the Kalman filter under zero measurement is that the estimate variance can still predicted from $\mathbf{M}_k = \Phi_k \mathbf{P}_{k-1} \Phi_k^T + \mathbf{Q}_{k-1}$. Periods of time where the filter is solely relying on integration of the system model, i.e. equation 4-8. It is shown in the results section that for unobservable systems this shows the drift in variance accordingly.

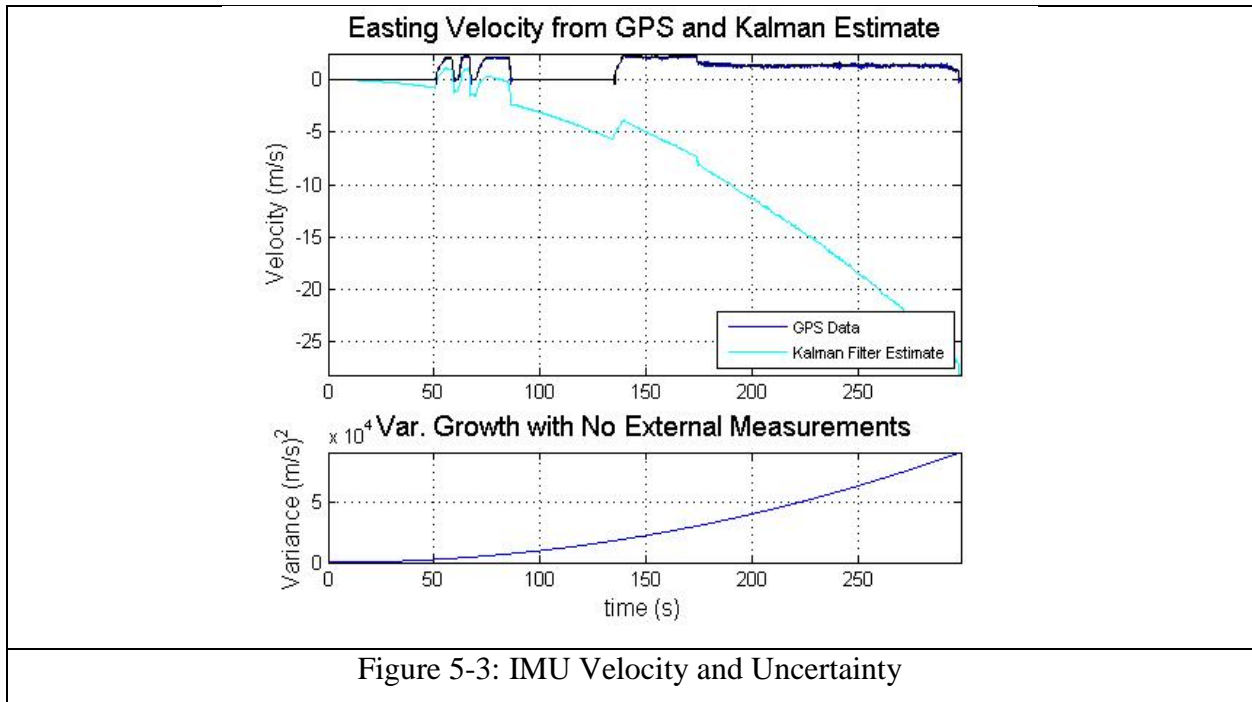


Figure 5-3 shows the velocity estimate vs. the GPS estimate as it grows without bound starting with a pre-computed set of initial conditions. An interesting note is that the uncertainty in velocity appears to grow as a quadratic, although the accelerations are only integrated once, and, according to the definition of a random walk which states the sample dependent variance growth is linear for the first integral of a random variable. The cause of this quadratic growth is caused by the compounding effects of the integration of body angular rates and resolving them into the navigation frame.

Initial conditions also contribute to the quickly drifting solution of a Kalman filter, and especially in the context of integrating attitude rates. The subtraction effect of gravity from acceleration can cause large sensed accelerations, and if the pitch and roll angles are imprecise, this leads to a large accumulation in error in both the velocity and position. For example, if the pitch angle were to be off by 1 degree, the corrected acceleration in the x axis would be,

	$\epsilon = 9.81 \cdot \sin\left(1 \times \frac{\pi}{180}\right)$	5-7
--	---	-----

Integration over 200 seconds would lead to a velocity error of 34.2416 m/s and positional error of 6.8 km. The next section will look at the calibration method used in this paper and discuss the implementation into the overall navigation solution.

5.2.3 Initial Alignment and Calibration Implementation

To account for the fact that pitch and roll are not directly observable when GPS is out, a cascading filter is used to achieve this based on the initial calibration and alignment methods as described in 2.2.4 for when the vehicle is stationary. When the motionless state of the vehicle is detected by the WSS and accelerometers, it is then possible to start estimating the orientation using a zeroth order KF which are augmented in as measurements. When the vehicle is no longer moving based on zero wheel speed and the vehicle suspension has settled determined by the magnitude of the accelerations, the roll and pitch angles can be estimated by the following from equation 2-18,

$$\mathbf{a}_b = \begin{bmatrix} -\beta_s \\ \beta_c \cdot \theta_s \\ \beta_c \cdot \theta_c \end{bmatrix} \mathbf{g}.$$

Similarly, the gyroscopic bias terms may be estimated as well, since it is assumed that the vehicle is not moving during this time. Note that when the vehicle speed is zero, it is assumed that the nominal acceleration is zero, however, in the presence of engine vibration and perhaps wind gusts, this is not necessarily the case.

Using a zeroth order Kalman filter [66], which is augmented with the gyroscope data to gyroscopic bias,

	$\begin{bmatrix} \hat{\mathbf{a}}_{b,k} \\ \hat{\boldsymbol{\omega}}_k \end{bmatrix} = \begin{bmatrix} \hat{\mathbf{a}}_{b,k-1} \\ \hat{\boldsymbol{\omega}}_{k-1} \end{bmatrix} + \mathbf{K}(\begin{bmatrix} \mathbf{a}_{b,k} \\ \boldsymbol{\omega}_k \end{bmatrix} - \begin{bmatrix} \hat{\mathbf{a}}_{b,k-1} \\ \hat{\boldsymbol{\omega}}_{k-1} \end{bmatrix})$	5-8
--	---	-----

where \mathbf{K} is the Kalman gain as is computed by algorithm one in 3.3 and $\hat{\mathbf{a}}_{b,k}$ is the estimated acceleration at time k .

For this reason, the filter design to estimate roll and pitch is based on a zeroth order linear Kalman filter of the measurements \mathbf{a}_b to give the estimated acceleration $\hat{\mathbf{a}}_b$ and then β and θ can be computed as,

	$\hat{\beta} = \left[\text{asin} \left(\frac{-\hat{a}_{b,x}}{g} \right) \right],$	5-9
--	---	-----

and

	$\hat{\theta} = \left[\text{asin} \left(\frac{\hat{a}_{b,y}}{g \cdot \cos(\hat{\beta})} \right) \right],$	5-10
--	---	------

where $\hat{a}_{b,y}$ is the estimated acceleration in the y direction.

With θ , β , and gyro bias now estimated, they can be augmented in the original Kalman filter equations as a measurement of pitch, and compensation terms for bias.

The benefit in modelling the estimate of the angle as a linear Kalman filter as opposed to augmenting the nonlinear equations into the main Kalman filter is that the model can be assumed to be perfectly known, i.e. during this time the roll and pitch angles are nominally constant, thus taking on a zeroth order linear model. The output of this filter can then be augmented into the main navigation EKF as measurements of the roll and pitch angles, i.e.

	$\mathbf{y}_{\text{imu}} = \begin{bmatrix} \hat{\theta} \\ \hat{\beta} \end{bmatrix},$	5-11
--	--	------

Which can then be augmented into the any of the measurement vectors shown above. For example, if GPS and WSS data are available,

5.2.4 Stationary Vehicle Measurement Vector

When the vehicle is stationary, an augmented measurement vector of the system model can be constructed to add the measurement of the pitch and roll angles as estimated by equation 2-18.

	$\hat{\mathbf{y}}_k = \mathbf{c}(\hat{\mathbf{x}}_k^-) = \begin{bmatrix} \hat{x}_{1,k}^- \\ \hat{x}_{2,k}^- \\ \hat{x}_{3,k}^- \\ \hat{x}_{4,k}^- \\ \hat{x}_{5,k}^- \\ \hat{x}_{6,k}^- \\ {}^b_n\mathbf{R}(\hat{x}_{7,8,9,k}^-) \times [\hat{x}_{4,k}^- \quad \hat{x}_{5,k}^- \quad \hat{x}_{6,k}^-]^T \\ \hat{x}_{8,k}^- \\ \hat{x}_{9,k}^- \\ \hat{x}_{7,k}^- \\ \hat{x}_{8,k}^- \end{bmatrix}$	5-12
--	--	------

Where the difference now is that there is redundant roll θ and now pitch β measurements, as seen in the last two rows of the vector.

And similarly, \mathbf{P}_{imu} will also be fed back directly into the original EKF for the total system for the measurement noise covariance.

Finally, to illustrate how the cascaded filter works, Figure 5-4 illustrates the Kalman filter with augmented measurements from the cascaded Kalman filter.

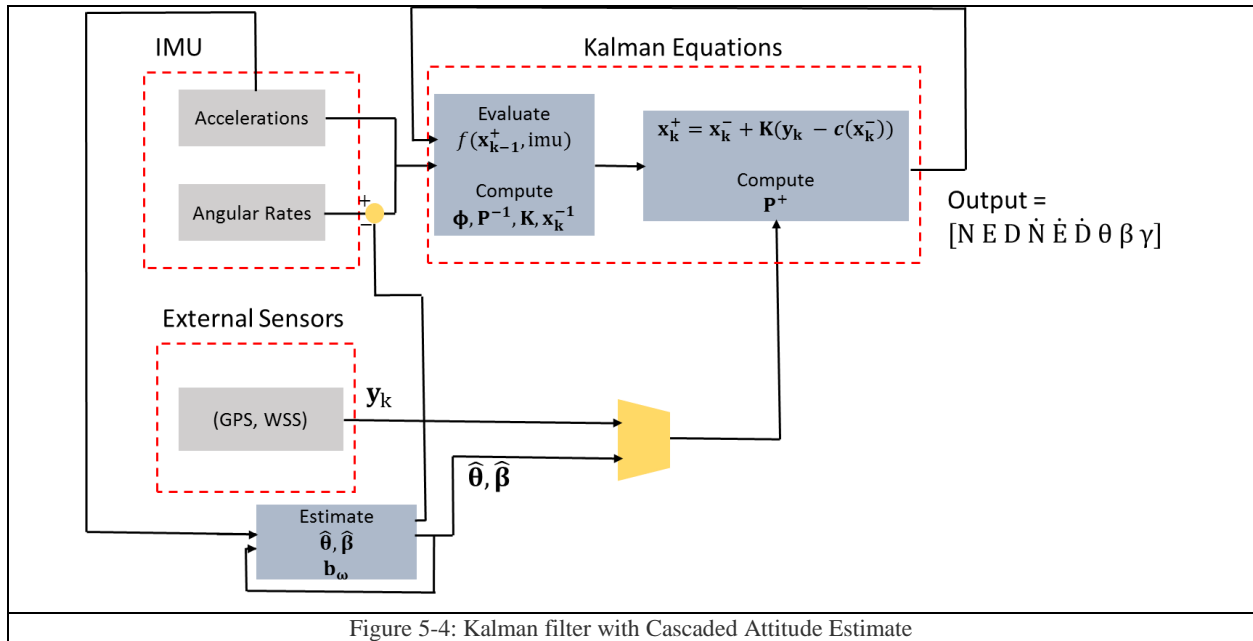


Figure 5-4: Kalman filter with Cascaded Attitude Estimate

Where the angular rates are compensated for the bias terms as calculated while the vehicle is stationary. Different scenarios where bias terms are unaccounted for and initial alignment terms are not done are examined in Chapter 6.

This chapter discussed the hardware implementation of each of the sensing platforms used for navigation. The electrical interface was described as well as a brief look at the performance if each were a standalone sensing package. Furthermore, the method used to implement a cascaded Kalman filter for attitude estimates using the calibration equations was shown. The baseline performance of each sensor gives the impression that any single sensor is in fact not sufficient for a navigation solution. The next chapter focuses on situations that an autonomous vehicle might experience during operation, such as the need to calibrate orientation and estimate biases.

Chapter 6: Results

This chapter focuses on the results of the implemented Kalman filter under the different cases proposed in chapter 4. Namely, the EKF using all available measurements, the EKF with GPS outage, and using the augmented alignment scheme. Different trajectories, such as a straight line path, and curved paths which push the use of the angular rate sensor. The general EKF is examined and compared against the GPS position and velocity solution their and corresponding accuracies are compared as well.

6.1 Attitude Estimation

This section focuses on the effects of initially estimating the attitude of the vehicle and bias associated with the gyroscopes as outlined in section 5.2.3 The accelerometers on the vehicle experience some acceleration as due to engine vibrations, so it is necessary to determine if the navigation method proposed is suitable in that type of environment.

The roll and pitch angles are estimated using the zeroth order filter as shown in 5.2.3 and subsequently to estimate how well the angles were estimated. Recall that the estimated angles are used to transform the acceleration data used to calculate the angles into the navigation frame before gravity is compensated, so it is critical to obtain a good estimate of these values.

Figure 6-1 shows the convergence of the estimate of the forces acting on the body during the first 20 seconds of an alignment stage. To see how quickly the estimate converges to a constant value, the difference in acceleration is shown in the top subplot, followed by the corresponding roll and pitch angles using the accelerometer data in the bottom subplot.

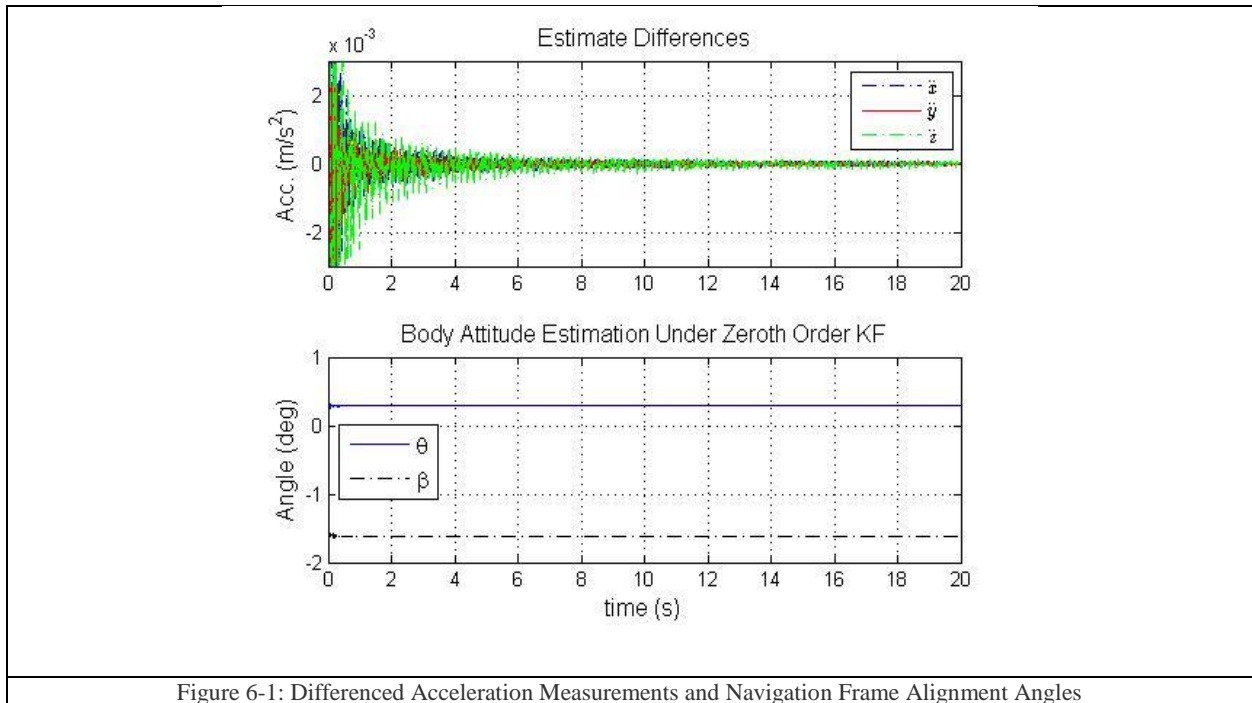


Figure 6-1: Differenced Acceleration Measurements and Navigation Frame Alignment Angles

Figure 6-1 show the differenced values of acceleration measurement and the corresponding attitude output. The estimated attitude angles converge to nearly constants within the first second.

Accordingly, the estimation covariance associated with the attitude estimate can also be tracked in the framework of the Kalman filter. Since this method used a zeroth order Kalman filter, the nonlinear transformation of the covariance is not captured using the proposed method. However, this estimate is for the variance on the *accelerations* and not the body attitude.

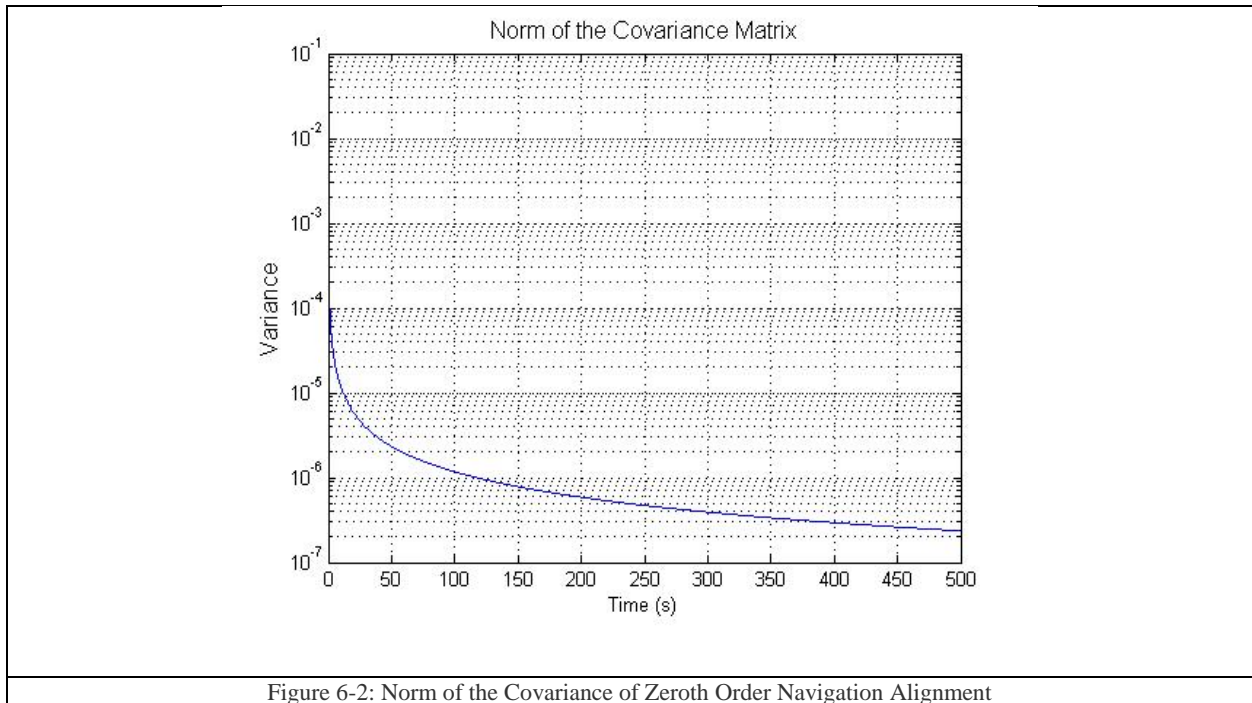


Figure 6-2: Norm of the Covariance of Zeroth Order Navigation Alignment
 Figure 6-2 shows the norm of the estimation covariance of the zeroth order filter.

The purpose of resolving the attitude angles externally from the main navigation equations is to decouple the dynamics of the angular rate equations as well as use the fact that if the vehicle is stationary, the angles can be assumed constant and hence the zeroth order model can be used. These estimates of attitude can then be used as measurements in the main navigation loop, and further, have an updating covariance based on the zeroth order filter. The covariance associated with the attitude estimate can now be used as the *measurement* covariance term in the main Kalman filter.

Figure 6-3 shows the validation method described above to the attitude angles calculated. The acceleration data that was taken while the vehicle was stationary that was also used to calculate the roll and pitch angles is transformed into the navigation frame, and then integrated to provide velocity and position in Figure 6-3.

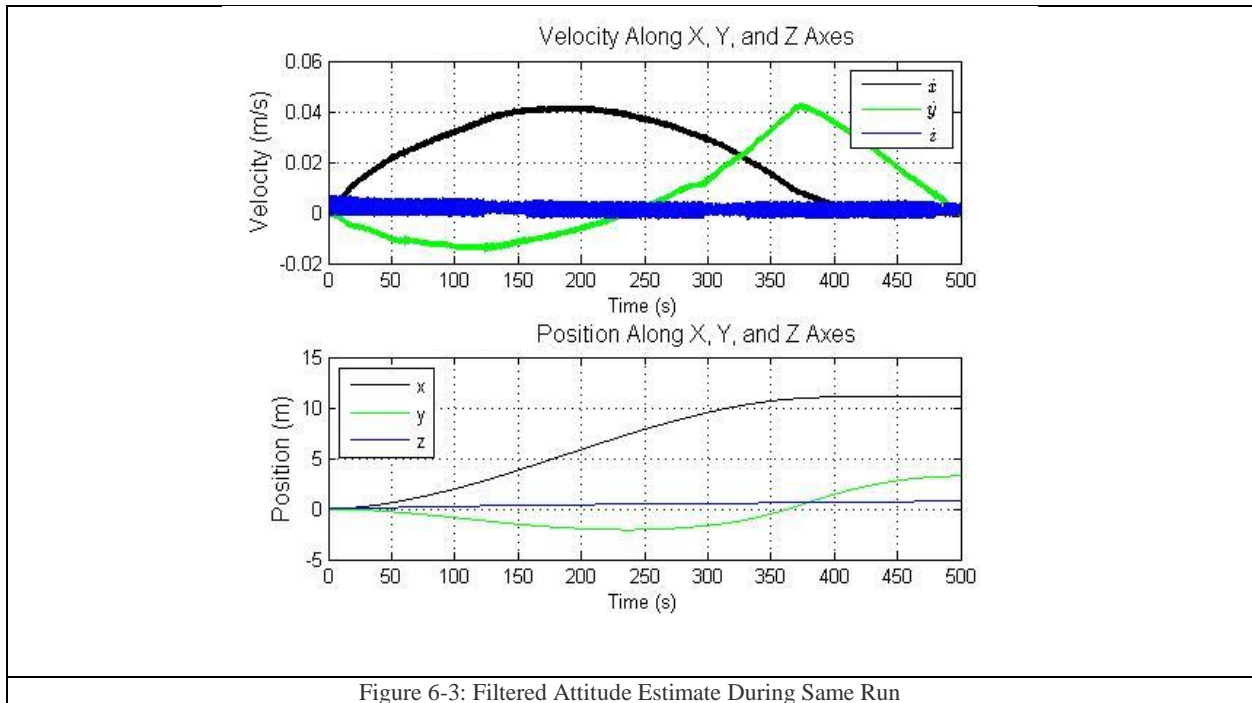


Figure 6-3: Filtered Attitude Estimate During Same Run

Figure 6-3 shows the transformed and integrated body accelerations using the attitude angles estimated previously, and the associated drift using the angles as found from the calibration technique. This shows relatively low amounts of integration drift due to the fact that the compensated gravity vector has limited effects when the IMU is transformed into the locally level frame using the angles found from the calibration method.

Conversely, if no attitude vector is estimated, and the accelerations are integrated in just the body frame, without attitude correction, then the velocity and position integrated will have the performance shown in Figure 6-4. The amount of drift in the two is reduced to a maximum of 10 meters in position after using the method from nearly a 4 km maximum drift without compensation.

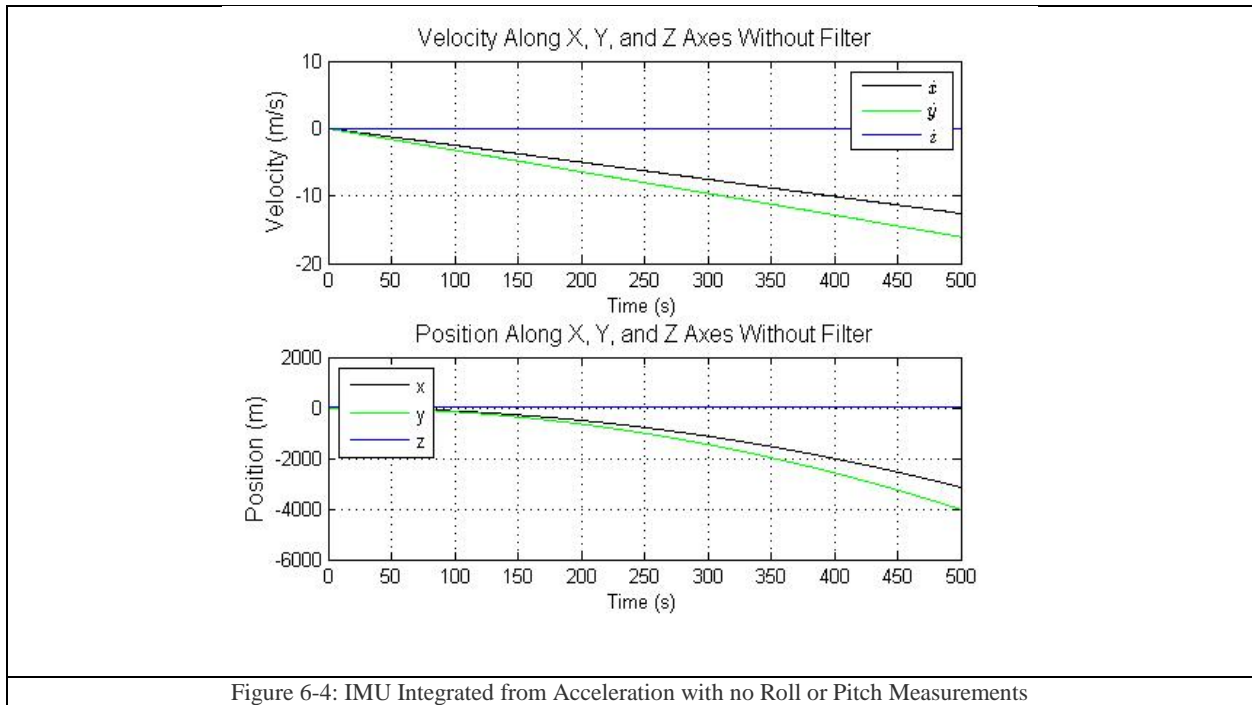


Figure 6-4: IMU Integrated from Acceleration with no Roll or Pitch Measurements

Figure 6-4 shows the effect of integrating accelerations in the navigation frame if the roll and pitch angles are incorrect/unaccounted for.

Section 5.2.3 also describes that while the vehicle is stationary, it is an ideal time to estimate the gyroscope bias. The gyroscope bias can be shown to have a major impact on the overall solution, as the integration of such bias will lead to a quickly drifting attitude, which is already shown to have significant impact of the velocity and positional estimates.

Figure 6-5 shows the effect of simply integrating the gyroscope outputs during the same stationary vehicle period without compensating for bias error in the measurement.

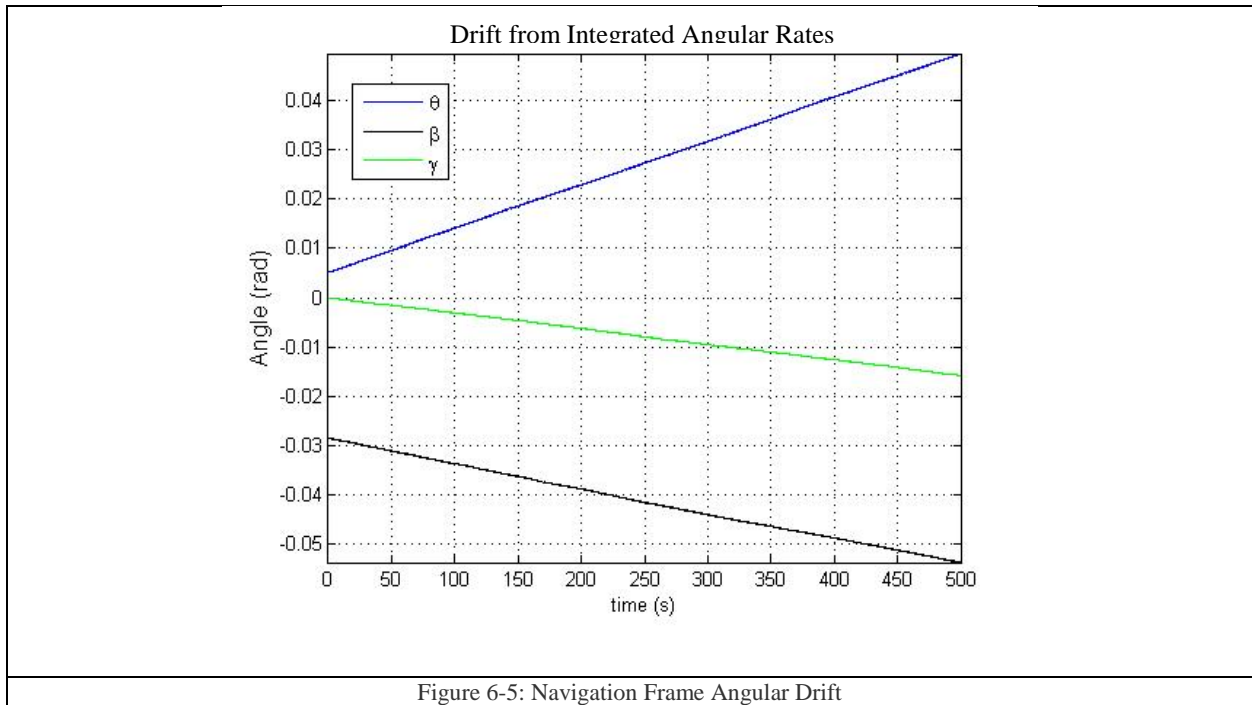


Figure 6-5: Navigation Frame Angular Drift

Figure 6-5 shows the effect of integrating a gyroscope measurement without compensating for, or estimating the bias is the signal. The largest drift over 200 seconds is seen to be .04 radians, or about 2.5 degrees.

To quantify what the biased attitude estimate would yield if these drifting angles were used as part of the navigation solution is, for example, if $\frac{9.789m}{s^2} \times \sin(.02 \text{ rad}) = .1960 \frac{m}{s^2}$ were integrated, for 100 seconds, then the integrated velocity drift is 19.5965 m/s.

By estimating the bias in real time while the vehicle is stationary using a zeroth order Kalman filter as shown in section 5.2.3 is illustrated in Figure 6-6 as a comparison to Figure 6-5 which has significant integration drift without compensating for bias terms.

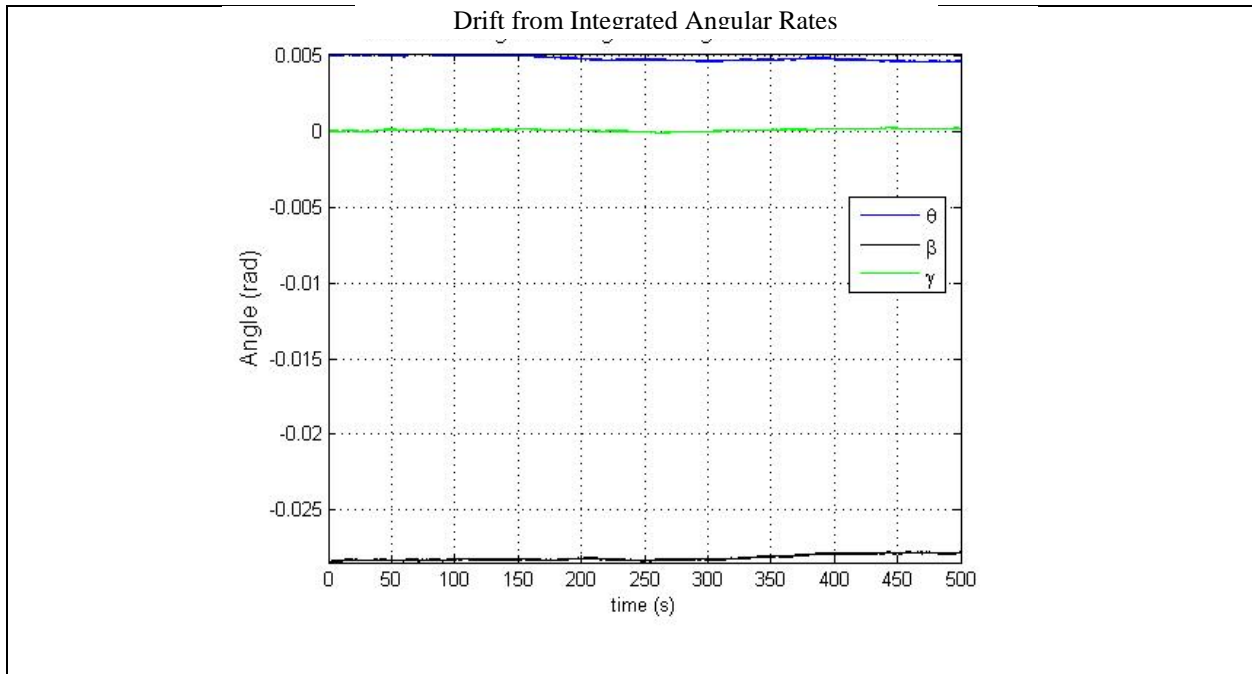


Figure 6-6: Reduction of Integration Drift with Bias Corrections

Figure 6-6 shows integrated gyroscope signals with the estimated bias compensation utilized. The amount of integration drift is reduced significantly, however, bias instability causes error over a long period of time.

Figure 6-7 shows an example of a dead reckoned navigation solution using a standalone IMU solution with bias correction and estimated roll and pitch under stationary vehicle conditions, and GPS provided initial conditions.

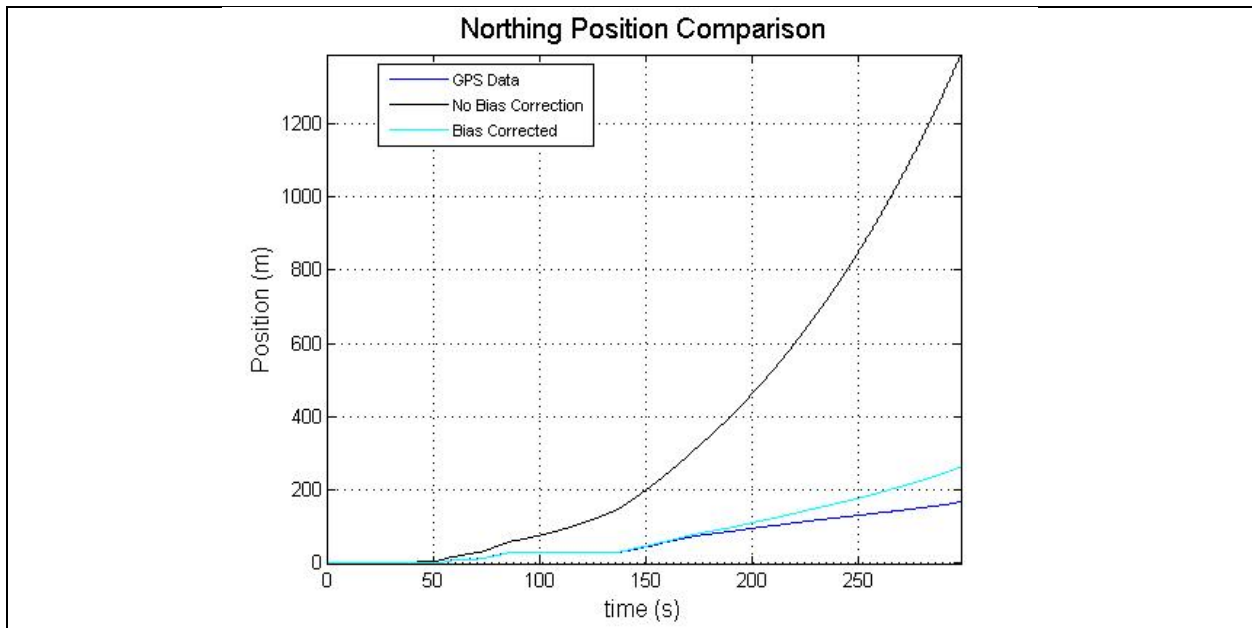


Figure 6-7: IMU Dead Reckoned Trajectory with Bias Corrected Gyros and Roll and Pitch Calculation

Figure 6-7 shows that without bias compensation, the northing position drifts by well over a thousand meters. This is also assuming pitch and roll were computed beforehand as well.

Similarly, Figure 6-8, show the northing velocity drift behavior.

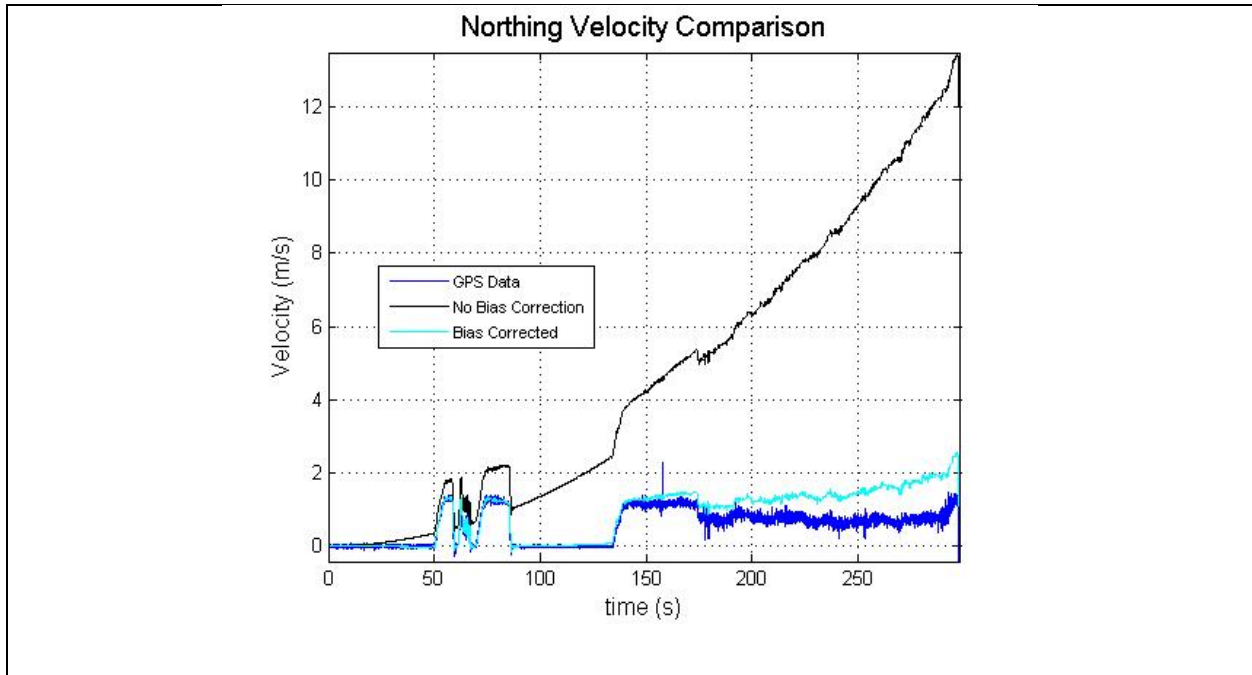


Figure 6-8: Northing Velocity Comparison

Figure 6-8 illustrates velocity drift with and without gyroscopic bias correction during an initial alignment phase.

In conclusion, if the attitude calculation through integration is off, and corrected during stationary vehicle periods, the accuracy and integrity of the IMU output will increase by an order of magnitude under conditions of no GPS reception or aiding WSS measurements. The effect of having an accurate IMU navigation scheme is so that there is a reliable safety net in the events of GPS outage or other sensor loss.

6.2 Test Case One – Full EKF Model

In this case, it is desirable to look at the full EKF that is used to see its performance during different GPS performance. For example, when a GDOP spike occurs, it is undesirable to have

the estimate in the vehicle ‘hop’ from one place to another. The general thought is that the other sensor information and holonomic constraints will prevent this from happening.

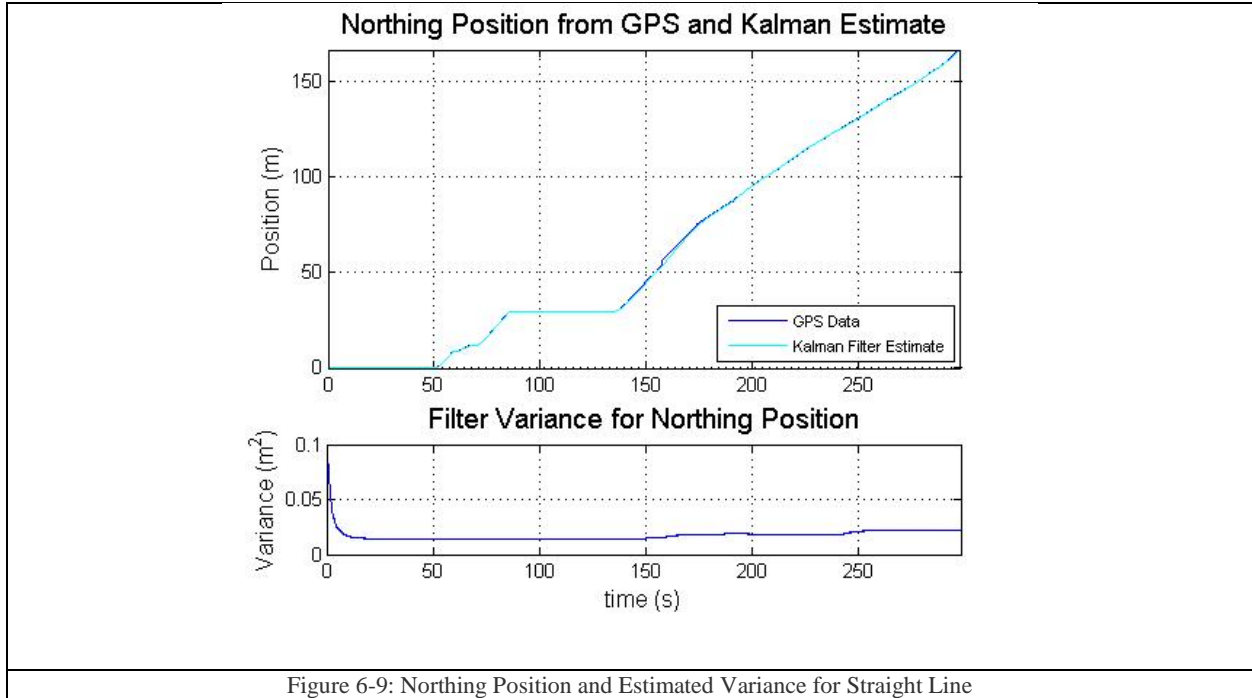


Figure 6-9 shows a northing trajectory given by GPS northing and the KF estimate. The estimation error variance is also shown. Beginning at about the 160 second mark, the GPS signal loses its integrity. This loss of GPS is highlighted in the next figure.

This trajectory shows that the GPS has very good performance during the first 150 seconds, and then jumps during a GPS pop. To show what this effect has on the GPS signal itself, an exploded view of the first large jump is shown at 158 seconds into the northing position trajectory in Figure 6-10 and the estimated northing velocity and GPS measurement in Figure 6-11.

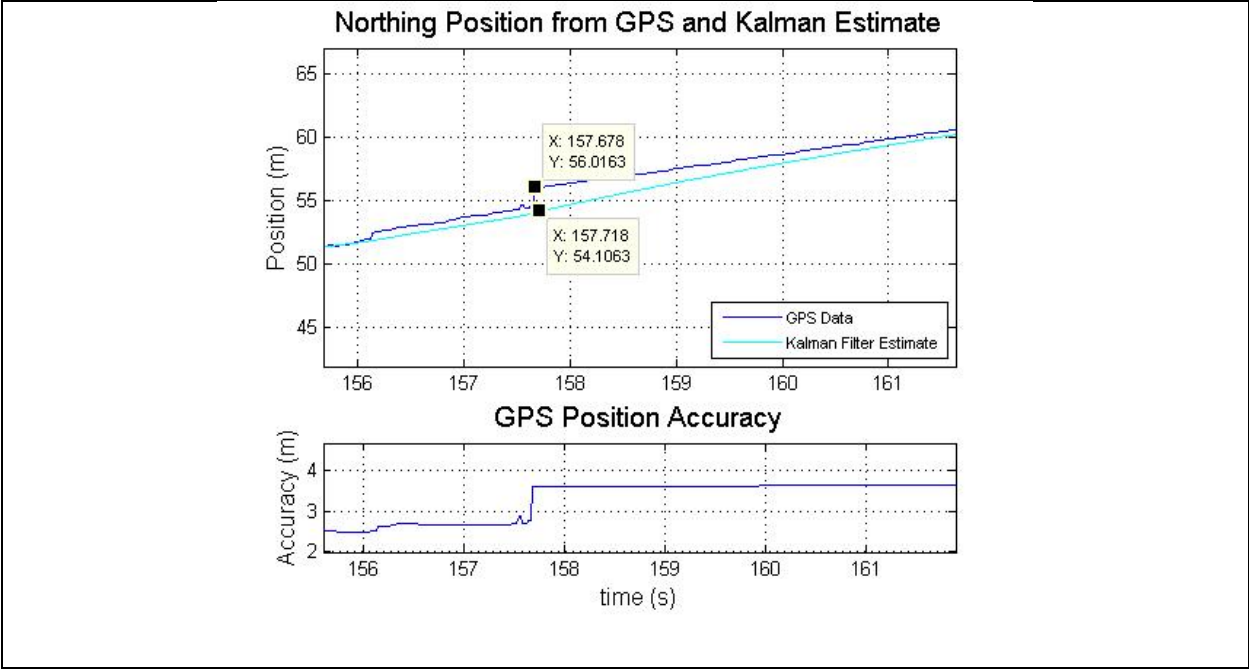


Figure 6-10: GPS Pop for Northing Trajectory and Kalman Estimate Rejection

Figure 6-10 illustrates a sudden jump in GPS data of about 1.9 meters to the north over one epoch. The EKF is shown to reject this sudden pop due to the constraints and changing measurement variance from the GPS positional accuracy.

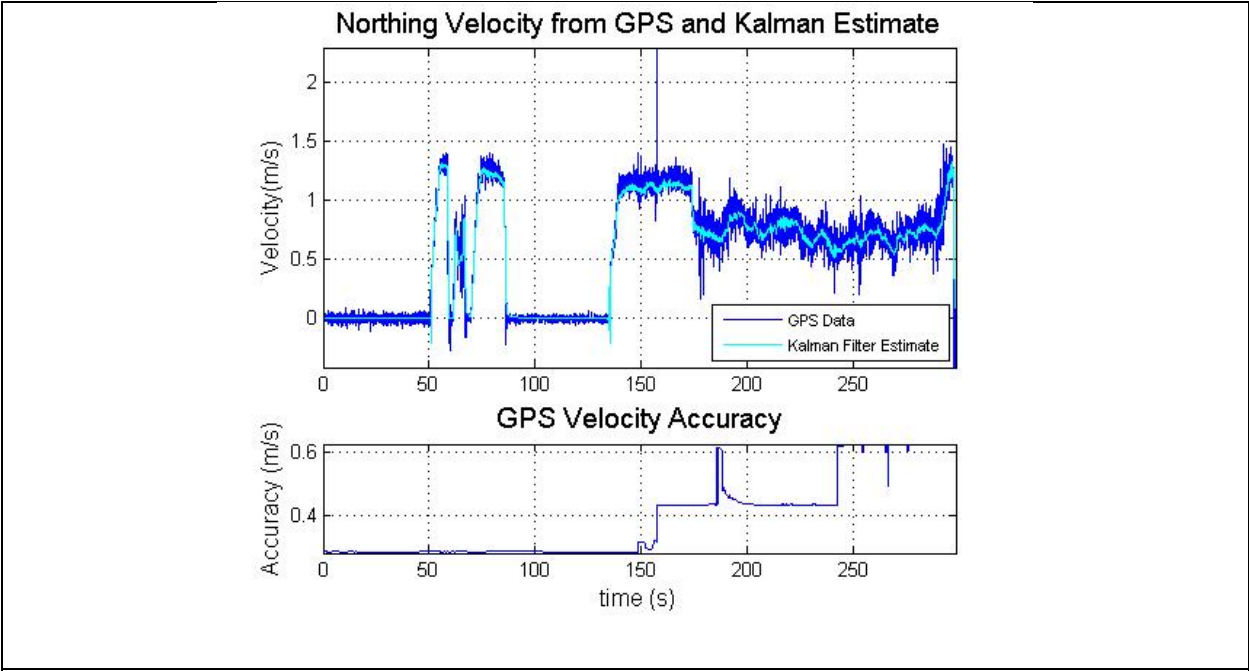
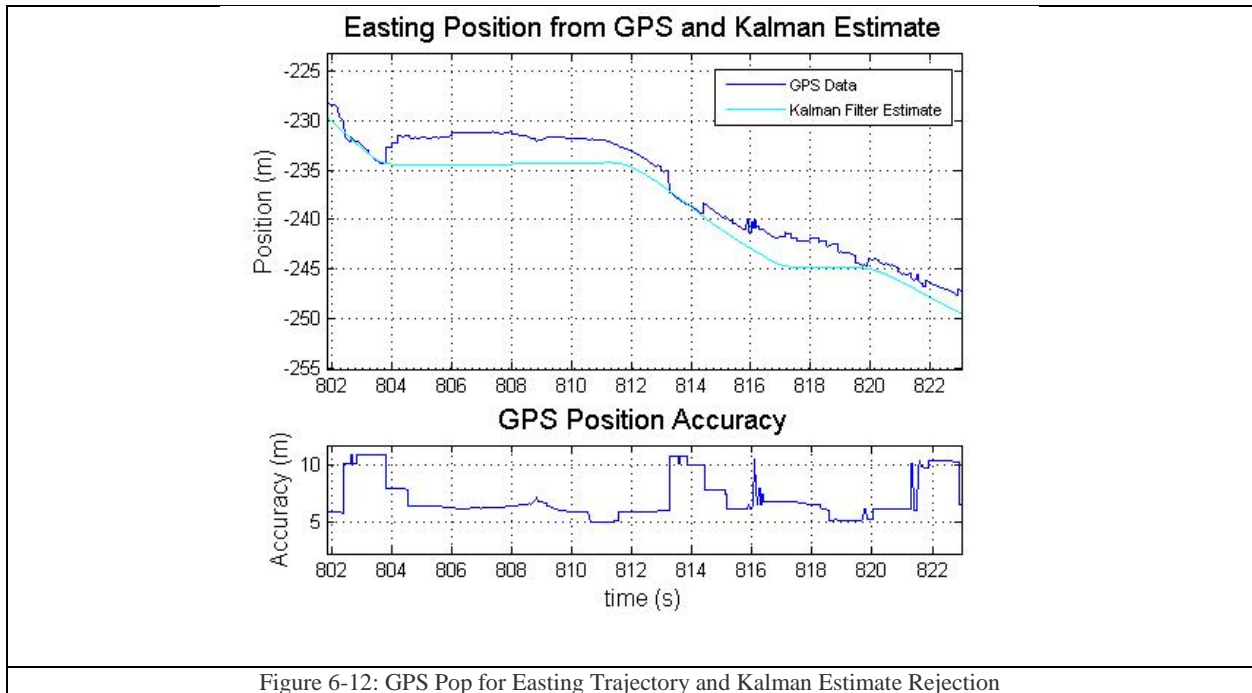


Figure 6-11: Northing Velocity - GPS vs. Kalman Estimation

Figure 6-11 shows the northing velocity during the same time as in Figure 6-10. Similarly, the large jumps in the GPS data are successfully rejected.

Figure 6-12 shows a different instance of consecutive GPS pops over 25 seconds.



The Kalman filter rejects the pop and maintains the trajectory that it was likely on. However, a point can be made about accuracy vs. precision for this event. The GPS measurement showed a sudden change in position, but this doesn't necessarily mean that it jumped further away or closer to the real position. It is impossible to know the true mean of the position because GPS receiver only reports accuracy, which is not necessarily centered on the true mean. For this reason, the autonomous vehicle must inevitably track GPS points because there is no other absolute information regarding position in this system. However, one of the requirements in this thesis is that the reference feedback be smooth, so that no abrupt or jagged control signals are sent to the controller which is achieved in the current implementation.

6.2.1 GPS Outage

In this section, a look at the behavior of the Kalman filter during GPS outage is examined. For example, the same trajectory shown above is used to compare the results of when the GPS cuts out shortly after initialization.

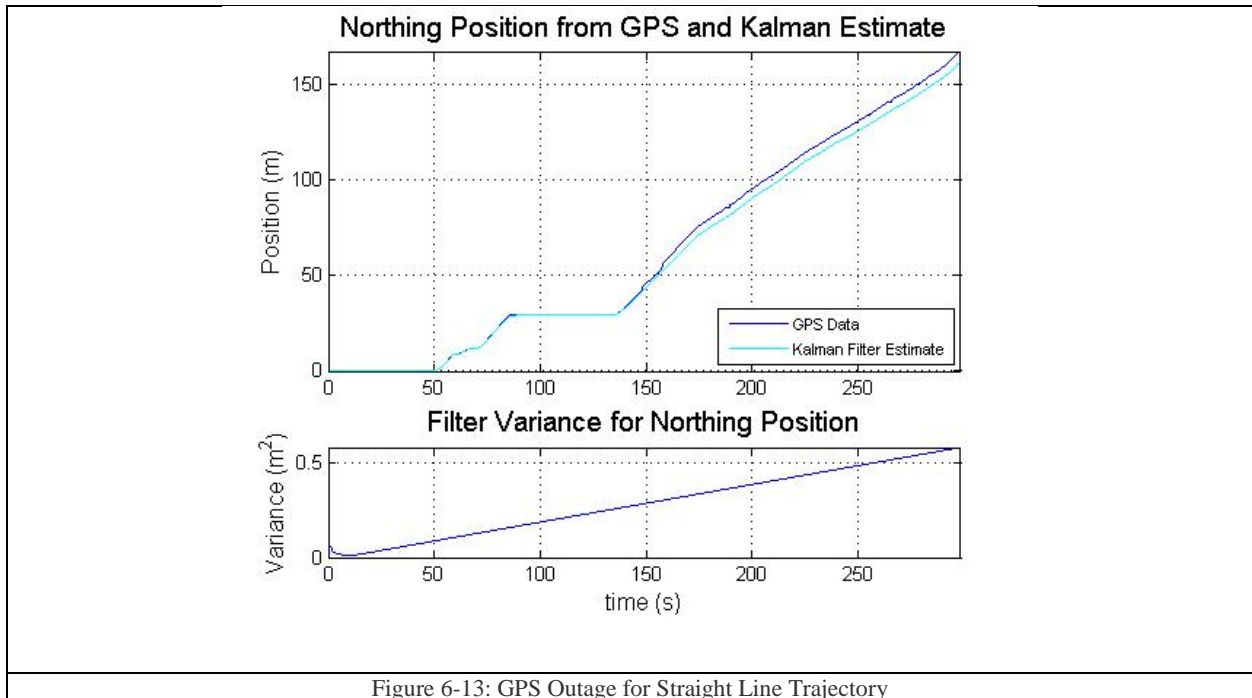


Figure 6-13: GPS Outage for Straight Line Trajectory

Figure 6-13 shows that the amount of drift in position is 5.8 meters after a short initialization of the GPS for heading reference. The filter performance shows a linearly increasing variance, as opposed to the quadratic growth seen previously when WSS was not utilized. However, the performance being tracked is somewhat futile, in that it does not account for deterministic error, such as bias.

The estimate variance grows during this time as the position must due to no absolute position measurement. Furthermore, it is interesting that the northing estimate grows linearly, although the estimate is dependent on both integrated angular velocity and acceleration as opposed to quadratically or worse as shown in Figure 5-3 which showed a quadratic increase in variance through the integration of angular rates, and coordinate transformed and integrated body accelerations. With the use of WSS data, the estimated variance during unobservable periods is contained significantly.

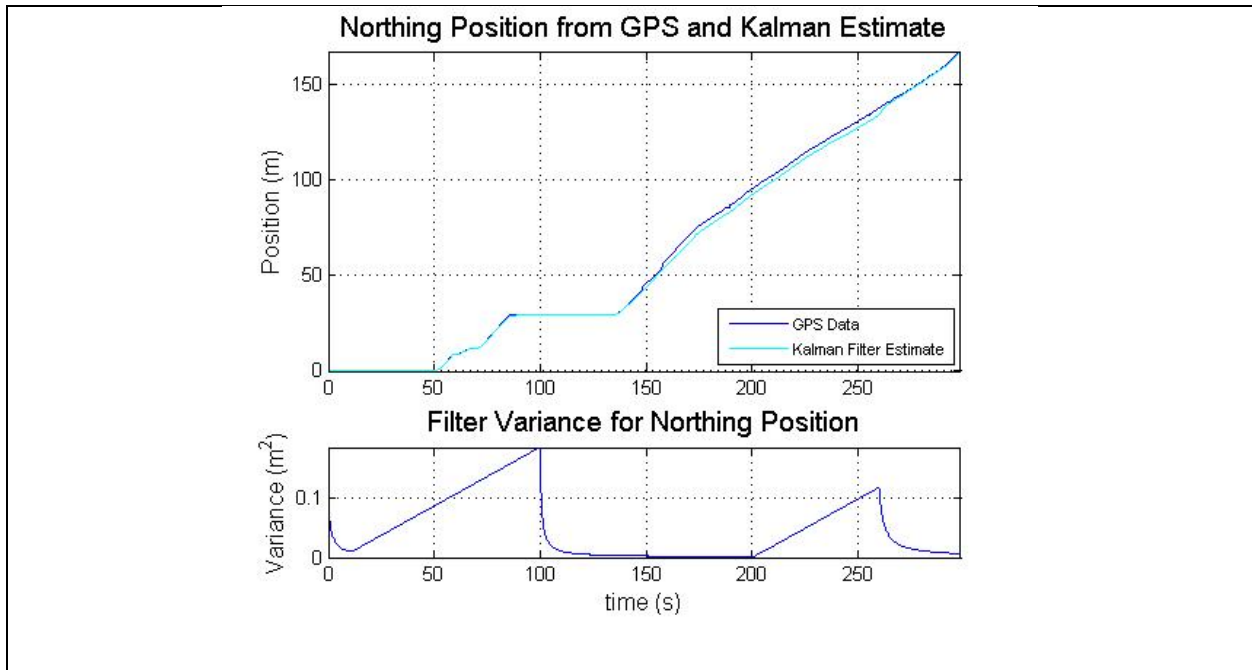


Figure 6-14: GPS Outage During Two Intervals and Estimated Performance

Figure 6-14 shows the performance and estimation variance of two GPS outages beginning at 10 seconds lasting for 90 seconds, and again at 200 seconds lasting for 60 seconds. The maximum amount of drift in either outage was 4 meters.

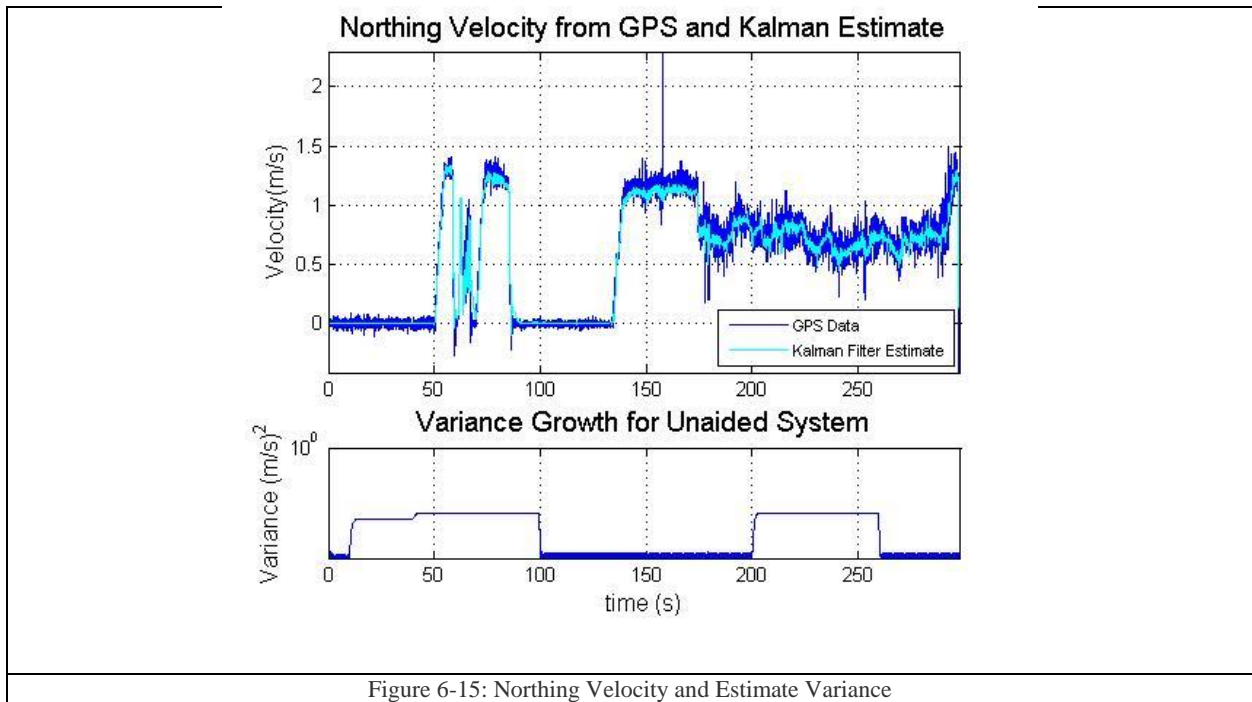


Figure 6-15: Northing Velocity and Estimate Variance

Figure 6-15 shows the velocity performance during two instances of GPS outage.

As one can see from Figure 6-14 and Figure 6-15, the estimate variance on velocity does not grow due to the fact that velocity is still measured absolutely and the integration drift on the gyroscopes is limited due to calibration. It does change, however, due to the lost information from the GPS which no longer provides redundant information and thus decrease the estimation variance. Positional variance is shown to grow as expected, and when GPS kicks back in, the transition is smooth

Finally, it is useful to look at how well the filter tracks performance under GPS denied circumstances and how reasonable it is to trust the filter accuracy readings. In Figure 6-13, it appears that the variance growth reach a maximum value of $0.6 m^2$, although the drift from the GPS signal is upwards of 6 m. This is due to the fact that deterministic errors are not accounted for in the Kalman variance estimate, and furthermore, without an error model to estimate the bias, scale factor, etc. it is not likely that the performance estimate of the Kalman filter can be trusted at all.

This chapter discussed the Kalman filter algorithm and the main components on how it works, namely, the prediction and correction phase and how that effects the estimate variance. The example used was northing velocity during a fast deceleration, and showed the rejection of a noisy prediction estimate to combine the other sensor data to output a cleaner, lower variance, estimate. Furthermore, this chapter showed results from aligning and estimating drift constants and the performance increase when this is done. The effect of GPS pop was examined and the rejection thereof by utilization of the whole sensor suite. Lastly, GPS outage performance was examined to see how well a GPS denied system could perform, and how the estimated variance corresponded to the actual drift.

Chapter 7: Conclusions and Future Work

This work was a reviewed and discussed the principles and application of strapdown inertial navigation in the framework of the extended Kalman filter. There have been many similar works on navigation, and this paper is by no means exhaustive or cover the all of the idiosyncrasies associated with navigation, but aimed to provide insight in the development and implementation of an EKF for multi-rate systems with other considerations regarding the development of the Kalman filter.

The Kalman filter is a widely accepted and used tool with highly practical applications in many systems, such as robotics, computer vision, and many others. In the case of strapdown inertial navigation, the methods presented in this thesis can be extended to other applications outside the scope of ground vehicles, such as for aerial vehicles, missiles, or marine vehicles which are all equipped with similar sensor packages.

7.1 Filter Model Construction

The filter model construction in this context was a somewhat unconventional application of Kalman filtering, where IMU measurements appeared in the state dynamics model. Normally, the system dynamics matrix is dependent on equations of motion, which may or may not be time varying. However, constructing the filter this way allows for seamless integration of the IMU into position and velocity with the updated position and velocity measurements as they come from the GPS and WSS. The Kalman filter provides a convenient framework to combine information from external sensors, constraints, and general intuition into the model to improve the overall solution.

Hardware selection must be done carefully when designing a navigation system, as it was shown that even with a navigation grade IMU, it is possible to have an erroneous solution from common errors that exceed the realm of minimum variance. Understanding the deterministic error can allow the design engineer to incorporate an error model, and estimate bias or scale factor online.

For low cost systems, a tilt sensor or reorientation of dual GPS antennas such that tilt angle could help measure bias in the accelerometer during coarse alignment [47].

7.2 Standalone Sensor Platforms

It was demonstrated that for highly precise localization as required for autonomous vehicles, any one sensor was not sufficient under all conditions, although the aided IMU with WSS could stay within 10 meters over a 400 meter trajectory. Furthermore, properties of the IMU were exploited to reinitialize and recalibrate the drifting attitude, as the alignment and bias appears to have the most influence on the degradation of the inertial navigation solution. However, with auxiliary sensors to support inertial navigation, it is possible to have an improved solution regardless of the presence of bias and scale factor in the IMU output. Without compensation of the deterministic error terms, the algorithm will lead to a quickly diverging solution in the event of GPS outage, as shown in section 6.1

The main source of drift in the standalone INS system was not, in fact, caused by the noisy measurements of the sensor, but rather the small variation in attitude and the correction of gravity term. The strapdown inertial navigation system requires a highly accurate sense of body attitude to properly cancel the effects of gravity. For a nonholonomic vehicle, this effect is amplified, especially in the forward direction where incorrect pitch angle will cause longitudinal velocity to grow according to $g \times \int_0^t \sin(\beta) d\tau$. It is believed also, that higher order integration methods of the gyroscopes would also alleviate some of the deviation from the true angles of the sensors.

In the context of autonomous vehicles, accuracy is only part of the equation, it is also desired to reduce the effects of jagged pop from the GPS. It is shown that in general, the extended Kalman filter reduces this effect in the state estimate. With an adapting measurement covariance matrix according to estimated accuracy as provided by the GPS receiver, it is possible to further mitigate these effects and at the very least give the filter a more accurate representation of the uncertainty.

7.3 Process and Measurement Noise

The design of the process and measurement covariance matrices were completed through the use of the autocorrelation functions associated with each sensor while the vehicle was stationary with the engine running, in an attempt to capture the true nature of the measurement variance during operation. However, since the WSS will measure zero during stationary operation, the variance will also be zero, causing \mathbf{R}_k to assume a perfect measurement. In fact, the nature of both GPS position and WSS is that they are not Gaussian noise, thus violating the assumptions of the optimal Kalman filter, and is compounded according due to the first order linearization truncation of the estimated statistics. Accordingly, due to the nonlinear transformations of all said sensors, the optimality of the KF is no longer valid under the conditions of minimum variance.

In this work, process noise was considered to be caused by the IMU output which was then further simplified as a conservative estimate of the nonlinear transformation of that process noise. However, this did not include the environmental effect or other stochastic inputs that may affect the solution. This could potentially lead to an inaccurate representation of the statistical awareness.

7.4 Benefits of Adaptation

To deal with the uncertain process noise and measurement noise, adaptation has been a proven way to estimate the covariance matrices in real time. However, due to the violation of the Gaussian assumption for GPS and WSS, this may cause adverse effects in the estimated covariance matrices. For example, during stationary vehicle periods, the distribution of the WSS is identically zero, which will then lead the filter to think there are perfect measurements from the WSS, and the GPS is influenced by deterministic error which may cause problems in the autocorrelation functions.

Other methods of using the EKF are to change the state variables to error terms based on the INS solution minus the auxiliary sensor aided Kalman filter. This method allows for the errors in the INS to be compensated for in real time, specifically, bias and scale factor are common error

terms to be estimated. The measurement terms in this structure take the form of INS measured position, velocity, and attitude minus the aiding sensors solution as well.

7.5 Future Work

The Kalman filter has been used extensively for INS/GPS navigation, ranging from the study of initial calibration to lowering the cost of the combination of the two for the best estimate of the navigation solution. This paper scratches the surface of GPS/IMU integration, but there are several areas worth exploring in the future.

For example, the cascaded model and augmented measurement matrix method used for coarse alignment was assumed to be a linear, zeroth order filter, which neglected the effects of the nonlinear transformation of the probability distribution function. Perhaps using an extended information filter in the cascaded framework to initialize attitude of the stationary vehicle would provide statistically more significant results. This will allow an infinite covariance/zero information at the beginning of each calibration, thus making no assumptions of the current knowledge of the system and feeding appropriate statistics to the filter. It would also be interesting to examine gyrocompassing in the aforementioned framework.

With regards to IMU/GPS integration, it is almost standard now to use an error model to estimate the sensor errors on the IMU. This has been shown to be effective and work in real time to compute sensor bias and scale factor, and thus provide a better IMU navigation solution. The method of integration in this work was simple Euler integration, whereas a higher order integration could be used to improve truncation error.

Other sensors could be incorporated, such as magnetometers, tilt sensors, and even computer vision to aid in IMU bias corrections. The main takeaway is that the Kalman filter can combine many different sources of data, estimate the deterministic error as states, and find a minimum variance solution for the random error associated with measurements and environment.

Bibliography

- [1] Y. Bar-Shalom, L. Rong and T. Kirubarajan, Estimation with application to tracking and navigation: theory algorithms and software, John Wiley & Sons, 2004.
- [2] M. S. Grewal, L. R. Weill and A. P. Andrews, Global Positioning Systems, Inertial Navigation, and Integration; Second Edition, Hoboken, New Jersey: Wiley, 2007.
- [3] K. R. Britting, Inertial navigation systems analysis, 2010.
- [4] U. Ozguner and C. Stiller, "Systems for Safety and Autonomous Behavior in Cars: The DARPA Grand Challenge Experiment," *Proceedings of the IEEE*, vol. 95, no. 2, pp. 397-412, 2007.
- [5] P. M. Kitner, Global Positioning System Theory and Design, 1999.
- [6] Y. F. Jiang, "Error Analysis of Analytic Coarse Alignment," *Aerospace and Electronic Systems*, vol. 34, no. 1, pp. 334-337, 1998.
- [7] C. a. S. M. o. I. N. S. Errors, "El-Diasty, Mohammed; Pagiatakis; Spiros," *Journal of Global Positioning Systems* , vol. 7, no. 2, pp. 170-182, 2008.
- [8] C. C. Ward and K. Iagnemma, "Model-based wheel slip detection for outdoor mobile robots," in *IEEE International Conference on Robotics and Automation*, Roma, 2007.
- [9] R. Isermann, R. Schwarz and S. Stolz, "Fault-tolerant drive-by-wire systems," *IEEE, Control Systems* , vol. 22, no. 5, pp. 64-81, 2002.
- [10] B. Oksendal, Stochastic Differential Equations, an Introduction with Applications; Sixth Edition, Berlin Heidelberg : Springer, 2013.
- [11] P. Corke, Robotics, Vision and Control, Berlin Heidelberg, Germany: Springer, 2011.

- [12] C. Hong, Z. Nanning and J. Qin, "Pedestrian detection using sparse Gabor filter and support vector machine," *Intelligent Vehicles Symposium IEEE*, pp. 583-587, 2005.
- [13] C. Kuo-Yu and L. Sheng-Fuu, "Lane Detection Using Color-Based Segmentation," *Intelligent Vehicles Symposium*, pp. 706-711, 2005.
- [14] C. Y. Low, H. Zamzur and S. Mazlan, "Simple Robust Road Lane Detection Algorithm," in *Intelligent and Advanced Systems 5th International Conference*, 2014.
- [15] P. King, *A Low Cost Localization Solution Using a Kalman Filter for Data Fusion*, Blacksburg: Virginia Tech, 2008.
- [16] C. Hide, T. Moore and M. Smith, "Adaptive Kalman Filtering for Low-cost INS/GPS," *The Journal of Navigation*, vol. 56, pp. 143-152, 2003.
- [17] Y. Ren and X. Ke, "Particle Filter Data Fusion Enhancements for MEMS-IMU/GPS," *Scientific Research*, vol. 2, pp. 417-421, 2010.
- [18] B. Southall, T. Haue, J. A. Marchant and B. F. Buxton, "An autonomous crop treatment robot: Part 1. A Kalman filter model for localization and crop/weed classification," *The international Journal of robotics research*, vol. 21, no. 1, pp. 61-74, 2002.
- [19] S. Y. Chen, "Kalman Filter for robot vision: a survey," *IEEE Transactions on Industrial Electronics*, vol. 59, no. 11, pp. 4409-4420, 2012.
- [20] S. Jeon, M. Tomizuka and T. Katou, "Kinematic Kalman Filter (KKF) for Robot End-Effector Sensing," *Journal of Dynamic Systems, Measurement, and Control*, vol. 131, no. 2, 2009.
- [21] novatel.com, "Novatel," Novatel, 20 04 2015. [Online]. Available: www.novatel.com. [Accessed 01 05 2015].

- [22] D. M. Bevly, "Global Positioning System (GPS): A low cost velocity sensor for correcting inertial sensor errors on ground vehicles," *Journal of Dynamic Systems, Measurement, and Control*, vol. 126, pp. 255-264, 2004.
- [23] H. Qi and J. B. Moore, "Direct Kalman Filtering Approach for GPS/INS Integration," *Aerospace and Electronic Systems, IEEE Transactions*, vol. 38, no. 2, pp. 687-693, 2002.
- [24] S. Gao, Y. Zhong, X. Zhang and B. Shirizadeh, "Multi-sensor Optimal Data Fusion for INS/GPS/SAR Integrated Navigation System," *Aerospace Science and Technology*, vol. 13, pp. 232-237, 2009.
- [25] J. Wendel and G. F. Trommer, "Tightly Coupled GPS/INS Integration for Missile Applications," *Aerospace Science and Technology*, vol. 8, pp. 627-634, 2004.
- [26] S. Sukkarieh, E. M. Nebot and H. F. Durrant-Whyte, "A High Integrity IMU/GPS Navigation Loop for Autonomous Land Vehicle Applications," *IEEE Transactions on Robotics and Automation*, vol. 15, no. 3, pp. 572-578, 1999.
- [27] P. Zhang, J. Gu, E. E. Milios and P. Huynh, "Navigation with IMU/GPS/Digital Compass with Unscented Kalman Filter," in *Proceeding of the IEEE International Conference on Mechatronics & Automation*, Niagra Falls, 2005.
- [28] A. Fakharian, T. Gustafsson and M. Mehrfam, "Adaptive Kalman Filtering Based Navigation: An IMU/GPS Integration Approach," in *Internations Conference on Networking, Sensing and Control*, Delft, the Netherlands, 2011.
- [29] A. Mohamed and K. Schwarz, "Adaptive Kalman Filtering for INS/GPS," *Journal of Geodesy*, vol. 73, no. 4, pp. 193-20, 1999.
- [30] S. Cooper and H. Durrant-Whyte, "A Kalman Filter Model for GPS Navigation of Land Vehicles," in *Intelligent Robots and Systems '94, Proceedings of the IEEE/RSJ/GI International Conference*, Munich, 1994.

- [31] S. Sukkarieh, "Low Cost, High Integrity, Aided Inertial Navigation Systems for Autonomous Land Vehicles," The University of Sydney, Sydney, 2000.
- [32] D. Titterton and J. L. Weston, Strapdown Inertial Navigation Technology, IET, 2004.
- [33] D. Simon and T. Chia, "Kalman Filtering with State Equality Constraints," *IEEE Trans. Aerospace Electronics Systems*, vol. 38, no. 1, pp. 128-136, 2002.
- [34] G. Dissanayake, S. Sukkarieh, E. Nebot and H. Durrant-Whyte, "The Aiding of a Low-Cost Strapdown Inertial Measurement Unit Using Vehicle Model Constraints for Land Vehicle Applications," *IEEE Transactions on Robotics and Automation*, vol. 14, no. 5, pp. 731-747, 2001.
- [35] "OmniStar," OmniStar, 2014. [Online]. Available: www.omnistar.com. [Accessed 20 04 2015].
- [36] D. Titterton and J. Weston, Strapdown Inertial Navigation Technology, Herts: The Institution of Electrical Engineers, 2004.
- [37] M. Grewal and A. Andrews, Kalman Filtering; Theory and Practice Using MATLAB, Third Edition, Hoboken, New Jersey: Wiley, 2008.
- [38] B. Barshan and H. F. Durrant-Whyte, "Inertial Navigation Systems for Mobile Robots," *IEE Transactions on Robotics and Automation*, vol. 11, no. 3, pp. 328-342, 1995.
- [39] N. El-Sheimy, H. Hou and X. Niu, "Analysis and Modeling of Inertial Sensors Using Allan Variance," *IEEE Transactions on Instrumentation and Measurement*, vol. 57, no. 1, pp. 140-150, 2008.
- [40] J. J. Craig, Introduction to Robotics: Mechanics and Control 3rd Edition, New Jersey: Prentice Hall, 2005.
- [41] W. E. L. M. a. W. G. P. Strange, "A Gravity Survey of the Island of Oahu, Hawaii," *Pacific Science*, vol. 19, no. 3, pp. 350-353, 1965.

- [42] J. E. Bortz, "A New Mathematical Formulation for Strapdown Inertial Navigation," *Aerospace and Electronics Systems, IEEE Transactions*, vol. 7, no. 1, pp. 61-66, 1971.
- [43] P. G. Savage, "Strapdown Inertial Navigation Integration Algorithm Design Part 1: Attitude Algorithms," *Journal of Guidance, Control, and Dynamics*, vol. 21, no. 1, pp. 19-28, 1998.
- [44] R. B. Miller, "A New Strapdown Attitude Algorithm," *Journal Of Guidance*, vol. 6, no. 4, pp. 287-291, 1983.
- [45] P. G. Savage, "Strapdown Inertial Navigation Integration Algorithm Design Part 2: Velocity and Position Algorithms," *JOURNAL OF GUIDANCE, CONTROL, AND DYNAMICS*, vol. 21, no. 2, pp. 208-221, 1998.
- [46] K. Atkinson and W. Han, *Elementary Numerical Analysis*, Hoboken, New Jersey: Wiley, 2004.
- [47] D.-W. H. Nebot E., "Initial Calibration and Alignment of Low Cost Inertial Navigation Units for Land Vehicle Applications," *Journal of Robotics Systems*, vol. 16, no. 2, pp. 81-92, 1999.
- [48] H.-S. Ahn and C.-H. Won, "Fast Alignment Using Rotation Vector and Adaptive Kalman Filter," *IEEE Transactions on Aerospace and Electronics Systems*, vol. 42, no. 1, pp. 70-83, 2006.
- [49] P. Batista, C. Silvestre, P. Oliveira and Cardeira, "Accelerometer Calibration and Dynamic Bias and Gravity Estimation: Analysis, Design, and Experimental Evaluation," *IEEE Control Systems Technology*, vol. 19, no. 5, pp. 1128-1137, 2011.
- [50] P. M. G. Silson, "Coarse Alignment of a Ship's Strapdown Inertial Attitude Reference System Using Velocity Loci," *IEEE Transactions on Instrumentation and Measurement*, vol. 60, no. 6, pp. 1930-1941, 2011.

- [51] A. Acharya, S. Sadhu and T. Goshal, "Improved self-alignment scheme for SINS using augmented measurement," *Elsevier Aerospace Science and Technology*, vol. 15, pp. 125-128, 2011.
- [52] T. Hamel and R. Mahony, "Attitude Estimation on $SO(3)$ Based on Direct Inertial Measurements," in *IEEE International Conference on Robotics and Automation*, Orlando, 2006.
- [53] Y. F. Jiang, N. Chiao Tung and Y. P. Lin, "On the Rotation Vector Differential Equation," *Aerospace and Electronic Systems, IEEE Transactions*, vol. 27, no. 1, pp. 181-183, 1991.
- [54] D. W. Stockwell, "Bias Stability Measurement: Allan Variance," [Online]. Available: <http://www.moog-crossbow.com/Literature>. [Accessed 20 4 2015].
- [55] S. Nasiri, "A Critical Review of MEMS Gyroscopes Technology and Commercialization Status," [Online]. Available: invensense.com. [Accessed 20 4 2015].
- [56] "GPS.gov," [Online]. Available: GPS.gov. [Accessed 20 4 2015].
- [57] J. Wendel, O. Meister, C. Schlaile and G. F. Trommer, "An Integrated GPS/MEMS-IMU Navigation System for an Autonomous Helicopter," *Aerospace Science and Technology*, vol. 10, pp. 527-533, 2006.
- [58] J. A. Farrell, T. D. Givargis and M. J. Brath, "Real-Time Differential Carrier Phase GPS-Aided INS," *IEEE Transactions on Control Systems Technology*, vol. 8, no. 4, pp. 709-721, 2000.
- [59] H. Hwang, "Kinematic GPS for differential positioning: Resolving integer ambiguities on the fly," *Navigation: J. Instt. Nac.*, vol. 38, no. 1, 1991.
- [60] A. Gelb, *Applied Optimal Estimation*, Cambridge: The Analytic Sciences Corporation, 1974.

- [61] R. Kalman, "A New Approach to Linear Filtering and Prediction Problems," *ASME*, vol. ?, no. ?, pp. 35-45, 1960.
- [62] N. Wiener, *Extrapolation, Interpolations, and Smoothing of Stationary Time Series With Engineering Applications*, Cambridge : M.I.T. Press, 1964.
- [63] R. Kalman and R. Bucy, "New Results in Linear Filtering and Prediction Theory," *Journal of Basic Engineering*, vol. 83, no. 1, pp. 95-108, 1961.
- [64] E. A. V. D. M. R. Wan, "The Unscented Kalman Filter for Nonlinear Estimation," in *Adaptive Systems for Signal Processing, Communications, and Control Symposium*, Lake Louise, 2000.
- [65] R. Mehra, "Approaches to Adaptive Filtering," *IEEE Transactions on Automatic Control*, vol. 17, no. 5, 1972.
- [66] P. Zarchan, *Fundamentals of Kalman Filtering- A Practical Approach*, 2nd Edition, Reston: American Institute of Aeronautics and Astronautics, Inc., 2005.
- [67] Y. Bulut, "Applied Kalman Filter Theory," Civil Engineering Dissertations, Paper 13, <http://hdl.handle.net/2047/d20003550>, 2011.
- [68] D. Simon, "Kalman Filtering with State Constraints: A Survey of Linear and Nonlinear Algorithms," *IET Control Theory Appl.*, vol. 4, no. 8, pp. 1303-1318, 2010.
- [69] E. Lefferts and F. L. Markley, "Kalman filtering for spacecraft attitude estimation," *Journal of Guidance, Control, and Dynamics*, vol. 5, no. 5, pp. 417-429, 1982.
- [70] A. Mourikis and S. Roumeliotis, "A multi-state Constraint Kalman Filter for Vision-aided inertial navigation," in *IEEE International Conference on Robotics and Automation*, Roma, 2007.
- [71] S. J. Julier and J. K. Uhlmann, "Unscented Filtering and Nonlinear Estimation," *IEEE*, vol. 92, no. 3, pp. 401-422, 2004.

- [72] M. Bando, Y. Kawamata and T. Aoki, "Dynamic Sensor Bias Correction for Attitude Estimation Using Unscented Kalman Filter in Autonomous Vehicle," *International Journal of Innovative Computing, Information, and Control*, vol. 8, no. 3B, pp. 2347-2358, 2012.
- [73] F. H. T. N. I. M. & S. C. Schlee, "Use of an External Cascade Kalman Filter to Improve the Performance of a Global Positioning System (GPS) Inertial Navigator," in *Aerospace and Electronics Conference IEEE*, Dayton, 1988.
- [74] D. M. P. B. Bevely, "Cascaded Kalman filters for accurate estimation of multiple biases, dead-reckoning navigation, and full state feedback control of ground vehicles.," *Control Systems Technology*, vol. 15, no. 2, pp. 199-208, 2007.
- [75] J. Farrell and M. Limestone, "Exact Calculation of Discrete-Time Process Noise Statistics of Hybrid Continuous/Discrete Time Applications," in *Proceedings of the 32nd Conference on Decision and Control*, San Antonio, 1993.
- [76] P. Y. Hwang, "Kinematic GPS: Resolving Integer Ambiguities on the fly," in *IEEE Symposium on Position Location and Navigation*, 1990.
- [77] J. Farrell, M. Grewal, M. Djodjat and M. Barth, "Differential GPS with Latency Compensation for Autonomous Navigation," in *Proceedings of the 1996 IEEE International Symposium on Intelligent Control*, Dearborn, MI, 1996.
- [78] D. Doberstein, *Fundamentals of GPS Receivers, A Hardware Approach*, New York: Springer, 2012.
- [79] W. Ding and J. Wang, "Precise Velocity Estimation with a Stand Alone Receiver," *The Journal of Navigation*, vol. 64, no. 2, pp. 311-325, 2011.
- [80] J. Pratt, P. Axelrad, K. M. Larson, B. Lesage, R. Gerren and N. DiOrio, "Satellite Clock Bias Estimation for iGPS," *GPS Solut*, vol. 17, no. 3, pp. 381-389, 2013.

- [81] S. G. L. Cao, "Multi-Objective Robust Initial Alignment Algorithm for Inertial Navigation System with Multiple Disturbances," *Aerospace Science and Technology*, vol. 21, pp. 1-6, 2012.
- [82] P. Dvidson, J. Hautamaki and J. Collin, "Using Low Cost MEMS 3D Accelerometer and One Gyro to Assist GPS Based Car Navigation System," in *Proceedings of 15th Saint Petersburg International Conference on Integrated Navigation Systems*, Saint Petersburg, 2008.
- [83] D. J. Simon and D. L. Simon, "Constrained Kalman Filtering via Density Function Truncation for Turbofan Engine Health Estimation," *International Journal of Systems Science*, vol. 41, no. 2, pp. 159-171, 2010.
- [84] M. Roth and F. Gustafsson, "An Efficient Implementation of the Second Order Extended Kalman Filter," in *14th International Conference on Information Fusion*, Chicago, 2011 .